NASA Contractor Report 182203

A Control-Volume Method for Analysis of Unsteady Thrust Augmenting Ejector Flows

Colin K. Drummond

Sverdrup Technology, Inc.
NASA Lewis Research Center Group
Cleveland, Ohio

November 1988

Prepared for
Lewis Research Center
Under Contract NAS3-25266

National Aeronautics and
Space Administration

Table of Contents

1. SUMMARY

A new method of analysis for predicting thrust augmenting ejector characteristics is presented and the results of computations for a test case discussed. The impetus for the development of the method is based on three simulation requirements: (1) a predictive analytic procedure is needed, (2) the method must accommodate some form of turbulent flow characterization and interchange, and (3) the final system of equations must be amicable to a real-time simulation objective. A literature search revealed an absence of ejector research consistent with these combined objectives *and* that was capable of describing *transient* flows.

Within the general framework of the control-volume formulation for continuity, momentum, and energy there exist time derivatives of field variable volume integrals. Since these volume integrals cannot be converted into surface integrals, an approximation for the field variable spatial distribution must be made. Under the assumption that the ejector mixing region physics dominate ejector performance characteristics, spatial sub-division of the mixing region permits each sub-volume to be approximated by characteristic velocity, pressure, and temperature profiles. A description of turbulent flow is provided with Abramovich-type self similar turbulent flow field variable profiles. Time derivatives of the volume integral reduce to time derivatives of the field variable characteristics, and, with treatment of the surface integrals in the "usual" way, a set of differential equations in time evolves. With the intent to focus primarily on results for ejector thrust, very few (less than ten) subdivisions of the mixing region are needed, and, therefore, a terse description of the ejector mixing region is obtained. Although a crude description of the turbulent ejector jet interaction is employed, the final system of equations can potentially provide real-time thrust predictions, thereby meeting the aforementioned objectives.

Since a step-change in the ejector driving nozzle flow is representative of typical ejector operation, an example prediction of this situation is employed as a test case for application of the methodology.

2. EJECTOR SIMULATION PERSPECTIVE

Role of the Simulation

Research on design methodologies for integrated aircraft and propulsion flight control systems requires accurate subsystem component simulations. In principle, these simulations must mimic steady-state *and* transient component effects. A NASA Lewis research program is currently underway to develop a "real-time" simulation -- including system transients -- for Short Take-Off Vertical Landing (STOVL) aircraft. Thrust augmenting ejectors are considered potentially valuable propulsion subsystem elements for the powered-lift aspect of STOVL aircraft. To explore ejector concepts further, the initial NASA Lewis STOVL system simulation requires a thrust augmenting ejector sub-system simulation. Unfortunately, an ejector simulation that includes ejector transients is not currently available; the purpose of the present work is to develop one.

An ejector is a mechanically simple fluidic pump composed essentially of two components: (1) a "primary" jet nozzle issuing into (2) a shroud. This arrangement permits entrainment and acceleration of a secondary flow (within the shroud) by the primary jet. A diffuser section attached to the shroud allows control over the ejector discharge pressure. Figure 1 illustrates a generic thrust augmenting ejector.

From a system simulation point of view, the ejector participates in the description of the aircraft "plant dynamics" as shown in figure 2.

Three Competing Requirements

There are three basic requirements the ejector simulation must meet:

1. The mathematical model must be *predictive* (not parametric) in nature.

2. Some approximation of turbulent flow characteristics inside the ejector mixing region must be made.

3. The final system of equations describing the ejector must be amicable to the NASA/Lewis real-time simulation objective.

To meet the first requirement, only two data sets should be prescribed: (a) the primary jet "control-valve" setting (with associated thermodynamic data), and (b) *free-stream* atmospheric properties. From this, the secondary inlet condition **and** the ejector thrust augmentation (as a function of time) are predicted. A parametric method would specify *all* primary and secondary conditions (in contrast to the predictive method where the latter is unknown).

Central to the idea of an *accurate* ejector simulation, the second requirement points out the need for *some* type of characterization of turbulent mixing and entrainment phenomena in the mixing region; a description of these effects is essential for transient-type analyses.

The third requirement emphasizes the ejector simulation must not become a CPU bottleneck in the final STOVL simulation.

At this point in time these simulation goals are at odds with each other; methods relying on first principles for the predictive facet of analysis are accurate, but not executable in real-time.

Perspective on Previous Work

Ejector research goes back about half a century and has resulted in a multitude of papers on various aspects of ejector performance, optimization, and analytic methods. Frequently referenced in recent literature is the work of Porter and Squires[1981] whose survey produced a compilation of over 1600 research papers on ejectors; much more research on ejectors has been done since that review. No attempt is made in the present work to extensively discuss the history of ejector research. Rather, it is more of interest to note that in the survey conducted for this work (see References) unsteady flow research focuses on the *pulsed* ejector flow problem. Such flows are of interest, for example, in chemical laser applications (see Anderson [1970a, 1970b, 1976], Johnson [1966], and Petrie, Addy, and Dutton[1985]). No papers were identified that dealt with transient *thrust augmenting ejector* flows in a way consistent with a real-time simulation goal.

Methods of analysis are extracted from either a control-volume or material-volume formulation. In the former, a set of algebraic equations is (often) based on quasi-one-dimensional and isentropic conditions, while in the latter a multidimensional non-linear system of differential equations is obtained. The first generally gives way to parametric studies while the second is more predictive in nature.

Although bases of analysis can be polarized as described above, there are many methods of implementation. For any specific perspective on formulation involving, for instance, a system of differential equations, details of analysis depend on the analyst's selection of a solution method, e.g., finite-difference, finite-element, or method of characteristics. We summarize the extremes of ejector simulation as follows:

1. A control volume analysis is by far the most straightforward and widely reported method, but, since the system of equations is under-determined (when only the ambient and primary nozzle conditions are given), some key parameters must be specified. Although the system has potential for real-time simulation, the need to prescribe, for instance, mass entrainment ratio yields that (in principle) this is at best a parametric method of analysis.

2. A material-volume analysis draws on the full Navier-Stokes and energy equations, and provides an opportunity for a fundamental introduction of tubulent flow characteristics. It is therefore possible to be predictive in nature, but only at a considerable CPU expense; these machine computations are not likely to fall within a real-time framework.

Present Approach

In order to generate a predictive method of analysis an empirically based model for the turbulent interaction region is explored within the framework of a control volume analysis. This approach provides a rational foundation for the introduction of steady flow data to "calibrate" an unsteady flow simulation; there is no intent here to provide a multi-dimensional CFD code based on first principles.

Elements of Current Work

A methodology for simulating thrust augmenting ejector performance is described in the present work. Section 3 describes some typical ejector approximations and considerations related to ejector operation and operating regimes. Since the final system of equations are extracted from a control-volume formulation, control-volume equations for an arbitrary ejector control volume are given in Section 4; this enables the general (time-dependent) surface velocity to be correctly introduced into the system. Section 4 also expands on the simplification of one-dimensional flow and application of the equations to the inlet, mixing region, and diffuser.

Section 5 remarks on the simplification offered by a steady-state analysis and provides a descriptive solution procedure and results from the same. Section 6 looks at three approaches for unsteady flow analysis and details the Finite-Volume adaptation used in the present work.

A test case is examined in Section 6; this leads the the concluding remarks in Section 8.

Appendicies A-J provide extensive detail on points of analyses traditionally assumed "intuitively obvious". Such information is contained in the present work for (a) completeness of documentation of the proposed method, (b) the capability to reproduce the derived results, and (c) illustration of inadvertently implicit assumptions.

3. PRELIMINARY CONSIDERATIONS

Qualitative Ejector Characteristics

A thrust augmenting ejector is often described as a fluidic pump that employs the momentum of a high velocity jet from the primary flow nozzle (drive flow) to entrain and pressurize a secondary (suction) stream; a typical thrust augmenting ejector consists of four basic components:

1. a high pressure nozzle to accelerate the primary flow,
2. an inlet section to accelerate the secondary flow
3. an intermediate mixing section to permit momentum exchange between the primary and secondary flows, and
4. a diffuser to match the discharge pressure (static) with the ambient.

Overviews of the characteristics for this general ejector configuration have been given recently by (among others) Koenig et. al.[1981], Minardi [1982], and Bevilaqua [1984]. Also, the proceedings of the 1981 Ejector Workshop for Aerospace Applications (Braden et. al. [1982]) covers many issues in ejector technology and simulation. It is well known that the (irreversible) mixing of the primary and secondary streams results in a local static pressure that is less than the ambient; this is the origin of the suction effect on the secondary stream. Recovery of the static pressure in the diffuser results in a net thrust component from the difference of the (integrated) pressure distribution of the diffuser and inlet[1]. It is therefore of interest in ejector design to contour the inlet and diffuser so as to maximize the suction effect and diffuser pressure recovery. A typical ejector wall pressure distribution is shown in Figure 3 (taken from Bernal and Sarohia [1983]; also see the work of Miller and Comings [1958]). Minimization of nozzle drag (direct and ram) is also important, as is the need to avoid shroud leakages. An approximate relation for the ejector system thrust is given by

$$T = \dot{m}_{1P} u_{1P} + \int_I p(\underline{I} \cdot \underline{n}) dA - \sum I_i \qquad (1)$$

where the first term is an approximation for the primary nozzle thrust, the second the net surface pressure integral, and the last the sum of viscous and pressure losses. The obvious design goal is to have an ejector where the third term is minimized. In analysis, the object is to predict the velocities and pressures such that all terms in the thrust equation can be evaluated; as a practical matter this is not an easy task and is the impetus for the variety of approximate methods that exist. For example, in a steady-state analysis the total thrust of the system can be computed from application of conservation of momentum and mass for a control volume corresponding to the duct boundary - in this case there is no need to integrate the pressure distribution over the

1 Analogous to the theory of lift on a wing in an inviscid flow, the inviscid thrust in an ejector is attributed to the net circulation that arises when the flow streamlines in the shroud are directed longitudinally from what would otherwise (in the absence of the shroud) be at an angle to the centerline.

wall of the shroud. At the other extreme finite-element or finite-difference methods of analysis are used to compute detailed flow velocities and pressures along the wall bounding the flow.

It is evident that (as in many other fluid flow problems) ejector analyses suffer from a lack of understanding of turbulent flow. Current mathematical descriptions of turbulent flow yield non-linear, time-dependent equations; non-unique solutions are also an important consideration. Phenomenological descriptions prevail, however, and "calibrated" versions seem to simulate flows well. Several ejector studies blend empirical results, aero-thermodynamics, and control volume (or numerical) approaches quite successfully in the analysis of ejector performance (see for instance, Salter [1975], or Tavella and Roberts [1984]). Nonetheless, experimental work continues to improve understanding (again, an example is the work of Bernal and Sarohia [1983]). Some conclusions from experimental studies assist in the characterization of ejector behavior:

1. The level of thrust augmentation does not vary noticeably with primary pressure ratio (the rate at which the primary jet spreads is not a function of its initial velocity).

2. Thrust augmentation increases nearly linearly with diffuser area ratio, up to an area ratio in the vicinity of 1.5. Augmentation levels off and/or decreases as the area ratio is increased further - the duct wall half-angle seems to influence the particular trend.

3. Ejector performance is very sensitive to inlet losses and the thrust efficiency of the nozzle, although skin friction losses appear to be very small. The extent of mixing of the flow discharge (flow skewness) has a significant impact on ejector performance. See Belivaqua [1974].

4. Velocity profiles in the mixing region tend to be self-similar.

5. Additional thrust augmentation can be realized for installed ejectors with the use of end plates - these cause an otherwise three-dimensional flow to be two-dimensional (the end plates block flow into the separated region and create a drop in pressure at the ejector exit, improving performance).

Reflecting on the last remark, the present work does not focus extensively on some of the aerodynamic installation problems of ejectors described, for instance, by Knott and Cudy [1986] or Lund, Tavella, and Roberts [1986], though this is not to say that such effects are unimportant or can be overlooked in future ejector examinations. Rather, two- vs three- dimensional effects are significant and have considerable bearing on the interpretation of experimental data.

Of principle interest here is that secondary mass flow entrainment and the extent of mixing (of the two streams at the ejector discharge station) are closely related to thrust augmentation, and influenced by (1) ejector geometry, (2) primary jet characteristics, and (3) physical fluid properties.

Efficiency and Thrust Augmentation Ratio

Ejector performance is often quantified by computation of the thrust augmentation ratio, ϕ, and the ejector efficiency, η. As would be expected, an increase in thrust augmentation occurs at the cost of a decreased efficiency, so the "optimum" ejector balances the two (in accordance with the prescribed mission). In the definition of ϕ it is useful to use as a reference the isentropic thrust obtained from the expansion of the primary jet to the ambient

$$\phi = \frac{T_{SYSTEM}}{F_{PRIMARY,IDEAL}} \tag{2}$$

Note that when an isentropic reference thrust is used it is easier to compare the performance of ejectors with different nozzles.

Several equations to characterize "efficiency" have been used in the literature:

1. The nozzle efficiency is given as the ratio of the system thrust and the sum of the thrust for the primary and secondary streams under ideal conditions,

2. The ejector efficiency can be measured as the ratio of the kinetic energy of the ejector efflux to the input energy of the primary nozzle,

3. A ratio of the input momentum to the discharge momentum could be used (for the nozzle or ejector),

4. Base the ejector efficiency on the concept of thermodynamic availability (see Minardi [1982]),

5. Compute the ratio of the enthalpy change of the mixed ejector flow to the ideal change in enthalpy of the primary flow (again, see Minardi [1982] for details and several versions on this).

Item 2 is chosen for the present work and described in more detail in Section 4.

Characteristic Surfaces

Mass flow characteristics can be expressed in a general way as a function of stagnation pressure and back-pressure ratios as

$$\mu = \frac{\dot{m}_S}{\dot{m}_P} = f\left(\frac{P_{1S,0}}{P_{1P,0}}, \frac{P_{atm}}{P_{1P,0}}\right) \tag{3}$$

where it is assumed that ejector geometry and fluid properties are known. Similarly, the secondary stream inlet Mach number can be expressed as

$$M_{S1} = f\left(\frac{P_{S1}}{P_{1P,0}}, \frac{P_{atm}}{P_{1P,0}}\right) \tag{4}$$

where P_{1S} is the static pressure of the secondary flow at the point of confluence of the two streams.

A significant contibution to ejector analysis is the work of Addy, Dutton, Mikkelson and co-workers [1974, 1981, 1986] who provide a clear view of overall ejector characteristics through the presentation of three-dimensional surfaces; the ordinate and abscissa use the arguments of the general relations given above. An overview of the more detailed discussion by Addy, Dutton, and Mikkelsen [1981] follows.

Three regimes of flow can be described with three-dimensional surfaces that have the parameters of equations (2) and (3) as axes; these surfaces are shown in figure 4. An important feature of the surface is the "break-off" curve that divides the "supersonic" and "saturated-supersonic" regimes and the "mixed flow" regime. In the latter, ϕ is a function of the ambient pressure level while the former are not. Although it is assumed the primary nozzle flow is choked, the distinction of the breakoff curve is to mark the development of sonic conditions in the mixing region. Under certain conditions the secondary stream velocity can reach sonic conditions at the inlet, in which case the flow is choked and the mixing region described by a saturated-supersonic regime (see figure 4). Subsonic flows are depicted by the mixed regime.

Thrust augmenting ejectors entrain a second fluid at ambient conditions and discharge to the (same) ambient a mixed primary and secondary fluid. In this situation

$$\frac{P_{1S,0}}{P_{1P,0}} = \frac{P_{atm}}{P_{1P,0}} \tag{5}$$

so a subset of the three-dimensional surface of figure 4 which is of interest is the two-dimensional slice shown in figure 5. Because the three-dimensional surface has been drawn in a general way, no specific intent to exclude or include the saturated-supersonic region has been made in the description of figure 5. The secondary flow characteristic surface of figure 6 illustrates that sonic inlet conditions are associated with the saturated-supersonic regime.

Obviously the problem before us is to establish specific numbers for the axes of the characteristic curves (as functions of time). Recognize that those numbers which are presently available (and supported by experimental data) are generally for steady-state ejector operation and therefore provide little with which to remark on transient behavior.

Remarks on the Analytic Approach

In the interest of (eventually) realizing a real-time simulation capability, it is rational to begin the ejector analysis with the development of (1-D, integral) control-volume equations for a partitioned ejector; nomenclature for an arbitrary control volume is given in figure 7. This type of analysis forms a general mathematical structure within which methods for providing a transient capability and imitation of the turbulent interactions can be explored.

To be sure, there are much more capable frameworks of analysis, but they have only been explored for steady flows and example calculations indicate the approaches are extremely CPU intensive. Shen et. al.[1981] investigate the high secondary mass flow scenario using finite element analysis. Hedges and Hill [1974] discuss finite-difference solutions and review the integral boundary layer analyses of significance.

Considerable attention is paid in Appendix A and B to the development of the integral equations since (a) the nature of the time-dependent terms is important, (b) a proper account of a control volume moving in space is required, and (c) an open discussion of "intuitively obvious" quantities (presented without derivation) is without rigor. The development of these equations is predicated on a point of view appropriate for ejectors - "appropriate" is given here by those arguments often presented and weathered scrutiny in the literature. Some elements of that point of view are discussed below:

Constant Area Mixing Section

The ejector shown in figure 1 reflects the assumption that the mixing region has a constant cross-sectional area; this selection is intentional and made on a theoretical basis. An alternate configuration is the "constant-pressure" ejector in which it is assumed the area of the mixing region varies such that, in the one-dimensional case, the integrated static pressure is constant over the mixing region cross-section. For this configuration, however, determining the necessary mixing section area distribution and the high-probability of off-design operation are problems.

As it turns out for the traditional steady-state control volume analyses, the constant-area and constant-pressure formulations predict comparable performance (see Dutton et. al.[1982], Dutton and Carroll [1986]). In fact, the constant area formulation leads to a doubled value solution in which the mixed flow is either subsonic or supersonic; the solutions for the Mach number are related by the relation for the Mach number across a normal shock. Selection of a solution is based on compliance with the second law of thermodynamics.

Minardi [1982] provides a discussion of considerations for which the constant-area geometry is a necessary, but not sufficient, condition for the analysis. This leads to the conclusion that all possible solutions for the mixing region will be obtained with the constant-area case, even though certain solutions are not likely to occur for typical ejector configurations.

Adiabatic Ejector Walls

It is almost a universal assumption in theoretical ejector studies that the ejector walls are insulated; this allows the surface heat flux term in the energy equation to be dropped. As will be discussed in detail later, this is not immediately an assumption that the flow is isentropic. If we consider the arguments on the creation of entropy in Appendix B,

$$\frac{Ds}{Dt} - \nabla\cdot\left(\frac{\kappa\nabla\cdot T}{T}\right) = \frac{\psi}{\rho T} + \frac{\kappa}{\rho}\left(\frac{\nabla T}{T}\right)^2 \geq 0 \qquad (6)$$

then entropy changes exist as long as the fluid is subject to viscous dissipation. The combination of adiabatic ejector walls and inviscid flow provides:

$$\frac{Ds}{Dt} = 0 \qquad (7)$$

from which a convenient steady flow integral arises:

$$-\int_I s\,d\dot{m} = 0 \qquad (8)$$

This relation is most often employed in the analysis of the inlet and diffuser. Since Bernoulli's equation can now be used for the description of pressure across those regions an alternate use of the entropy balance is realized; generally speaking, the entropy balance becomes a condition on the simultaneous solution for the equations of mass, momentum, and energy (mechanical).

Inviscid Interaction Region

For ejector flow conditions where the static pressure of the secondary flow is less than that of the primary flow ($P_{S1} < P_{P1}$), the primary flow expands and interacts with the secondary flow to provide the interface boundary shown in figure 8. Note the formation of an "aerodynamic throat", that is, a minimum cross-sectional area downstream of the inlet associated with the boundary of the inviscid interaction of the two streams. If the secondary flow is subsonic upstream of this station, then the peak flow velocity at the constriction will be at or below sonic conditions. The "supersonic" operating regime is described when $M_{S2}=1$, and the "mixed" region given where $M_{S2}<1$. At very low secondary flow rates the secondary flow is effectively "sealed off" from the primary flow. A number of investigators (Anderson [1974a,b], Addy and co-workers [1974, 1981]) have taken advantage of these "partitioned" flows, as originally characterized by Fabri[1958]. Of interest here are the admission of the following assumptions for this "inviscid interaction" region:

1. The primary and secondary streams are distinct and do not mix between the point of confluence and station 2.

2. Viscous interactions occur along the interface of the two streams (mechanism of energy exchange between the primary and secondary flow).

3. Each stream is treated as irrotational.

4. Although the average pressure of the streams is (potentially) different at each streamwise station, the local static pressure is equal at the boundary.

In the work of Addy et. al. [1981] both streams are treated with an isentropic flow assumption (mixed and supersonic regimes). Anderson [1974a] allows that the secondary flow is isentropic, but determines the primary flow field from the method of characteristics (in his treatment of supersonic flow only). Quain et. al.[1984] relax the assumption that the secondary flow is isentropic, but the discussion of results from that work is not possible at this time (the paper is written in Chinese, abstract in English).

Implementation of an inviscid interation region may simplify the analysis of the mixing region, but this does not relax the requirement of an iterative solution methodology. Nonetheless, the use of this modelling approach offeres some analytic simplification and is worthwhile to pursue if the conditions which precipitate the approximation can be identified in advance.

The low-secondary-flow rate regime is only properly treated with a two-dimensional flow field analysis. As such, the euphoria surrounding a one-dimensional approach is mitigated by these types of flows and asks that the computational burden be assumed (for the correct analysis) or the degredation in solution accuracy announced.

Thermodynamic Considerations

Some elementary thermodynamic assumptions are often made in ejector analyses; identification of them here is appropriate:

1. The state principle of thermodynamics provides that, for a gas, a given thermodynamic variable can be described in terms of <u>two</u> thermodynamic properties.

2. Below a gas temperature of (approximately) 600^{o}K, air has essentially a constant specific heat, and therefore qualifies as a perfect gas; for generality, though, an ideal gas would be used.

3. For a perfect gas the entropy and enthalpy of the gas are expressible as a function of temperature only.

4. Application of Dalton's law of partial pressure to a constant volume mixing process yields the properties of the mixed flow at station 3 (see Appendix F).

Rarely does it come to pass the need to distinguish between an ideal and a perfect gas; both are described by the equation of state, but the specific heat of an perfect gas is constant, but in an ideal gas the specific heat is a function of temperature. This minor point can have significant impact on computational speed if temperature is unknown and the specific heat then extracted by an iterative method.

Summary

In the present simulation effort, an ejector with a constant area mixing region and adiabatic walls will be used to provide thrust augmentation through the mixing of two ideal gas streams. A phenomenological approach is taken to the turbulent interaction problem, consistent with the objective to formulate a system description amicable to real-time simulation.

4. CONTROL-VOLUME EQUATIONS FOR ONE-DIMENSIONAL FLOW

Overview

A control volume description of the ejector is perceived to be the most efficient method of analysis for the real-time simulation goal of the present work. This section outlines the application of the general control volume equations (developed in Appendix A) to the ejector shown in figures 1 and 10. Note the ejector is partitioned into an inlet, mixing, and diffuser region. Development of the mass, momentum, and energy equations for each component intends to provide three results: (a) a summary of the integral form of the equation, (b) a form useful for the transient ejector analysis, and (c) the version obtained if a piecewise-constant velocity is assumed at stations of inflow and efflux. Prior to those developments some remarks on the one-dimensional flow approximation are made below.

One-dimensional flow approximation

Compressible flow in channels is often treated in (practical) control volume analyses under the assumption that a quasi-one-dimensional flow exists; the basic simplification offered is that velocity gradients can occur along (not across) the streamwise axis of the channel (longitudinal axis). See figure 9.

A real-flow velocity profile is not (necessarily) symmetric and would reflect the presence of any viscous, blockage, and Reynolds number effects. In the absence of separation the real flow in the vicinity of the boundary must be parallel to the wall. In the present work these effects can only be accounted for as far as the continuity equation allows.

Analysis of "traditional" one-dimensional flow yields that the accuracy of this assumption depends on the axial gradient of the cross-sectional area. If dA/dx is small the assumption is well received (For the analysis of a stream-tube the "approximation" is exact). It is worth noting the comparison given by Thompson [1972] between nozzle data and the result for a one-dimensional flow analysis.

Particular attention should be paid to the generosity of the one-dimensional flow assumption for the expansion of the primary jet issuing from the nozzle. There is considerable breakdown in the approximation - and therefore in the accuracy of the analysis - when the secondary static pressure is significantly less than that of the primary jet. Recognize, of course, the extreme subsonic case (discussed previously) where the secondary flow is effectively "sealed-off" and the flow field must be treated as two-dimensional (recall figure 8).

Often it is assumed that the one-dimensional flow is also piecewise constant; this allows for multiple streams of constant one-dimensional velocity to be considered and provides for very convenient forms of the control volume equations.

Some accommodation of real-flow effects can be provided through a "skewness factor" which mitigates the asumption that the discharge velocity from a duct is completely mixed. As a practical matter, such an account is particularly useful for examination of ejector configurations where experimental data is available.

Skewness Factor

In order to include (partially, anyway) non-ideal mixing characteristics in the ejector analysis, there is often introduced a skewness factor for the flow at the exit of a mixing region and for the diffuser exit. It is assumed that knowledge of friction losses in the shroud and the value of the skewness factor are adequate for the characterization of the net effects of non-ideal mixing (even though local flow details cannot be extracted).

Consider the spatially averaged velocity given by

$$\langle v \rangle = \frac{1}{A}\int v\,dA \tag{1}$$

for the definition

$$\beta = \left(\int v^2\,dA\right) \Big/ \left(\langle v \rangle^2 A\right) \tag{2}$$

If v is uniform, the skewness factor is unity; in a non-uniform flow $\beta > 1$. To get a feeling for the magnitude of β, Bevilaqua [1974] notes that a typical ejector inlet region has a skewness factor on the order of 1.8, while the skewness factor at the exit of a (well-designed) mixing duct is approximately 1.02.

The skewness factor is constant for self-similar velocity profiles.

Salter [1975] discusses a theoretical approach to the prediction of the skewness factor, based on the turbulent jet theory of Abramovich [1963].

Continuity

For a control volume moving through space with velocity *U(t)* the continuity equation is

$$\frac{d}{dt}\int_V \rho\,dV + \oint_A \rho(\underline{u}-\underline{U})\cdot\underline{n}\,dA = 0 \tag{3}$$

Define at any instant in time the mass contained in the control volume by

$$m_{cv} = \int_V \rho\,dV \tag{4}$$

and introduce the relative velocity

$$\underline{v} = \underline{u}-\underline{U} = v\underline{i} \tag{5}$$

where the unit normal is defined as positive outward from the surface of the control volume. Also, define the mass flowrate past station k as

$$\dot{m} = -\int \rho_{A_k} (\underline{v} \cdot \underline{n}) dA \tag{6}$$

Emphasis is placed on (a) the use of the relative velocity, and (b) the presence of the negative sign. The impact of the latter is that an inflow is described by a *positive* mass flow; since

$$(\underline{v} \cdot \underline{n})_k = v_k(-\underline{i} \cdot \underline{i}) = -v_k \tag{7}$$

then for an inflow

$$\dot{m}_k = \int \rho \underline{v}_k dA \tag{8}$$

and for an outflow

$$(\underline{v} \cdot \underline{n})_{k+1} = v_{k+1}(\underline{i} \cdot \underline{i}) = v_{k+1} \tag{9}$$

$$\dot{m}_{k+1} = -\int_{A_k} \rho v_k dA \tag{10}$$

Returning to the continuity equation, substitution yields

$$\frac{d}{dt}\{m_{cv}\} = \sum_k \dot{m}_k \tag{11}$$

This has the intuitively desireable result that when the inflow exceeds the outflow, the accumulation of mass is a positive quantity. Although superficially this may appear a trivial result, reflect on a formulation involving u instead of v in the definition of the mass flowrate; the impact on the latter is significant.

Introduction of the skewness factor requires the assumption of a constant density over the cross-section,

$$\dot{m} = \int_{A_k} \rho v_k dA = \bar{\rho} \int_{A_k} v_k dA = \rho_k < v > A \tag{12}$$

Integrals dissapear on the right hand side of the continuity equation if the density is considered piecewise constant; the mass flux accross station k is

$$\dot{m}_k = (\rho v A)_k \tag{13}$$

and therefore

$$\frac{dm_{cv}}{dt} = (\rho v A)_k - (\rho v A)_{k+1} \tag{14}$$

Momentum

Application of the integral momentum equation to an ejector with adiabatic walls and where gravitational effects are neglected provides

$$\frac{d}{dt}\int_V \rho \underline{u} dV = -\oint_A \rho \underline{u}(\underline{u} - \underline{U}) \cdot \underline{n} dA + \oint_A \underline{n} \cdot \underline{S}' dA - \oint_A n \cdot (p I') dA \tag{15}$$

Introduce the relative velocity, then

$$\frac{d}{dt}\int_V \rho(\underline{v} + \underline{U}) dV = -\oint_A \rho(\underline{v} + \underline{U}) \underline{v} \cdot \underline{n} dA - \oint_A \underline{n} \cdot (p \underline{I}') dA + \oint_A \underline{n} \cdot \underline{S}' dA \tag{16}$$

Define the net force acting on interior surfaces (thrust) to be characterized by the sum of the surface integral of the deviatoric stress tensor and the interior pressure forces

$$\underline{F} = \oint_\Gamma \underline{n} \cdot \underline{S}' dA - \oint_\Gamma \underline{n} \cdot (p \underline{I}) dA \tag{17}$$

It is important to note that no shear stresses are assumed to be acting over the inlet or outlet regions. Also note that the area Γ represents the (fixed) interior surfaces of the ejector unit - those are the areas responsible for the exchange of forces (between the fluid and ejector surfaces) to provide the system thrust.

Expand the time derivative in the momentum equation

$$\frac{d}{dt}\int_V \rho(\underline{v} + \underline{U}) dV = \frac{d}{dt}\int_V \rho \underline{v} dV + \frac{d}{dt}\int_V \rho \underline{U} dV \tag{18}$$

and recognize

$$\frac{d}{dt}\int_V \rho \underline{U}\, dV = \frac{d}{dt}(\underline{U} m_{cv}) \tag{19}$$

Recalling that the reference velocity U is constant over the surface (but remains *time dependent*), then

$$\frac{d}{dt}(\underline{U} m_{cv}) = \underline{U}\frac{dm_{cv}}{dt} + m_{cv}\frac{d\underline{U}}{dt} \tag{20}$$

Also

$$-\oint_A \rho(\underline{v}+\underline{U})\underline{v}\cdot n\, dA = -\oint_A \rho \underline{v}(\underline{v}\cdot\underline{n})dA - \underline{U}\oint_A \rho v\cdot \underline{n}\, dA$$

$$= -\oint_A \rho \underline{v}(\underline{v}\cdot\underline{n})dA + \underline{U}\frac{dm_{cv}}{dt} \tag{21}$$

The momentum equation becomes

$$\frac{d}{dt}\int_V \rho \underline{v}\, dV + m_{cv}\frac{d\underline{U}}{dt} = -\oint_A \rho \underline{v}(\underline{v}\cdot n)dA - \oint_A \underline{n}\cdot(pI)dA + F \tag{22}$$

where A implies those surfaces at the inlet and outlet of the control volume, not the internal surfaces used in the definition of F.

Important Note: The volume integral represents the time rate-of-change of the momentum of all particles inside the control volume at an instant in time. It cannot be converted into a surface integral and requires some estimate of field conditions in the ejector mixing region.

Some simplification of the momentum equation results from a piecewise constant velocity, density, and pressure assumption. In this case

$$-\oint_A \rho \underline{v}(\underline{v}\cdot\underline{n})dA = \sum_k \underline{v}_k \dot{m}_k \tag{23}$$

$$-\oint_A \underline{n}\cdot(pI)dA = -\sum_k P_k \underline{n}_k A_k \tag{24}$$

and therefore

$$\frac{d}{dt}\int_V \rho \underline{v}\, dV + m_{cv}\frac{d\underline{U}}{dt} = \sum_k \underline{v}_k \dot{m}_k - \sum_k P_k n_k A_k + F \tag{25}$$

An alternate modification involves the skewness factor. For a uniform cross-sectional area,

$$\int \rho v^2 dA = \rho \beta < v >^2 A$$

$$= \beta \dot{m} < v > \qquad (26)$$

then substitution in the appropriate locations in the momentum analysis above provides the desired result.

Energy

Ejector analyses typically assume all surfaces are adiabatic, but (as mentioned earlier) this is not immediately an implication that any of the transport processes are isentropic. With this in mind the control volume formulation of the energy equation is:

$$\frac{d}{dt}\int_V (\rho H - P) dV = \oint_A p \underline{U} \cdot \underline{n} dA - \oint_A \rho H (\underline{u} - \underline{U}) \cdot \underline{n} dA \qquad (27)$$

Note the *absolute velocity* participates in the definition of the stagnation enthalpy

$$H = h + \frac{u^2}{2} \qquad (28)$$

From this the ideal gas assumption yields

$$\rho H = \rho c_p T_0 \qquad (29)$$

then

$$\frac{d}{dt}\int_V (\rho c_p T_0 - P) dV = \oint p \underline{U} \cdot \underline{n} dA - \oint_A \rho c_p T_0 \underline{v} \cdot \underline{n} dA \qquad (30)$$

which is the desired integral form.

As before, a piecewise constant velocity, density, and temperature simplifies the equation

$$\frac{d}{dt}\int_V (\rho c_p T_0 - P) dV = U \sum_k P_k A_k (\underline{i}_U \cdot \underline{n}_k) + \sum_k H_k \dot{m}_k (\underline{i}_v \cdot \underline{n}_k) \qquad (31)$$

but does not eliminate the volume integral on the RHS.

Entropy

In integral form the entropy equation acts as a condition on the solution of the mass, momentum, and enegy equations; from Appendix A,

$$\frac{d}{dt}\int_V \rho s dV + \oint_A \rho s \underline{v}\cdot\underline{n} dA + \oint_A \frac{1}{T}\underline{q}\cdot\underline{n} dA \geq 0 \qquad (32)$$

Acknowledging that the last term vanishes by virtue of the adiabatic ejector assumption, a non-zero entropy balance arises from viscous dissipation.

If the mass flowrate is introduced

$$\frac{d}{dt}\int_V \rho s dV - \oint_A s d\dot{m} \geq 0 \qquad (33)$$

then the uniform one-dimensional flow assumption yields

$$\frac{d}{dt}\int_V \rho s dV - \sum_k s\dot{m}(i_v\cdot\underline{n}) \geq 0 \qquad (34)$$

Summary of Basic Equations

Four basic control volume equations form the foundation of the analysis of the transient ejector:

Mass

$$\frac{d}{dt}\{m_{cv}\} = \sum_k \dot{m}_k$$

Momentum

$$\frac{d}{dt}\int \rho_V \underline{v} dV + m_{cv}\frac{d\underline{U}}{dt} = -\oint_A \rho \underline{v}(\underline{v}\cdot\underline{n})dA - \oint_A \underline{n}\cdot(p\underline{I})dA + \underline{F}$$

Energy

$$\frac{d}{dt}\int_V (\rho c_p T_0 - P)dV = \oint \rho U\cdot n dA - \oint_A \rho c_p T_0 v\cdot n dA$$

Entropy

$$\frac{d}{dt}\int_V \rho s\, dV \;-\; \oint_A s\, d\dot{m} \;\geq\; 0$$

For the momentum, energy, and entropy equations, the simplified one-dimensional relations are:

$$\frac{d}{dt}\int_V \rho \underline{v}\, dV \;+\; m_{cv}\frac{d\underline{U}}{dt} \;=\; \sum_k \underline{v}_k(\underline{i}_v \cdot \underline{n}_k)\dot{m}_k \;-\; \sum_k P_k \underline{n}_k A_k \;+\; \underline{F}$$

$$\frac{d}{dt}\int_V (\rho c_p T_0 - P)\, dV \;=\; U\sum_k P_k A_k(\underline{i}_U \cdot \underline{n}_k) \;+\; \sum_k H_k \dot{m}_k(\underline{i}_v \cdot \underline{n}_k)$$

$$\frac{d}{dt}\int_V \rho s\, dV \;-\; \sum_k s\dot{m}(\underline{i}_v \cdot \underline{n}) \;\geq\; 0$$

An important goal in transient ejector analysis is finding an accurate approximation to the time dependent volume integrals on the left hand side of each equation.

Remarks on Supplementary Equations

Overview

Application of the general, one-dimensional flow, control-volume equations to the ejector of figure 10 is intended to provide a framework for ejector performance prediction in terms of the primary nozzle flow, initial conditions from which the secondary fluid is drawn, and ambient conditions. In application to the mixing region, the assumptions involved are critical since it is within this region that the most complex physical phenomena occur.

In anticipation of the section 6 discussion on methods of solution for the complete (time dependent) one-dimensional ejector equations developed above, the simplification of steady-flow is explored in section 5. That excursion is of value in situations where a quasi-steady flow can be assummed to exist. That discussion also addresses some concepts to closure common to the unsteady flow problem formulation. This allows section 6 to focus on the difficult issue of evaluating the time-dependent volume integral terms. A summary of the solution options that exist and the reccommended approach in the provision of a complete system of equations is then made.

The control volumes used in the applications to follow are illustrated in figures 1 and 10. Since it is assumed (for this phase of the work) that the primary nozzle flow characteristics are known, no control volume is drawn for it. An important assumption is that the nozzle and the shroud are adiabatic - as discussed earlier this is not (immediately) an assumption that the flow is isentropic; the latter is allowable only if viscous dissipation is absent from the flow (as you would have, for instance, in an ideal, irrotational flow).

To set the stage for application of the control volume equations to the ejector, some remarks on the character of some unknowns and the working medium follow:

1. The state principle allows that local thermodynamic states are expressible in terms of two thermodynamic variables; in the present work the static pressure and temperature have been chosen.

2. The assumption of an ideal gas provides the entropy and enthalpy are functions of temperature only. Density is given as a function of T and P through the ideal gas law.

3. The local mass flowrate is defined in the one-dimensional case as a function of velocity, temperature, and static pressure.

4. It is assumed that the force on the shroud can be constructed as the sum of empirical relations for duct flows, including such effects as losses due to expansion or contraction of cross-sections. The empirical constants will reduce the unknowns in the function for F to velocity, temperature, and static pressure. Geometric characteristics are assumed known.

5. In general, entropy is employed in arguments related to the admissability of solutions, not in the direct solution for specific velocity, temperature, and static pressures.

6. Velocities at the inlet duct and primary nozzle discharge are uniform and one-dimensional, but distributions internal to the mixing region are expressable in some "appropriate" self-similar form.

7. The default unknown velocity is the relative velocity, v, since the absolute velocity, u, and the frame of reference velocity, U, are related by $v = u - U$. For the present work it is assumed that U is known. Actually U is generally not, but if the ejector GDE's are coupled with those for the aircraft then U can, in principle, be determined (in general, as a function of time).

8. Possible existance of shock waves is recognized, but an account here would require they are normal and stationary with respect to the shroud (diffuser, inlet, and mixing region) frame-of-reference. In the present work subsonic flight is assumed for the operational envelope the ejector participates in.

We suspect in the primary flight mode the ejector is involved in will not be supersonic flight.

Supplemental Equations

The framework of analysis is constructed through application of the control-volume equations to the inlet region, mixing region, and diffuser. The assumptions of the previous section introduce the following supplemental equations:

$$\dot{\underline{m}} = \rho \underline{v} \cdot \underline{n} \Gamma$$

$$\rho = P/RT$$

$$\underline{v} = \underline{u} - \underline{U}$$

$$\underline{F} = \underline{F}(P, T, \underline{v})$$

$$h = h(T)$$

$$s = s(T)$$

The principle unknows at this point are the following (field) variables: velocity, *v(x,t)*; static pressure, *P(x,t)*; temperature, *T(x,t)*. The steady-state solution for these unknowns is discussed in the next section; Section 6 describes the approach for the transient situation.

5. STEADY FLOW ANALYSIS

Overview

Although it is the intent of the present work to focus on unsteady ejector flows, the steady-flow solution methodology is of interest for several reasons:

- The steady-state solution is the starting solution for the unsteady analysis,
- Many of the subroutines generated for the steady-state version of the program are common to the transient program; a successful steady-state solution is a useful check on those routines,
- The steady-state ejector performance program can be a useful theoretical tool for interpreting data from the NASA Lewis PLF.

Presentation of typical steady-state ejector performance equations highlights the mathematical benefits of disposing of time-dependent terms in the ejector analysis and, by default, provides the system of equations one would use in a quasi-steady flow analysis. For instance, the section 6 assumption of a quasi-steady inlet and diffuser flow means the steady-state inlet and diffuser equations discussed below are applicable. Additionally, many details associated with the execution of the general ejector "problem" (and coincident with an unsteady flow analysis) are easily illustrated with a description of the solution of the steady flow equations. The present work draws partially upon the discussions of Belivaqua [1974], Salter [1975], and Alperin and Wu [1983a,b].

System of Equations

In a steady-state ejector flow scenario, time-dependent control volume terms would not be involved in the system of equations. Recalling the general system and auxiliary equations presented in section 4, it is important to note the steady flow assumption leaves three governing equations and (only) nine unknowns for the description of the mixing region. Although there is some variation in specific analyses, closure to this problem is usually obtained by prescribing one or more of the following:

1. confluence static pressure ratio at the inlet,
2. primary and secondary inlet velocities,
3. static pressure at exit,
4. stagnation temperatures at the inlet.

Often, if there is not a direct prescription of, for instance, the stagnation conditions at the inlet, an isentropic flow is assumed between the (assumed known) free-stream conditions and the inlet cross-section, thereby facilitating calculations of the inlet temperature and pressure.

For the present steady-flow analysis, the three conditions for closure are obtained by prescribing (a) primary flow inlet conditions, (b) static pressure at the diffuser exit, and (c) an isentropic inlet and diffuser. A detailed discussion of the system of equations follows.

Mixing Region

Considerable simplification of the system of equations is realized by invoking the steady-state assumption; the system is given by:

Mass:

$$0 = \dot{m}_{1P} + \dot{m}_{1S} - \dot{m}_3 \qquad (1)$$

Momentum:

$$0 = v_{1P}\dot{m}_{1P} + v_{1S}\dot{m}_{1S} - \beta < v_3 > \dot{m}_3 + \left(P_{1P} - P_3\right)A_3 + \underline{F} \qquad (2)$$

Energy:

$$0 = \dot{m}_{1P}H_{0,1P} + \dot{m}_{1S}H_{0,1S} - \dot{m}_3 H_{0,3} \qquad (3)$$

The entropy equation remains a condition on the solution, as discussed earlier (also, see Appendix B). Some assumptions often applied to the system are:

1. All skin friction and blockage losses are neglected.
2. The primary flow is fully expanded at the point of confluence of the two jets (equal static pressure at the inlet region, station 1).
3. Specific heat of each gas stream is assumed equal.
4. The ejector is stationary in space (test stand set-up).
5. Gases are assumed thermodynamically perfect (constant specific heat) and described by the equation of state.

Only assumptions 1, 3, and 5 are used in the present work.

Non-dimensionalization of the system of equations above clarifies the participation of each equation in the solution; related manipulations are outlined below.

i. Continuity

A useful non-dimensional form of the mass flowrate equation is (see Appendix G.6)

$$\frac{\dot{m}}{PA}(RT)^{1/2} = M\left\{\gamma\left(1+\frac{\gamma-1}{2}M^2\right)\right\}^{1/2}$$

$$= f_6(\gamma, M) \tag{4}$$

where it is understood that the specific heat ratio is known or can be computed from Dalton's law (Appendix F). From conservation of mass

$$\dot{m}_P + \dot{m}_S - \dot{m}_3 = 0 \tag{5}$$

in non-dimensional form

$$\frac{\dot{m}_3}{P_P A_P} = \frac{\dot{m}_P}{P_P A_P} + \frac{\dot{m}_S}{P_P A_P} = \frac{\dot{m}_P}{P_t A_P}(1+\mu)$$

$$= \left(R_P T_{0,P}\right)^{-1/2} f_6\left(\gamma_P, M_P\right)(1+\mu)$$

If the mass flowrate equation for station 3 is normalized by the primary flow conditions

$$\frac{\dot{m}_3}{P_P A_P} = \frac{P_3 A_3 f_6(\gamma_3, M_3)}{P_P A_P \sqrt{R_3 T_{0,3}}} \tag{7}$$

then by comparison with the result derived above

$$\frac{P_3}{P_P} = \frac{A_P}{A_3}\sqrt{\frac{R_3 T_{0,3}}{R_P T_{0,P}}}\frac{f_6(\gamma_P, M_P)}{f_6(\gamma_3, M_3)}\{1+\mu\} \tag{8}$$

the entrainment ratio itself can be expressed as a function of f_6 in a similar form:

$$\mu = \frac{\dot{m}_s}{\dot{m}_p} = \frac{P_S A_S}{P_P A_P}\sqrt{\frac{R_P T_{0,P} f_6(\gamma_S, M_S)}{R_S T_{0,S} f_6(\gamma_P, M_P)}} \tag{9}$$

so that the static pressure ratio is given by

$$\frac{P_P}{P_S} = \frac{A_S}{A_P}\sqrt{\frac{R_P T_{0,P} f_6(\gamma_S, M_S)}{R_S T_{0,S} f_6(\gamma_P, M_P)}}\frac{1}{\mu} \tag{10}$$

In general, the stagnation pressures are assumed to be related isentropically to the static pressures at the same station by the function

$$P_0 = \left\{1 + \frac{(\gamma - 1)}{2} M^2\right\}^{\gamma/\gamma-1} P = f_3(\gamma, M) P \tag{11}$$

then the stagnation pressure ratio is

$$\frac{P_{0,S}}{P_{0,P}} = \frac{P_S f_3(\gamma_S, M_S)}{P_P f_3(\gamma_P, M_P)} \tag{12}$$

ii. Momentum Equation

In non-dimensional form, the momentum equation is given by

$$1 + \frac{P_S A_S}{P_P A_P} - \frac{P_3 A_3}{P_P A_P} + \frac{\rho_P v_P^2}{P_P} + \frac{\rho_P v_S^2}{P_P} - \beta \frac{\rho_3 < v_3 >^2}{P_P} = 0 \tag{13}$$

The velocity terms can be written

$$\frac{\rho v^2}{P} = \frac{v^2}{RT} = M^2 \gamma \tag{14}$$

so that the momentum equation can be written

$$\left\{1 + \gamma_P M_P^2\right\} + \frac{P_S A_S}{P_P A_P}\left\{1 + \gamma_S M_S^2\right\} - \frac{P_3 A_3}{P_P A_P}\left\{1 + \beta \gamma_3 M_3^2\right\} = 0$$

Re-arrange the previous result for the static pressure ratio

$$\frac{P_S A_S}{P_P A_P} = \sqrt{\frac{R_S T_{S,0}}{R_P T_{P,0}} \frac{f_6(\gamma_P, M_P)}{f_6(\gamma_S, M_S)}} \mu \tag{16}$$

so the momentum equation is

$$0 = \left(1 + \gamma_P M_P^2\right) + \mu \left\{\frac{R_S T_{S,0}}{R_P T_{P,0}}\right\}^{1/2} \frac{f_6(\gamma_P, M_P)}{f_6(\gamma_S, M_S)} \mu \left(1 + \gamma_S M_S^2\right)$$

$$- (1 + \mu) \left\{\frac{R_3 T_{3,0}}{R_P T_{P,0}}\right\}^{1/2} \frac{f_6(\gamma_P, M_P)}{f_6(\gamma_3, M_3)} \left(1 + \beta \gamma_3 M_3^2\right) \tag{17}$$

then

$$0 = f_7(\gamma_P, M_P) + \mu\left\{\frac{R_S T_{S,0}}{R_P T_{P,0}}\right\}^{1/2} f_7(\gamma_S, M_S) - (1+\mu)\left\{\frac{R_3 T_{3,0}}{R_P T_{P,0}}\right\}^{1/2} f_7(\gamma_3, M_3) \quad (18)$$

where

$$f_7(\gamma, M) = \left(1+\beta\gamma M^2\right)/f_6(\gamma, M) \quad (19)$$

The solution for M_3 is now given in the form

$$f_7(\gamma_3, M_3) = \left\{\frac{R_3 T_{3,0}}{R_P T_{P,0}}\right\}^{-1/2} (1+\mu)^{-1}\{f_7(\gamma_P, M_P) + \mu\left\{\frac{R_S T_{S,0}}{R_P T_{P,0}}\right\}^{1/2} f_7(\gamma_S, M_S)\} \quad (20)$$

For given primary and secondary conditions the right-hand-side is a constant

$$f_7(\gamma_3, M_3) = K_1 \quad (21)$$

An expression for M_3 is derived by re-introducing the definition of the function f_7

$$1 + \beta\gamma M^2 = K_1 M\left(\gamma\left\{1+\frac{\gamma-1}{2}M^2\right\}\right)^{1/2} \quad (22)$$

since

$$\left(1+\beta\gamma M^2\right)^2 = 1 + 2\beta\gamma M^2 + \beta^2\gamma^2 M^4 \quad (23)$$

then

$$1 + 2\beta\gamma M^2 + \beta^2\gamma^2 M^4 = K_1^2 M^2 \gamma + K_1^2 M^4 \gamma\left(\frac{\gamma-1}{2}\right) \quad (24)$$

This is re-arranged to yield

$$1+\left(2\beta\gamma-K_1^2\gamma\right)M^2+\left(\beta^2\gamma^2-K_1^2\gamma\left(\frac{\gamma-1}{2}\right)\right)M^4 \;=\; 0 \qquad (25)$$

so

$$A \;=\; \beta^2\gamma^2-K_1^2\gamma\left(\frac{\gamma-1}{2}\right) \qquad (26)$$

$$B \;=\; 2\beta\gamma-K_1^2\gamma \qquad (27)$$

$$C \;=\; 1 \qquad (28)$$

The solution for M_3 is therefore obtained from the solution to the quadratic equation

$$A\left(M_3^2\right)^2 \;+\; BM_3^2 \;+\; C \;=\; 0 \qquad (29)$$

which is given by

$$M_3^2 \;=\; \frac{-B\pm\sqrt{B^2-4AC}}{2A} \qquad (30)$$

The root is expressed in functional form as

$$M_3 \;=\; f_{17}\left(\beta,\gamma_3,K_1\right) \qquad (31)$$

iii. Energy Equation

Introduction of the entrainment ratio in the energy equation yields:

$$\hat{c}_3T_{3,0} \;=\; \frac{\dot{m}_P}{\dot{m}_3}\hat{c}_PT_{P,0}+\frac{\dot{m}_S}{\dot{m}_3}\hat{c}_ST_{S,0} \qquad (32)$$

where $\hat{c}$ is the specific heat at constant pressure. Rearranging,

$$T_{3,0} \;=\; \frac{\dot{m}_P}{\dot{m}_P+\dot{m}_S}\left\{\frac{\hat{c}_P}{\hat{c}_3}T_{P,0}+\mu\frac{\hat{c}_S}{\hat{c}_3}T_{S,0}\right\} \qquad (33)$$

and therefore

$$T_{3,0} = \frac{1}{(1+\mu)\hat{c}_3}\frac{\hat{c}_P}{}\left\{T_{P,0} + \mu\frac{\hat{c}_S}{\hat{c}_P}T_{S,0}\right\} \quad (34)$$

Expressed as a ratio:

$$\frac{T_{3,0}}{T_{P,0}} = \frac{1}{1+\mu\hat{c}_3}\frac{\hat{c}_P}{}\left\{1 + \mu\frac{\hat{c}_S}{\hat{c}_P}\frac{T_{S,0}}{T_{P,0}}\right\} \quad (35)$$

iv. Inclusion of Frictional Effects

Salter [1975] provides corrections for friction effects through an equivalent pressure loss:

$$\Delta P_f = \left(fL\rho v^2\right) \; / \; \left(2D_h\right) \quad (36)$$

where f is the friction factor and D_h is the hydraulic diameter. Also, a momentum correction factor, K_m, is applied to the mixing region exit to account for incomplete mixing of the primary and secondary streams; use of the momentum correction factor means the momentum equation is to be written explicitly in v (rather than in terms of the mass flow rate), the result:

$$\begin{aligned} 0 = {} & \rho A_{1P} v_{1P}^2 + \rho A_{1S} v_{1S}^2 - K_m \rho A_3 v_3^2 \\ & + \left(P_{1S} - P_3\right) A_3 - \Delta P_f A_3 \end{aligned} \quad (37)$$

Bevilaqua [1974] and Kentfield [1978] take a slightly different tack and invoke an incompressible flow assumption to simplify their analysis (they also remark on the error introduced in this approximation).

v. Mixing Region Equation Summary

Solutions for the pressure, velocity, and temperature at station 3 are obtained by analysis of the mixing region; since conditions at the primary station are given, the field variables at station 3 are functions of the unknown conditions at station 1S.

Manipulation of the equation of continuity in conjunction with the equation of state yields the ratio of pressure at the mixing region exit and at the primary nozzle discharge:

$$\frac{P_3}{P_P} = \frac{A_P}{A_3}\sqrt{\frac{R_3 T_{0,3}}{R_P T_{0,P}}}\frac{f_6\left(\gamma_P, M_P\right)}{f_6\left(\gamma_3, M_3\right)}\left\{1+\mu\right\}$$

this is implicitly a function of conditions at station 1S, via the entrainment ratio,

$$\mu = \frac{\dot{m}_s}{\dot{m}_p} = \frac{P_S A_S}{P_P A_P}\sqrt{\frac{R_P T_{0,P}}{R_S T_{0,S}}}\frac{f_6(\gamma_S, M_S)}{f_6(\gamma_P, M_P)}$$

From the momentum equation, the Mach number at station 3 was derived in terms of the Mach number at the primary and secondary flow conditions at station 1,

$$M_3 = f_{17}(\beta, \gamma_3, K_3)$$

Through the energy equation the relation between the stagnation temperature at station 3 and the stagnation temperature at the primary and secondary stations was found to be:

$$\frac{T_{3,0}}{T_{P,0}} = \frac{1}{(1+\mu)}\frac{\hat{c}_P}{\hat{c}_3}\left\{1 + \mu\frac{\hat{c}_S}{\hat{c}_P}\frac{T_{S,0}}{T_{P,0}}\right\}$$

In summary, the prediction of P_3, v_3, and T_3 is a function of P_S, M_S, T_{S0}, and the pressure matching condition at the diffuser exit (more discussion on this point later). Analysis of the inlet region will exchange the unknown pressure, temperature, and velocity at station 1 for those at infinity.

Recall that, for this particular predictive situation, the secondary inlet conditions are not known in advance since the secondary flow conditions are a consequence of conditions in the mixing region, not a cause for the same. No real reduction in the number of unknows is gained from the addition of these relations but is a necessary development for the complete system of equations. Relations for the diffuser are similar to those for the inlet and provide closure for the final system of equations.

Here, it is of benefit to realize that for the thrust augmenting ejector the static pressure at station 4 should, in general, be equal to that of the ambient.

The system of equations for the inlet and diffuser are discussed next.

Inlet

The inlet is given as the region between infinity and station 1S; application of the principles of mass, momentum, and energy to that region are described below. As a first approximation isentropic conditions are assumed to prevail.

i. Mass

For a single-stream flow, the mass flowrate is unity,

$$\frac{\dot{m}_S}{\dot{m}_P} = 1 \qquad (38)$$

so that

$$\rho_S v_S A_S = \rho_\infty v_\infty A_\infty \tag{39}$$

or (see Figure 1)

$$\rho_S v_S A_S = \rho_0 v_0 A_0 \tag{40}$$

since the characteristic area at infinity is undefined.

ii. Momentum

A balance of momentum for an ideal nozzle flow provides

$$P_S A_S + \dot{m}_S v_S = P_\infty A_\infty + \dot{m}_\infty v_\infty \tag{41}$$

then

$$\frac{P_S}{P_\infty}\left\{1 + \frac{\dot{m}_S v_S}{P_S A_S}\right\} = \frac{A_\infty}{A_S}\left\{1 + \frac{\dot{m}_\infty v_\infty}{P_\infty A_\infty}\right\} \tag{42}$$

$$\frac{P_S A_S}{P_\infty A_\infty} = \left\{\frac{1 + \gamma_\infty M_\infty^2}{1 + \gamma_S M_S^2}\right\} \tag{43}$$

An alternate expression for this ratio is given in terms of the mass flow function, $f6$

$$\frac{P_S A_S}{P_\infty A_\infty} = \left\{\frac{R_S T_{0,S}}{R_\infty T_{0,\infty}}\right\}^{1/2} \frac{f_6(\gamma_\infty, M_\infty)}{f_6(\gamma_S, M_S)} \tag{44}$$

but for an isentropic flow it can be shown the two ratios are not independent.

iii. Energy

Conservation of energy provides the simple statement that the stagnation temperatures in the free-stream and at station 1S are equal

$$T_{0,\infty} = T_{0,S} \tag{45}$$

this result relies on the adiabatic inlet assumption. If local properties are related to local stagnation conditions isentropically, then

$$T_0 = T\left(1 + \frac{\gamma + 1}{2} M^2\right) \tag{46}$$

from which

$$\frac{T_S}{T_\infty} = \frac{T_{0,S}}{T_{0,\infty}} \left\{ \frac{1 + \frac{\gamma_\infty - 1}{2} M_\infty^2}{1 + \frac{\gamma_S - 1}{2} M_S^2} \right\}$$

$$= \frac{f_2(\gamma_\infty, M_\infty)}{f_2(\gamma_S, M_S)} \tag{47}$$

The assumption of isentropic flow simplifies the integrated form of Gibbs' relation to

$$\frac{\gamma}{\gamma - 1} \ln\left(\frac{T}{T_0}\right) - \ln\left(\frac{P}{P_0}\right) = 0 \tag{48}$$

and therefore

$$\frac{P_S}{P_\infty} = \frac{P_{S,0}}{P_{\infty,0}} \left\{ \frac{T_S^*}{T_\infty^*} \right\} \tag{49}$$

where

$$T^* = T^{\gamma/\gamma - 1} \tag{50}$$

Since the ideal gas law provides that

$$\frac{P_S}{P_\infty} = \frac{T_S^*}{T_\infty^*} \tag{51}$$

it is evident the stagnation pressures must be equal for an isentropic flow

$$P_{S,0} = P_{\infty,0} \tag{52}$$

and so the static pressure ratio is

$$\frac{P_S}{P_\infty} = \frac{f_3(\gamma_\infty, M_\infty)}{f_3(\gamma_S, M_S)} \tag{53}$$

This is a slightly more convenient expression than that derived from the momentum equation since the area ratio is not required in the present result (but an isentropic flow assumption is).

iv. Remarks

In the general case of analysis the free-stream velocity, static pressure, and static temperature are known so the stagnation temperature and pressure can therefore be computed. If isentropic flow conditions are assumed to exist (adiabatic ejector, frictionless flow) then the stagnation temperature and pressure at station 1S are equal to those in the free-stream. When the velocity at station 1S has been determined, the static temperature and pressure can be computed.

For situations where the isentropic flow assumption is not valid, we return to the momentum equation and account for frictional effects. As a first approximation of the "answer", an incompressible flow is assumed to exist. Recognize that in such a case, the differential formulation of momentum is preferred since Bernoullis' equation can be extracted. This provides an equation applicable to any inlet streamline. The analysis of Salter[1975] introduces a correction factor for real-flow effects with the use of an inlet loss coefficient, K_1, and the loss due to the impedance of the nozzles to the free-stream flow, C_D,

$$P_{1S} = P_\infty - \frac{1}{2}\rho\left(v_{1S}^2 - v_\infty^2\right) - \frac{1}{2}\rho v_0^2\left(K_1 + C_D\frac{A_{nozzle}}{A_0}\right) \tag{54}$$

Given the free-stream velocity, conservation of mass is used to find the first approximation to the secondary inlet velocity,

$$v_{1S} \sim \frac{A_\infty}{A_{1S}} v_\infty \tag{55}$$

and therefore

$$P_{1S} = p_\infty - \frac{\rho}{2} v_\infty^2\left(\left(\frac{A_\infty}{A_{1S}}\right)^2 - 1\right) \tag{56}$$

Diffuser

Pressure recovery in the diffuser is a function of the area ratio, and becomes an important parameter in ejector design. For the thrust augmenting ejector the exit static pressure is (generally) intended to be that of the ambient, but real flow effects may dictate otherwise. Nonetheless, in principle the overall (isolated) ejector pressure ratio is unity.

Equations governing the conservation of mass, momentum, and energy in the diffuser are similar to those for the inlet, but a brief discussion is presented below to highlight the pressure matching condition at the diffuser discharge.

i. Mass

For a single-stream flow, the mass flow rate is unity,

$$\frac{\dot{m}_3}{\dot{m}_4} = 1 \tag{57}$$

ii. Momentum

In the absence of frictional effects, the adiabatic diffuser is characterised by

$$\frac{P_4 A_4}{P_3 A_3} = \left\{ \frac{1 + \gamma_3 M_3^2}{1 + \gamma_4 M_4^2} \right\} \tag{58}$$

In this result the Mach number is modified by the mixing effectiveness parameter when an account of non-uniform mixing is desired.

iii. Energy

As before, the adiabatic diffuser assumption allows that

$$\frac{T_4}{T_3} = \frac{f_2(\gamma_3, M_3)}{f_2(\gamma_4, M_4)} \tag{59}$$

from which the additional assumption of isentropic flow permits

$$\frac{P_4}{P_3} = \frac{f_3(\gamma_3, M_3)}{f_3(\gamma_4, M_4)} \tag{60}$$

and since

$$P_{0,4} = P_{0,3} \tag{61}$$

$$P_4 = P_\infty \tag{62}$$

then the exit velocity can be computed from

$$f_3(\gamma_4, M_4) = \frac{P_{0,4}}{P_4} \tag{62}$$

iv. Remarks

For the assumption that the discharge pressure is equal to that of the ambient we find that the momentum equation can be used to predict the "appropriate" exit velocity for the given station 3 conditions. Recognize here that the station 3 condition reflects on the original velocity assumption at station 1S. The correct assumption will be that for which the mass flow rates at stations 3 and 4 are equal.

As a first approximation to the compressible flow solution the use of an incompressible assumption is of convenience; Bevilaqua [1975] and Salter [1975] provide more detials on those approximations.

Primary nozzle conditions

All of the thermodynamic and flow variables required to describe the primary nozzle discharge can be derived from three input conditions: mass flowrate, stagnation temperature, and static pressure. A discussion of the relationships involved - including an account for choked flow - is given below.

i. Primary nozzle pressure ratio

Manipulation of the mass continuity equation provides the relation

$$\frac{\dot{m}}{A} = \sqrt{\frac{\gamma}{R}}\frac{P}{\sqrt{T_0}} M \sqrt{1 + \frac{\gamma - 1}{2} M^2} \tag{63}$$

where

$$\frac{P_0}{P} = \left(1 + \frac{\gamma - 1}{2} M^2\right)^{\gamma/\gamma - 1} \tag{64}$$

It is intended the nozzle pressure ratio be expressed in terms of the mass flowrate, stagnation temperature, specific heat ratio, and nozzle geometry. To do this, the equation above is rearranged so that

$$\left\{\frac{\dot{m}}{PA}\sqrt{\frac{RT_0}{\gamma}}\right\}^2 = M^2\left(1 + \frac{\gamma - 1}{2} M^2\right) \tag{65}$$

Since the isentropic pressure ratio gives the Mach number as

$$M^2 = \frac{2}{(\gamma - 1)}\left\{\left(\frac{P_0}{P}\right)^{\gamma - 1/\gamma} - 1\right\} \tag{66}$$

then

$$0 = -\frac{\dot{m}^2 T_0 R}{P^2 A^2 \gamma}\left(\frac{\gamma-1}{2}\right) - \left(\frac{P_0}{P}\right)^{\gamma-1/\gamma} + \left(\frac{P_0}{P}\right)^{2(\gamma-1/\gamma)} \tag{67}$$

The nozzle pressure ratio is extracted from the solution to the quadratic equation; the result is:

$$\left(\frac{P_0}{P}\right)^{\gamma-1/\gamma} = \frac{1}{2} \pm \frac{1}{2}\left\{1 + 4\left(\frac{\dot{m}^2 T_0 R}{P^2 A^2 \gamma}\left(\frac{\gamma-1}{2}\right)\right)\right\}^{1/2} \tag{68}$$

from which we establish the relation (notice the "+")

$$\left(\frac{P_0}{P}\right) = \left(\frac{1}{2} + \frac{1}{2}\left\{1 + 4\left(\frac{\dot{m}^2 T_0 R}{P^2 A^2 \gamma}\left(\frac{\gamma-1}{2}\right)\right)\right\}^{1/2}\right)^{\gamma/\gamma-1} \tag{69}$$

This equation is valid for choked and unchoked flow; in the latter situation, however, there arises a convenient relation from the concept that the mass flowrate per unit area is a maximum for choked flow and coincides with a Mach number of unity.

A solution for the nozzle static pressure as a function of stagnation pressure, stagnation temperature, and specific heat is given in Appendix J.

Returning to the first equation of this section and eliminating the static pressure from the RHS provides

$$\frac{\dot{m}}{A} = \sqrt{\frac{\gamma}{R}}\frac{P_0}{\sqrt{T_0}} M\left\{1 + \left(\frac{\gamma-1}{2}\right)M^2\right\}^{-\frac{\gamma+1}{2(\gamma-1)}} \tag{70}$$

then for a Mach number of unity

$$\frac{\dot{m}}{A^*} = \sqrt{\frac{\gamma}{R}\left(\frac{2}{\gamma+1}\right)^{\gamma+1/\gamma-1}} \frac{P_0}{\sqrt{T_0}} \tag{71}$$

For air at standard conditions

$$\gamma = 1.4$$

$$R = 53.304 \frac{ft - lb_f}{lb_m R}$$

we substitute and obtain Fliegners's formula

$$\frac{\dot{m}}{A^*} = 0.532\frac{P_0}{\sqrt{T_0}} \tag{72}$$

The nozzle pressure ratio is then

$$\frac{P_0}{P_\infty} = 1.88\frac{\sqrt{T_0}}{P_\infty}\left(\frac{\dot{m}_P}{A_P}\right) \tag{73}$$

which is in a convenient form for hand calculations.

ii. Primary nozzle thrust for isentropic flow

From the steady-state momentum equation the thrust of a nozzle, choked or unchoked flow, provides

$$T = \dot{m}_e v_e + A_e(P_e - P_\infty) \tag{74}$$

Introduce now the idea for maximum thrust in which the area ratio is such that the exit pressure is the same as that of the ambient; furthermore, allow the exit velocity to be given by the relationship for isentropic flow,

$$v_e = c_0\left(\frac{2}{(\gamma-1)}\left\{1-\left(\frac{P_e}{P_0}\right)^{\gamma-1/\gamma}\right\}\right)^{1/2} \tag{75}$$

The primary isentropic thrust is therefore given as

$$T_s = \dot{m}_e\sqrt{\gamma R T_0}\left(\frac{2}{(\gamma-1)}\left\{1-\left(\frac{P_e}{P_0}\right)^{\gamma-1/\gamma}\right\}\right)^{1/2} \tag{76}$$

It seems that for unchoked flow the static exit pressure is equal to the ambient (for the ideal case); if the nozzle pressure ratio is defined by

$$NPR = \frac{P_0}{P_\infty} \tag{77}$$

then the isentropic thrust equation takes on a convenient form for evaluation of flow conditions.

For choked flow from a convergent nozzle the exit pressure is not, in general, equal to the ambient. It is then necessary in the analysis of choked flow to return to the original expression for thrust and account for this fact:

$$T_g = \dot{m}_e \sqrt{\gamma R T_0 \frac{2}{(\gamma-1)}\left\{1-\left(\frac{P_e}{P_0}\right)^{\gamma-1/\gamma}\right\}} + A_e(P_e - P_a) \qquad (78)$$

where the subscript a referes to the ambient condition. Now, with the substitutions

$$\dot{M}_e = \rho_e v_e A_e$$

$$P_e = \rho_e R T_e$$

$$A_e = \frac{\dot{m}_e r T_0}{P_e v_e}$$

and the additional relations that

$$v_e = \sqrt{2c_p T_0}\sqrt{1-\left(\frac{P_e}{P_0}\right)^{\gamma-1/\gamma}}$$

$$c_p = \frac{\gamma}{\gamma-1} R$$

then the isentropic thrust equation becomes

$$T_g = \dot{m}_e \sqrt{\gamma R T_0}\left(\frac{2}{(\gamma-1)}\left\{1-\left(\frac{P_e}{P_0}\right)^{\gamma-1/\gamma}\right\}\right)^{1/2} + \frac{\dot{m} R T_e}{v_e}\left(\frac{P_e}{P_a}-\frac{P_a}{P_e}\right)$$

$$T_g = \dot{m}_e \sqrt{\gamma R T_0}\left(\frac{2}{(\gamma-1)}\left\{1-\left(\frac{P_e}{P_0}\right)^{\gamma-1/\gamma}\right\}\right)^{1/2} + \frac{\dot{m} R T_e \left(1 - P_a/P_e\right)}{\sqrt{2c_p T_0}\sqrt{1-(P_e/P_a)^{\gamma-1/\gamma}}} \qquad (79)$$

Now,

$$\frac{R T_e}{\sqrt{2c_p T_0}} = \frac{T_e}{T_0}\left(\frac{R\sqrt{T_0}}{\sqrt{2c_p}}\right) \qquad (80)$$

$$\frac{R T_e}{\sqrt{2c_p T_0}} = \frac{T_e}{T_0}\sqrt{\frac{R T_0(\gamma-1)}{\gamma}} \qquad (81)$$

and for choked flow

$$\frac{P_*}{P_0} = \left(\frac{2}{\gamma+1}\right)^{\frac{\gamma}{\gamma-1}} \tag{82}$$

then

$$1 - \left(\frac{P_*}{P_0}\right)^{\frac{\gamma-1}{\gamma}} = \frac{\gamma-1}{\gamma+1} \tag{83}$$

so

$$T = \dot{m}\sqrt{T_0}\left\{\sqrt{\frac{2\gamma R}{\gamma-1}}\sqrt{\frac{\gamma-1}{\gamma+1}} + \sqrt{\frac{R(\gamma-1)}{2\gamma}}\left(\frac{T_*}{T_0}\right)\sqrt{\frac{\gamma+1}{\gamma-1}}\left(1-\frac{P_a}{P_*}\right)\right\} \tag{84}$$

Continuing,

$$\frac{T_*}{T_0} = \left(\frac{P_*}{P_0}\right)^{\frac{\gamma-1}{\gamma}} = \frac{2}{\gamma+1} \tag{85}$$

$$\frac{P_a}{P_*} = \frac{P_0 P_a}{P_* P_0} = \left(\frac{\gamma+1}{2}\right)^{\frac{\gamma}{\gamma-1}} \frac{P_a}{P_0} \tag{86}$$

which provides the result

$$T = \dot{m}\sqrt{T_0}\left\{\sqrt{\frac{2\gamma R}{\gamma+1}} + \sqrt{\frac{R(\gamma+1)}{2\gamma}}\left(\frac{2}{\gamma+1}\right)\left(1-\left(\frac{\gamma+1}{2}\right)^{\gamma/\gamma-1}\frac{P_a}{P_0}\right)\right\} \tag{87}$$

Combine the terms

$$\sqrt{\frac{R(\gamma+1)}{2\gamma}}\left(\frac{2}{\gamma+1}\right) = \sqrt{\frac{2R}{\gamma(\gamma+1)}} \tag{88}$$

then we obtain the desired result for the isentropic thrust for a choked nozzle:

$$T = \dot{m}\sqrt{T_0}\sqrt{\frac{2R}{\gamma(\gamma+1)}}\left\{\gamma + 1 - \left(\frac{\gamma+1}{2}\right)^{\gamma/\gamma+1}\frac{P_a}{P_0}\right\} \tag{89}$$

Thrust, thrust augmentation, and ejector efficiency

As previously mentioned the ratio of the total momentum increment and the thrust that would be obtained from the primary nozzle under ideal conditions yields the thrust augmentation ratio,

$$\phi = \frac{T_{SYS}}{F_{1P,IDEAL}} \tag{90}$$

where the system thrust is given by

$$T_{SYS} = \dot{m}_4(v_4 - v_\infty) \tag{91}$$

and the thrust from the nozzle under isentropic flow conditions is

$$F_{1P,IDEAL} = \dot{m}_{1P}v^*_{1P} \tag{92}$$

where

$$\frac{v^*_{1P}}{C_{1P}} = \left(\frac{P_{0,1P}}{P_{1P}}\right)^{(\gamma-1)/2\gamma}\left\{\frac{2}{\gamma-1}\left(1-\left(\frac{P_{1P}}{P_{0,1P}}\right)^{(\gamma-1)/\gamma}\right)\right\}^{\frac{1}{2}} \tag{93}$$

The efficiency of the energy transfer process is given by the ratio of the kinetic energy of the efflux and the energy input at the primary nozzle; the energy efflux is

$$KE_4 = \frac{1}{2}\dot{m}_4\beta < v_4 >^2 \tag{94}$$

and the energy input is

$$E_{1P} = v_{1P}A_{1P}(P_{0,1P} - P_{1P}) \tag{95}$$

Solution Options

In the previous section there were (for the general case of analysis) presented 9 equations describing ejector physics in terms of 12 unknowns. The difference between control-volume analyses generally centers around the manner in which closure is provided. Two basic approaches are distinguished in the present work according to

intent - the "direct solution" is used for parametric analyses and the "iterative solution" used for predictive analyses. The iterative approach is obviously preferred in the present work.

Direct Solution

From a computational point of view, a parametric analysis involves a direct solution to the system of equations. That is, it is a simple matter to specify a broad range of secondary inlet conditions and compute a corresponding set of discharge conditions. In those cases where multi-valued solutions exist, selection of the "correct" solution is assisted by the entropy condition. No attention need be paid to extracting which of the solutions are naturally occuring, only that the solution correspond with the prescribed conditions at the secondary inlet that, for whatever reason, in fact have arisen.

The parametric approach is not in line with the objectives of the present work so there is no need for further discussion. Complete coverage of the parametric viewpoint is given in the works of Addy, Dutton, Mikkelson, and co-workers (see references).

Iterative Solution

Although the iterative solution involves the same set of equations as the direct solution, it is the objective in the former to seek the appropriate inlet velocity which provides an exit static pressure corresponding with the ambient. So rather than select arbitrary inlet velocities, a reasonable estimate at the correct value is used (through, for instance an incompressible flow analysis) that meets ambient pressure conditions, and the result then refined - by iteration - until convergence is reached. A typical solution approach is presented below, although, as alluded to earlier, other solution procedures given in the literature may vary in some details of the steps involved.

i. A Typical Solution Procedure

The procedure outlined below reflects the assumption of insentropic inlet and diffuser physics; the impedance of the nozzle to the flow and other "real-flow" effects are ignored for the present discussion. We have:

1. *Compute the free-stream stagnation pressure and temperature* Use the given free-stream static pressure, static temperature and velocity in the following:

$$V_\infty = |\underline{U}| \sin\alpha$$

$$M_\infty = V_\infty / c_\infty$$

$$P_{0,\infty} = P_\infty f_3(\gamma_\infty, M_\infty)$$

$$T_{0,\infty} = T_\infty f_2(\gamma_\infty, M_\infty)$$

2. *Compute the primary nozzle discharge conditions* Use the (prescribed) discharge mass flowrate, stagnation temperature, and static pressure in the following procedure (Appendix J describes the modification if the stagnation pressure is given instead):

(i) Compute the NPR based on the assumption that the discharge pressure is the same as the ambient:

$$NPR = \left(\frac{1}{2} + \frac{1}{2} \left\{ 1 + 4 \left(\frac{\dot{m}^2 T_0 R}{P^2 A^2 \gamma} \left(\frac{\gamma - 1}{2} \right) \right) \right\}^{1/2} \right)^{\gamma/\gamma - 1}$$

(ii) Compute the NPR for choked flow ($M = 1$)

$$NPR^* = \left(\frac{\gamma + 1}{\gamma} \right)^{\frac{\gamma}{\gamma - 1}}$$

(iii) If $NPR > NPR^*$, the nozzle flow is choked; use Fliegner's formula to compute the stagnation discharge pressure,

$$P_{0,1P} = 1.88 \sqrt{T_0} \left(\frac{\dot{m}_P}{A_P} \right)$$

and the actual NPR is then based on the ratio of this stagnation pressure and the actual back pressure.

(iv) If $NPR < NPR^*$, the nozzle flow is subsonic. Use the static pressure at the nozzle discharge (an input condition) to compute the ratio

$$\frac{P_{0,1P}}{P_{1P}} = \left(\frac{1}{2} + \frac{1}{2} \left\{ 1 + 4 \left(\frac{\dot{m}^2 T_0 R}{P^2 A^2 \gamma} \left(\frac{\gamma - 1}{2} \right) \right) \right\}^{1/2} \right)^{\gamma/\gamma - 1}$$

then compute the actual NPR from the known back pressure condition.

(v) With the correct stagnation pressure now established, the computation of the static temperature and exit velocity can be made

$$T_{1P} = T_{0,1P} / f_2(\gamma_{1P}, M_{1P})$$

$$V_{1P} = M_{1P} c_{1P}$$

3. *Assume M1S* The solution to the steady-state problem is an iterative procedure; in the present work a "starting solution" must be given. An initial Mach number assumption of 0.01 has been found a convenient starting point for the computations of the present work.

4. *Compute station 1S conditions.* The known free-stream flow conditions, the Mach number at station 1S, and the assumption of an isentropic inlet are sufficient to estimate station 1S conditions. The isentropic assumption allows one to equate the free-stream and station 1S stagnation temperature and pressure:

$$P_{0,1S} = P_{0,\infty}$$

$$T_{0,1S} = T_{0,\infty}$$

Then

$$P_{1S} = P_{0,1S} / f_3(\gamma_{1S}, M_{1S})$$

$$T_{1S} = T_{0,1S} / f_2(\gamma_{1S}, M_{1S})$$

The mass flowrate at station 1S can then be computed; enough information now exists to compute the mass entrainment ratio.

5. *Compute properties at station 3.* Apply the system of equations from section 4.2.1.5:

$$T_{3,0} = F_8(\mu, T_{s,0}, T_{p,0})$$

$$M_3 = f_{17}(\beta_3, \gamma_3, K_3)$$

$$T_3 = T_{0,3} / f_2(\gamma_3, M_3)$$

$$\frac{P_3}{P_P} = \frac{A_P}{A_3}\sqrt{\frac{R_3 T_{0,3}}{R_P T_{0,P}}\frac{f_6(\gamma_P, M_P)}{f_6(\gamma_3, M_3)}}\{1 + \mu\}$$

$$P_{3,0} = P_3 f_3(\gamma_3, M_3)$$

The mass flowrate at station 3 can be computed with these results.

6. *Compute properties at station 4* The isentropic flow approximation and the assumption that the discharge pressure is equal to that of the ambient introduces

$$P_4 = P_\infty$$

$$P_{4,0} = P_{3,0}$$

$$M_4 = \sqrt{\frac{2}{\gamma - 1}\left\{\left(\frac{P_{4,0}}{P_4}\right)^{\gamma/(\gamma-1)} - 1\right\}}$$

This velocity represents that which, if the station 1S velocity were correct, would match the stagnation condition at station 3 to the static condition at station 4. Once the static temperature is computed

$$T_4 = T_{0,4} / f_2(\gamma_4, M_4)$$

enough information exists to compute the mass flowrate at station 4.

7. *Compare the mass flowrates at stations 3 and 4.* In general it is unlikely the initial guess for the station 1S velocity is correct, so the mass flow rate at station 3 will not be equal to the mass flowrate at station 4 (the latter based on a static discharge pressure equal to the ambient). If this is the case, the "surge" is given by,

$$\dot{m}^* = \dot{m}_3 - \dot{m}_4$$

and the mass flowrate at station 1S given by

$$\dot{m}_{1S} = \frac{1}{2}\dot{m}^*$$

from which the new inlet velocity at station 1S can then be computed.

8. *Repeat steps 4 - 7 until the solution converges.* The convergence criteria is that

$$|\dot{m}^*| < \epsilon = 0.1$$

9. *Proceed with the computation of thrust, thrust augmentation ratio, and ejector efficiency.*

This solution procedure is summarized in figure 11.

REMARKS:

1. Step 6 is based on an unknown value of the exit pressure (station 4), allowing for the general situation where the exit pressure is not equal to the ambient. Some modification of the procedure is allowable when the latter is true. In such a case the computed P_4 is compared with the ambient and modification of the inlet velocity based on the error in pressure prediction.

2. There is required a second iteration contained within each timestep if an ideal gas is used instead of a perfect gas. Figure 12 provides the computational steps for the inlet region. These steps are typical for each control volume and differ only by the subscripts of the variables used.

Sample Computations

A FORTRAN program for the Steady-state Ejector Analysis (SEA) performs computations for the methodology outlined above (Preparation of a user's manual for this routine is currently in-progress).

For the purpose of comparing theoretical predictions with experimental data, some preliminary data from the DeHaviland ejector tests at the NASA Lewis PLF facility have been made available to the present work; an overview of this data is presented in Appendix K.

Results

Input data to simulate PLF ejector runs 223-239 were considered adequate for the test of the steady-flow methodology since

A. The nozzle mass flowrates were between 18.7 lbm/s and 46.97 lbm/s -- a range broad enough for the primary nozzle to be choked somewhere inbetween (about 30 lbm/s), and

B. The primary nozzle stagnation temperature of 760 ^{o}R was considerably higher than the 540 ^{o}R ambient stagnation temperature.

Figure 13 illustrates that the steady flow analysis presented here is capable of predicting both the magnitude and the trends obtained in the experiments; note the mirroring of the "dip" in the vicinity of choked primary nozzle flow.

6. UNSTEADY FLOW ANALYSIS

Focus on Transient Ejector Flow

Fluid flows characterized by *time-dependent* velocity fields are termed *unsteady*. More revealing descriptions are linked to time-asymptotic flow behavior. A transient flow is a 'temporary' unsteady flow, associated with, for example, a change in ejector operation from one steady-state condition to another. Contrast this with oscillatory flows in which a periodic time-asymptotic flow character is exhibited. Ejectors utilizing pulsed primary nozzle flows are of the latter type. In the present simulation the focus on transient, not oscillatory, ejector phenomena descends from flight-critical aircraft flight control scenarios; an example would be transition to forward flight from vertical take-off.

Effects the transient ejector simulation should capture are:

1. Ejector response to the primary jet actuation,

2. Momentary depletion of net thrust due to reallocation of engine fan air to the ejector,

3. Feeder line delays (related to actuator transients).

Upon integration of the ejector, engine, and airframe simulations, incipient vertical deceleration effects (due to thrust lag) can be quantified.

Remarks on the Energy Exchange Process

In connection with recent research on the coherent structure of turbulent flows, it appears that even steady-state ejector operation relies on (local) unsteady flow processes[1]. That is, in a coherent flow there are continuously deforming boundries whose motion can (in principle) be tracked - not time averaged as in classical theory - so that there is a distinctly traceable mechanism for work by pressure to be done and therefore energy (attributable to pressure) between streams to be exchanged. Additional energy exchange is provided by viscous shear forces, but these do not rely on the motion of the boundary. Since the pressure-exchange process (non-dissipative) is very short in duration relative to the (dissipative) process of mixing (viscous-dominated), there is potential that a pressure-exchange dominated process is likely to be more efficient than a viscous dominated process. This notion is supported by the marked increase in performance of (correctly designed) ejectors with pulsed primary flows in comparison with their steady-state counterparts.

Since the literature reveals that most unsteady ejector studies concern pulsed laser operation, it is of interest to employ the conclusions from these studies in the present work (especially for work containing comparisons with experimental data). Such may

---

1 This "unsteadiness" in a turbulent flow has, of course, been known for a long time, it has just traditionally been a practice to use time averaged quantities in, for instance, the Navier-Stokes equations. See Liepmann [1979], and Hussain [1981] for discussions of "classic" vs coherent turbulent flow modelling.

not be the case, however, since there is a distinct domination of pressure-exchange mechanisms in pulsed jets that cannot be assumed to remain in a steady-flow turbulent jet entrainment scenario for thrust augmenting ejectors[2].

The present work employs the concept of kinetic energy exchange between the primary and secondary streams for the transient secondary velocity prediction. There is a limitation to this approach in that an emprical correction is needed for closure. However, there is significant technical antecedant for the correction factor and its use follows from the work of Korst and Chow [1966]. It is important to remark that the creation of a kinetic energy balance for this purpose requires deletion of the corresponding kinetic energy balance terms from the energy equation for the control volume (what remains is the thermal energy equation).

Three Levels of Approximation

From a technical standpoint difficulties in real-time ejector simulation arise from evasion and compromise. By "evasion" it is meant we are in search of the "answer" without mandating recourse to solving the full unsteady Navier-Stokes equations; in terms of "compromise", there is a need to balance the level of approximation used (for which empirical calibration of the theory is then intensified) and the expectations for the accuracy of the simulation. Three levels of approximation can be considered:

1. Quasi-Steady Flow: Assume that the characteristic time for changes in the forcing function (boundary conditions) is greater than the characteristic time for response of the fluid - that the fluid is "very agile" and therefore permits the steady-state equations of motion to be used at each instant in time.

2. Characteristic Volume Approach: Allow that the mixing region can be partitioned into three characteristic volumes; one domain characterizing secondary flow effects, another for the primary nozzle flow, and one to characterize the mixed flow domain (the size of the control volumes are time dependent).

3. Finite Volume Approach: Identify a finite number of control volumes of fixed size, partitioned only in the streamwise direction (the size of the control volumes are time independent). This approach introduces a relationship between the primary and secondary flows with the use of the self-similar profiles.

Remarks

In the analysis of a given unsteady flow problem, it is quite convenient mathematically if a quasi-steady formulation can be assumed valid. This leads to the use of steady flow equations in an unsteady flow analysis; at each instant in time the flow is assumed to instantly respond to boundary condition transients. A basic issue, however, is whether the characteristic time of the forcing function is the same order of magnitude as the relaxation time of the flow.

There is no need to remark on the details of the system of equations for this approach since this is, by default, already given in the steady flow discussion.

---

2 An interesting note here is that, at the other extreme, for pulsed flow there exists an entrainment even in a laminar flow for those geometries where a secondary streaming (a viscous phenomena) is present.

In the case of external unsteady flows the Strouhal number (a characteristic parameter for the unsteady flow frequency) plays a significant role as the criterion by which to (or not to) invoke the use of a quasi-steady formulation (see Drummond [1985, 1986]). Although the Strouhal number is also a convenient characteristic unsteady flow parameter in internal flows, there appears no technical antecedents on which to base the prescription of a threshold for quasi-steady ejector fluid-dynamic operation. Only testing would allow this assumption to be made a-priori.

An appropriate application of the characteristic volume approach is for flows that exhibit distinct flow regime characteristics, like, for instance, the inviscid interaction region discussed in section 3. Time lags for this system are generated through imposition of lag coefficients between field variables of the characteristic region; although this is a simple approach, it relies on accurate knowledge of the lag coefficients for the simulation to be accurate (read: analysis cannot be divorced from transient experimental data). This would be a new method in the approximation of transient ejector performance, but is not explored further in the present work.

The finite volume application of this work is also new in ejector analysis, but it is anticipated to be more accurate than the characteristic method since considerably more elements are employed; as expected, though, execution is likely to be more CPU intensive. Here, a hybrid approach is based on the work of Drummond [1985], and Seldner, Mihaloew, and Blaha [1972]. Note that an important feature of the method is that steady-state data (not transient) can be used in the calibration of the method. It employs control volume elements of constant volume and assumes the mixing region flow is expressable in self-similar form.

Finite Volume Approach

It is evident that the quasi-steady and characteristic methods of analysis previously discussed really make no specific assumption about the nature of the flow in the mixing region. The finite volume approach attempts to overcome this problem. Indeed, a fundamental philosophical point to be made is that in exchange for the ability to more accurately depict conditions (than you would otherwise have) inside a given sub-region, a more complex form of the surface integrals must be accommodated.

In the present work the inlet and diffuser regions are permitted to be represented by a quasi-steady approximation, and the finite volume method of analysis applied only to the mixing region. This is based on the perception of the inlet and diffuser physics to be driven by imposed pressure gradients, and the mixing region dominated by turbulent viscous interaction. Obviously, the notion is that the physics of the mixing region are the cause of a situation that yields the pressure gradient effect in the inlet and diffuser.

The fundamental assumption in the finite volume approach is that the mixing region is divided into N sub-regions of known volume and whose individual velocity, temperature, and pressure can be given by characteristic quantities. A significant departure from previous discussions is that the characteristic quantities are not necessarily uniform over the sub-region, but do relate to characteristic distributions. These distributions relieve us from a specific treatment of, for instance, an inviscid interaction region, though by default such a phenomenon should be predicted within the domain of an accurate solution methodology for the problem.

Corresponding with the finite volume method of analysis is the need for specific statements about the characteristic distribution within each sub-region. A discussion of the profiles used in the present work follows an overview of the basic control volume equations for the mixing region. Then, application of the finite volume method to the continuity, momentum, and energy equations for the mixing regions is discussed. Lastly, the complete system of equations for the ejector are assembled and the proposed method of solution presented.

Figure 14 illustrates the finite volume nomenclature and some typical elements. A virtual grid representation is given in figure 15.

General system of equations

The basic form of the control volume equations are:

Mass

$$\frac{d}{dt}\{m_{cv}\} = \sum_k \dot{m}_k \tag{1}$$

Momentum

$$\frac{d}{dt}\int_V \rho \underline{v}\, dV + m_{cv}\frac{d\underline{U}}{dt} = -\oint_A \rho \underline{v}(\underline{v}\cdot\underline{n})dA - \oint_A \underline{n}\cdot(p\underline{I})dA + \underline{F} \tag{2}$$

Energy

$$\frac{d}{dt}\int_V P\,dV = -\oint_A \gamma P \underline{v}\cdot\underline{n}\,dA - (\gamma-1)\oint_A P\underline{U}\cdot\underline{n}\,dA \tag{3}$$

Entropy

$$\frac{d}{dt}\int_V \rho s\,dV - \oint_A s\,d\dot{m} \geq 0 \tag{4}$$

Again, the presence of the surface integrals (that in the steady flow analysis were simple sums of average quantities) reflects the idea that one cost of incorporating a simple turbulence model in the time dependent volume integrals is given by increased surface flux term complexity.

Note the *heat equation* has replaced the *general power equation* for the energy equation (see derivations in Appendix A). Application of the self-similar profiles is in fact easier for the heat equation than it is for the power equation, but both are eventually needed in the analysis. As mentioned earlier, the kinetic energy components will be accounted for in a separate balance intended to predict the secondary flow magnitude; this will be detailed later.

Turbulent Jet Approximation

A diagram of the present turbulent jet geometric characteristics is given in figure 16. Extending from the mixing region inlet plane there exists a *potential-core* region characterized by a fairly uniform centerline velocity, with no transverse component. This is distinguished from the *mixed-flow* region where the centerline velocity decay arises from momentum transport to the entrained fluid.

This section extablishes the basic features of the potential- and mixed-flow regions for use in the finite-volume analysis.

i. Jet spreading approximation

Two jet angles are associated with the growth of the turbulent jet. One portrays the decay of the potential core region and the other bounds the outer jet boundary layer growth. Rectilinear profile assumptions for both have an analytic foundation and empirical verification. Although the outer jet expansion angle depends on the ejector pressure gradient and inlet velocity ratio, the inner jet expansion seems more exclusively a function of the latter. To eliminate the introduction of additional unknowns in the ejector problem formulation it is worthwhile to explore an analytic approximation for the inner boundary length, b_I ; see the potential core region of figure 16. Below, some remarks on the outer jet expansion follow a discussion of the potential core approximation.

ii. Potential core region length

Characterization of the potential core region is given in the present work by "calibrating" an analytic model; calibration is done with ejector data. Abramovich [1963] derives the length of the initial region for 2-D planar co-flowing jets as:

$$\frac{L}{b_0} = \frac{1 + r}{c_1(1-r)(0.416 + 0.134r)} \qquad (5)$$

where the velocity entrainment ratio is

$$r = v_{1S}/v_{1P} \qquad (6)$$

and the empirical coefficient for free jets given by

$$0.2 < c_1 < 0.3$$

Alternate models are presented by Abramovich for multiple jets that link the increase in thickness of the jet proportionally to the intensity of turbulence in the stream (those models also assume a loss of single jet identity loss for multiple jet configurations). We find it convenient to use the expression above with a corrected constant

$$c_1 = 0.4$$

which is based on the experimental work of Bernal and Sarohia [1983]. Prediction of L/b_0 of 15.5 for a 2-D single jet corresponds fairly well with a value of 18 extracted from their plots of nondimensional centerline velocity. In this regard the work of Krothapalli et. al. [1980] is of interest since multiple rectangular *free* jets were considered and the dimensionless length estimated (from their plots) to be in the vicinity of 14-20. This is the basis for the earlier remark that, at least for the ejector configurations of interest, the rate of the potential core spreading is influencedmore so by inlet velocity than longitudinal pressure gradient. For the limited purpose of establishing the non-dimensional potential core jet length the free turbulent jet results are applicable. Bear in mind that unlike the free turbulent jet an axial pressure gradient is assumed for the ejector.

Figure 17 illustrates the non-dimensional centerline velocity as a function of the non-dimensional centerline distance for a typical multiple free jet. The potential core region is important since the total non-dimensional length of the mixing region under consideration is on the order of 20-30.

iii. Outer jet boundary expansion

A linear representation for the outer jet boundary is illustrated by the boundary b_{II} in figure 16. This is based on the interpretation of data by Abramovich for incompressible planar jets (free and submerged). Data from Donsi et al [1979] supports this trend for extremely large pressure gradients (experiments were for fluidized beds with jetting). We therefore have

$$b = kz \tag{7}$$

and note Abramovich's simple expression for the constant has the attractive result

$$\frac{b}{z} = c_1 \frac{1-r}{1+r} \tag{8}$$

where c_1 is the same as used previously. An account of jet growth as a function of longitudinal pressure gradient could be nested in the constant. Due to the time-dependence of the pressure gradient for transient ejector operation the (outer) jet growth -- and therefore the proportionality constant -- is also a function of time. Since the development of Abramovich is based on continuity the present work follows suit, but from a finite volume standpoint. This ensures the finite-volume method will satisfy continuity without an ad-hoc construction of $b(x)$.

It is interesting, though, to remark on a test case for the correlation above where $r=0.35$ and an ejector mixing region pressure gradient of 14 lb_f/ft^2 is given. The 9^o expansion angle from finite volume continuity considerations compares reasonably well with the 10.1^o value from the Abramovich model (with $c_1=0.4$) and, as expected, is higher than the 5^o value found with c_1 for a free jet with no longitudinal pressure gradient.

Self-similar profiles

In the characterization of an element of the mixing region the velocity description simplifies with the 2-D planar turbulent jet self-similar profiles of Abramovitch [1963] for co-flowing jets:

$$\frac{v - v_e}{v_m - v_e} = \left\{ 1 - \left(\frac{x}{b} \right)^{1.5} \right\}^2 \tag{9}$$

Alternate co-flowing jet profiles are used, for instance, in the work of Korst and Chow [1966] or Lund, Tavella, and Roberts [1966], but the polynomial form is more applicable to the physics of interest here.

Introduce the dimensionless radial coordinate,

$$\xi = \frac{x}{b} \tag{10}$$

so that in general form

$$\frac{v - v_e}{v_m - v_e} = \Phi(\xi) = \left\{ \begin{matrix} \left(1 - \xi^{1.5}\right)^2, & 0 \le \xi < 1 \\ 0, & 1 \le \xi \le \hat{\xi} \end{matrix} \right\} \tag{11}$$

then

$$v = v_e(1 - \Phi) + v_m \Phi = f(\Phi) \tag{12}$$

where

$$\hat{\xi} = B/b \tag{13}$$

and B is the maximum value of the jet half-width, b. For an incremental volume of length Δz, width y, and height x, only part of the jet consumes the element. Therefore, the general velocity profile is written

$$v(\xi) = \left\{ \begin{matrix} f(\Phi), & 0 \le \xi < 1 \\ v_e, & 1 \le \xi \le \hat{\xi} \end{matrix} \right\} \tag{14}$$

The description above makes no account for the potential core for the initial jet region; for this we note

$$b = b_{II} - b_I \tag{15}$$

and the dimensionless radial coordinate becomes

$$\xi = \frac{x - b_I}{b_{II} - b_I} = \frac{x - b_I}{b} \tag{16}$$

Recognizing the inner boundary vanishes outside the potential core region (by definition), then by default the dimensionless coordinate takes the correct form if we define

$$b_I = \begin{Bmatrix} b_0 - z\tan\theta, & z < z_I \\ 0, z \geq z_I \end{Bmatrix} \tag{17}$$

where z_I is the length of the potential core region. In the discussion to follow distinction between the potential core and mixing regions is not necessary if the appropriate non-dimensional parameters are understood.

To allow for a density variation across the jet a basic self-similar profile is assumed,

$$\frac{\rho - \rho_e}{\rho_m - \rho_e} = \Lambda(\xi) \tag{18}$$

where

$$\Lambda(\xi) = \begin{Bmatrix} 1, & 0 \leq \xi < \xi^* \\ 0, & \xi^* \leq \xi \leq \bar{\xi} \end{Bmatrix} \tag{19}$$

and obviously

$$\rho = \rho_e(1 - \Lambda) + \rho_m \Lambda \tag{20}$$

The value of ξ^* used in the present work is unity, though fluidized bed data suggests a value of 0.9 allows more interaction between the jet boundary layer and the free-stream. For a constant cross-sectional density there is no need for a self-similar approximation; thus

$$\rho = \bar{\rho} \tag{21}$$

Pressure is assumed to have a profile similar to that for density,

$$\frac{P - P_o}{P_m - P_o} = \Lambda(\xi) \tag{22}$$

Again, this profile need not be invoked if the assumption of a uniform transverse pressure gradient is specified.

Temperature profiles are shown by Abramovich [1963] to have the dimensionless profile

$$\frac{T - T_o}{T_m - T_o} = \Psi(\xi) = 1 - \xi^{1.5} \tag{23}$$

derived as the square root of the velocity profile.

Transformation of coordinates require that derivatives of ξ be determined. If it is assumed that b is in general only a function of z and t (not x), then,

$$\frac{d\xi}{dx} = \frac{1}{b} \tag{24}$$

so, for example, the generic area integral across the mixing region is,

$$\begin{aligned} \zeta = \int_0^B z(\psi)\,dA &= \int_0^B z(\psi) W\,dx \\ &= W\left\{\int_0^b z(\psi)\,dx + \int_b^B z(\psi)\,dx\right\} \\ &= Wb\left\{\int_0^1 z(\psi)\,d\xi + \int_1^\xi z(\psi)\,d\xi\right\} \end{aligned} \tag{25}$$

and the integral for the complete cross-section would be

$$Z = \sum_{i=1}^{N} \zeta_i (\underline{i} \cdot \underline{n}) \tag{26}$$

i. Example Application: Average velocity computation

Computation of the average mixing-region velocity at station k is a simple example of the use of the self-similar profile integrals. Define the average velocity by

$$\bar{v}_k = \frac{1}{A_k}\int_A v\,dA \tag{27}$$

we have for "N" nozzles that

$$\bar{v}_k = \frac{2NW}{A_k}\int_0^B v\,dx \tag{28}$$

and through a change of variable

$$\bar{v}_k = \frac{2NWb_k}{A_k}\int_0^{\xi} v_i\,d\xi \tag{29}$$

Application of the self-similar profiles yields

$$\bar{v}_k = \frac{2NWb_k}{A_k}\int_0^{\xi}\left\{v_o(1-f_1)+v_m f_1\right\}d\xi \tag{30}$$

where

$$f_1 = \begin{cases}\left(1-\xi^{1.5}\right)^2, 0\le\xi<1\\ 0, 1\le\xi\le\bar{\xi}\end{cases} \tag{31}$$

Completion of the integral yields

$$\bar{v}_k = \frac{2NWb_k}{A_k}\left\{v_m\int_0^1 f_1\,d\xi + v_o\int_0^1(1-f_1)d\xi + v_o\int_1^{\xi}(1)d\xi\right\} \tag{32}$$

Let

$$A^* = \frac{2NWb_k}{A_k} \tag{33}$$

then

$$\bar{v} = A^*\left\{v_m(1-0.8+0.25)+v_o(0.8-0.25)+v_o(\bar{\xi}-1)\right\} \tag{34}$$

and finally

$$\bar{v} = A^*\left\{0.45v_m+v_o(\bar{\xi}-0.45)\right\} \tag{35}$$

Application of the finite volume method

The assumptions and profiles outlined in the previous section are applied to the equations of mass conservation, momentum conservation, and balance of energy.

Application to conservation of mass

For the generic sub-region k, bounded by surfaces at k and $k+1$,

$$\left(\frac{dm}{dt}\right)_k = \dot{m}_k - \dot{m}_{k+1} \tag{36}$$

where

$$\dot{m}_k = 2NW\int_0^B \rho_k v_k dx \tag{37}$$

From the similarity profiles

$$\dot{m}_k = 2NWb_k\int_0^\xi \{\rho_o(1-\Lambda)+\rho_m\Lambda\}\{v_o(1-\Phi)+v_m\Phi\}d\xi \tag{38}$$

As discussed earlier, an account of real-flow effects is provided in part through an empirically obtained jet spreading function $b(z,t)$ that defines the jet boundary. This is a common function explored in turbulent jet analyses. In general, the spreading function is dependent on space **and** time, although for the present preliminary study considerable simplification is obtained by ignoring the time dependence. It suffices for the present work to admit a quasi-steady approximation for the jet expansion; this approximation can be checked when ejector data is available.

After substitution of self-similar profiles the mass flux integral becomes

$$\dot{m} = 2NWb\int_0^\xi \{\rho_m v_m \Lambda\Phi + \rho_o v_m(1-\Lambda)\Phi + \rho_m v_o\Lambda(1-\Phi) + \rho_o v_o(1-\Lambda)(1-\Phi)\}d\xi \tag{39}$$

then (see Appendix H)

$$F_1 = \int \Lambda\Phi d\xi = 0.45 \tag{40a}$$

$$F_2 = \int \Phi(1-\Lambda)d\xi = 0 \tag{40b}$$

$$F_3 = \int \Lambda(1-\Phi)d\xi = 0.55 \tag{40c}$$

$$F_4 = \int (1-\Lambda)(1-\Phi)d\xi = \hat{\xi} - 1 \tag{40d}$$

where

$$\hat{\xi} = \frac{B}{b} \tag{41}$$

and the numerical values are for the mixed flow region.

Now,

$$\dot{m} = 2NWb\left(\rho_m v_m F_1 + \rho_a v_m F_2 + \rho_m v_a F_3 + \rho_a v_a F_4\right)$$

$$= 2NWb\left(Z_1\right) \tag{42}$$

The mass in the elemental volume is also given by

$$m = \int_V \rho dV = 2NW\Delta z \int_0^B \bar{\rho} dx$$

$$= 2NWb\Delta z \int_0^{\hat{\xi}} \bar{\rho} d\xi \tag{43}$$

where the characteristic density approximation for the finite volume has been used

$$\bar{\rho} = \frac{1}{2}\left(\rho_k + \rho_{k+1}\right) \Rightarrow \rho_{k+1} \tag{44}$$

If now

$$\int_0^{\xi} \rho d\xi = \rho_m E_1 + \rho_a E_2 \tag{45}$$

where

$$E_1 = \int_0^{\xi} \Lambda d\xi \tag{46a}$$

$$E_2 = \int_0^{\xi} (1-\Lambda) d\xi \tag{46b}$$

then

$$m = 2NWb\Delta z\left(\rho_m E_1 + \rho_a E_2\right) \tag{47}$$

The continuity equation now has the form

$$\bar{b}\Delta z\left\{E_1\left(\frac{d\rho_m}{dt}\right)+E_2\left(\frac{d\rho_e}{dt}\right)\right\} = \left\{b_k Z_{1_k}-b_{k+1}Z_{1_{k-1}}\right\} \tag{48}$$

i. Uniform transverse density approximation

A uniform jet density in the transverse direction simplifies computations by eliminating the distinction between entrained and primary flow density. This does not ignore the marked extreme of secondary amd primary flow, rather, treats the combined flow with a characteristic density extracted from thermal exchange upon mixing. With this assumption the elemental volume mass becomes

$$m = 2NW\Delta z\bar{\rho}B \tag{49}$$

and the result for the finite volume density derivative is

$$\left(\frac{d\rho}{dt}\right)_k = \frac{b_k Z_{1_k}-b_{k+1}Z_{1_{k-1}}}{B\Delta z} \tag{50}$$

ii. Computation of θ_{II}

Continuity conditions across the first mixing region finite volume (steady flow case) allow an approximation for the outer jet spreading angle. The approximation is based on the following

1) constant secondary velocity, and
2) constant primary and secondary flow densities.

In practice, these assumptions provide the jet spreading angle as a simple transformation from "top-hat" profiles to those of a self-similar form. Since

$$\dot{m}_1 = 2NWb_jZ_1 \tag{51}$$

then

$$b_j = \frac{\dot{m}_1}{2NWZ_1} \tag{52}$$

where

$$b_j = b_{II}-b_I \tag{53}$$

and the outer boundary layer then defines the jet expansion angle. A more convenient expression is given by an explicit representation of b as a function of the primary and secondary inlet velocities. Recall that

$$Z_1 = \rho_m v_m F_1 + \rho_e v_m F_2 + \rho_m v_e F_3 + \rho_e v_e F_4 \tag{54}$$

where

$$F_1 = \frac{b_I}{b} + 0.45 \tag{55a}$$

$$F_2 = 0.0 \tag{55b}$$

$$F_3 = 0.55 \tag{55c}$$

$$F_4 = \frac{B - b_I}{b} - 1 \tag{55d}$$

By substitution

$$\dot{m}_1 = 2NW\left\{\rho_m v_m\left(b_I + 0.45b\right) + \rho_m v_e(0.55b) + \rho_e v_e\left(B - b_I - b\right)\right\} \tag{56}$$

then the expression for the boundary layer thickness is

$$b = \frac{\dot{m}_1 - 2NW\rho\left\{b_I v_m + \left(B - b_I\right)v_e\right\}}{2NW\rho\left\{0.45v_m - 0.45v_e\right\}} \tag{57}$$

The outer jet expansion angle is therefore

$$\theta_{II} = arctan\left(\frac{b_{II} - b_0}{z_I}\right) = \left(\frac{b_I + b_I - b_0}{z_1}\right) \tag{58}$$

The expansion angle is determined at the time of initialization of the flow and, as a first approximation, remains constant in time thereafter. This assumes the inner boundary layer is not a deciding influence on the overall jet boundary layer characteristic. The form of the inner boundary layer used in the present work is primarily a function of the primary and secondary velocity ratio. On the other hand, the outer jet boundary is influenced more by the longitudinal pressure gradient than by inlet velocity ratio. Providing that the free-stream (inlet) and discharge pressures remain fairly constant, the constant boundary layer assumption will, as a first approximation, not significantly impact the gross characterization of ejector physics.

Application to the momentum equation

The integral form of the momentum equation for the elemental volume is given by

$$\frac{d}{dt}\int_V \rho \underline{v} dV + m_{cv}\frac{d\underline{U}}{dt} = -\oint_A \rho \underline{v}(\underline{v}\cdot\underline{n})dA - \oint_A \underline{n}\cdot(p\underline{I})dA + \underline{F} \qquad (59)$$

i. Time rate of change of momentum

Computation of momentum within an elemental volume is given by the volume integral of the density and velocity product,

$$M_k = \int_V \rho v dV = 2NW\Delta z\int_0^B \rho v dx \qquad (60)$$

For simplicity the average density concept from the continuity equation discussion is used here; furthermore, an average element velocity is assumed characterized by the velocity at station $k+1$,

$$M_k = 2NW\Delta z\bar{\rho}\int_0^B v_k dx \qquad (61)$$

this yields

$$M_k = 2NWb\Delta z\bar{\rho}\{v_m(F_1+F_2)+v_a(F_3+F_4)\} \qquad (62)$$

from which the time derivative is

$$\frac{dM_k}{dt} = 2NWb\Delta z\Big(\frac{d\rho}{dt}\{v_m(F_1+F_2)+v_a(F_3+F_4)\} + \rho(F_1+F_2)\frac{dv_m}{dt}+\rho(F_3+F_4)\frac{dv_a}{dt}\Big) \qquad (63)$$

ii. Momentum flux

The momentum flux across station k is

$$\dot{M}_k = \int_A \rho v^2 dA$$

$$= 2NW\int_0^B \rho_k v_k^2 dx$$

$$= 2NWb_k\int_0^\xi \rho_k v_k^2 d\xi \qquad (64)$$

Scalars are used in the above since the directions (signs) are understood at each station to be given by:

$$-\left(\underline{i}_v \cdot \underline{n}\right)_k = +1 \tag{65a}$$

$$+\left(\underline{i}_v \cdot \underline{n}\right)_{k+1} = -1 \tag{65b}$$

Recall that

$$v = v_o(1-\Phi) + v_m\Phi$$

where

$$\Phi(\xi) = \left\{\begin{matrix}\left(1-\xi^{1.5}\right)^2, & 0 \le \xi < 1 \\ 0, & 1 \le \xi \le \hat{\xi}\end{matrix}\right\}$$

then

$$v^2 = v_o^2(1-\Phi)^2 + v_m^2\Phi^2 + 2v_o v_m\left(\Phi - \Phi^2\right)$$

and so

$$\dot{M} = 2NWb\int_0^{\xi}\left\{\rho_o(1-\Lambda) + \rho_m\Lambda\right\}\left\{v_o^2(1-\Phi)^2 + v_m^2\Phi^2 + 2v_o v_m\left(\Phi-\Phi^2\right)\right\}d\xi \tag{67}$$

Performing the multiplications,

$$\begin{aligned}\dot{M} = 2NWb\int_0^{\xi}\{&\rho_o v_o^2(1-\Phi)^2(1-\Lambda) + \rho_m v_o^2(1-\Phi)^2\Lambda \\ &+\rho_o v_m^2(1-\Lambda)\Phi^2 + \rho_m v_m^2\Lambda\Phi^2 \\ &+ 2\rho_o v_o v_m(1-\Lambda)\left(\Phi-\Phi^2\right) + 2\rho_m v_o v_m\Lambda\left(\Phi-\Phi^2\right)\}d\xi\end{aligned} \tag{68}$$

Introduce a set of integrals G_i

$$G_1 = \int \Lambda\Phi^2 d\xi = 243/770 \tag{69a}$$

$$G_2 = \int \Lambda(1-\Phi)^2 d\xi = 320/770 \tag{69b}$$

$$G_3 = 2\int \Lambda\left(\Phi - \Phi^2\right)d\xi = 414/1540 \tag{69c}$$

$$G_4 = \int (1-\Lambda)\Phi^2 d\xi = 0 \tag{69d}$$

$$G_5 = \int (1-\Lambda)(1-\Phi)^2 d\xi = \hat{\xi} - 1 \tag{69e}$$

$$G_6 = 2\int (1-\Lambda)\left(\Phi - \Phi^2\right)d\xi = 0 \tag{69f}$$

so that

$$\dot{M} = 2NWb\{\rho_m v_m^2 G_1 + \rho_m v_a^2 G_2 + \rho_m v_a v_m G_3 + \rho_a v_m^2 G_4 + \rho_a v_a^2 G_5 + \rho_a v_a v_m G_6\} \tag{70}$$

$$\dot{M} = 2NWb\{Z_2\} \tag{71}$$

The net momentum flux is therefore

$$-\oint_A \rho v^2 (\underline{i}_v \cdot \underline{n})\underline{i}_v dA = \left(\dot{M}_k - \dot{M}_{k+1}\right)\underline{i}_v$$

$$= 2NW\left(b_k Z_{2_k} - b_{k+1} Z_{2_{k-1}}\right)(+\underline{i}_v) \tag{72}$$

iii. Static pressure integral

The surface pressure integral is re-written as

$$-\oint_A P(\underline{I}\cdot\underline{n})dA = -\int_{A_k} P(+i\cdot(-i))dA - \int_{A_{k-1}} P(+\underline{i}\cdot\underline{i}))dA \tag{73}$$

so application of the self-similar profiles is restricted to the equation

$$\int_A P\,dA = 2NWb\int_0^{\xi} P\,d\xi \tag{74}$$

from which we obtain

$$\int_A P\,dA = 2NWb\int_0^{\xi}\{P_o(1-A)+P_m A\}d\xi$$

$$= 2NWb\{P_m E_1 + P_o E_2\}$$

$$= 2NWb Z_0 \qquad (75)$$

where E_1 and E_2 have been previously defined.

The surface pressure integral is now given by

$$-\oint_A P(\underline{I}\cdot\underline{n})dA = +2NW\{b_k Z_{0,k} - b_{k+1} Z_{0,k+1}\} \qquad (76)$$

iv. Wall friction

Frictional effects are considered an explicit function of velocity, pressure, and temperature (or density)

$$\underline{F}_k = \underline{F}_k(\rho_i, v_i, P_i) \qquad (77)$$

but in the first approximation frictional effects are neglected.

v. Summary of components

The modified form of the momentum equation is given by summary of the components discussed above, the result is

$$2NWb_{k+1}\,\Delta z\{\frac{d\rho}{dt}\{v_m(F_1+F_2)+v_o(F_3+F_4)\}$$

$$+\frac{dv_m}{dt}\rho(F_1+F_2)+\frac{dv_o}{dt}\rho(F_3+F_4)\}$$

$$= 2NW(b_k Z_2 - b_{k+1} Z_2) + 2NW(b_k Z_0 - b_{k+1} Z_{0_k}) \qquad (78)$$

The last term has the simple interpretation of the *net* momentum flux,

$$\dot{M}_{Net} = 2NWb_k(Z_{2_k}+Z_{0_k}) + 2NWb_{k+1}(Z_{2_{k+1}}+Z_{0_{k+1}}) \qquad (79)$$

where at the ejector inlet

$$\dot{M}_{Net_1} = A_{1P}(P_{1P}+\rho_{1P}v_{1P}^2)+A_{1S}(P_{1S}+\rho_{1S}v_{1S}^2) \qquad (80)$$

A solution for the time derivative of velocity can now be extracted

$$\frac{dv_m}{dt} = \frac{\dot{M}_{Nel}}{2NWb_{k+1}\Delta z} - \frac{d\rho}{dt}\frac{1}{\rho}\left\{v_m + v_a\left(\frac{F_3+F_4}{F_1+F_2}\right)\right\} - \frac{dv_a}{dt}\left(\frac{F_3+F_4}{F_1+F_2}\right) \qquad (81)$$

Application to the energy equation

The form of the energy equation most conveniently adapted to the finite volume analysis is the heat equation, given in integral form as

$$\frac{d}{dt}\int_\Omega p\,dV = -\gamma\oint_S p\underline{v}\cdot\underline{n}\,dA - (\gamma-1)\oint_S p\underline{U}\cdot\underline{n}\,dA \qquad (82)$$

Distinction between this interpretation of the energy equation and the *mechanical* and *general power* equations is described in appendicies A and B. Term by term evaluation follows; in all discussions use has been made of the uniform transverse pressure and density assumption.

i. Surface flux terms

Since pressure and density have similar representations, the pressure energy-flux term is similar to the mass flux term; by direct analogy

$$\dot{e}_p = -\gamma\oint_s p\underline{v}\cdot\underline{n}\,dA = \dot{e}_k - \dot{e}_{k+1} \qquad (83)$$

where

$$\dot{e}_k = \gamma 2NWb_k p\left\{v_m(F_1+F_2)+v_a(F_3+F_4)\right\}$$
$$= \gamma 2NWbZ_4 \qquad (84)$$

and where the self-similar profile integrals F_i are the same as defined previously.

The pressure-energy flux associated with the free-stream is

$$-(\gamma-1)\oint_S p\underline{U}\cdot\underline{n}\,dA = (\gamma-1)UA(p_k - p_{k+1}) \qquad (85)$$

If desired, the area term can be re-written as

$$A_k = 2NWb_k(E_1+E_2) \qquad (86)$$

or

$$A_k = 2NWb_k\xi_k = 2NWB \tag{87}$$

ii. Time rate-of-change of energy

The volume integral of pressure cast in finite volume form is (see discussion on conservation of mass)

$$\int p\,dV = 2NWB\Delta z\,p \tag{88}$$

and has the time derivative

$$\frac{d}{dt}\int p\,dV = 2NWB\Delta z\left(\frac{dp}{dt}\right)_k \tag{89}$$

Considerable simplification of the time-derivative is realized from the approximation that static properties at station k are characteristic of the finite-volume element. This is not a statement of *uniform* volume thermodynamic properties, rather, that the reference for derivative computations can be approximately given at either station k or $k+1$.

iii. Summary of components

In modified form the heat equation is

$$2NWB\Delta z\left(\frac{dp}{dt}\right)_k = \gamma\, 2NW\left(b_kZ_1 - b_{k+1}Z_1\right) + (\gamma-1)U\,2NW\left(b_kZ_0 - b_{k+1}Z_0\right) \tag{90}$$

from which

$$\left(\frac{dp}{dt}\right)_k = \frac{\gamma}{\Delta zB}\left(b_kZ_1 - b_{k+1}Z_1\right) + \frac{\gamma-1}{\Delta zB}U\left(b_kZ_0 - b_{k+1}Z_0\right) \tag{91}$$

Homentropic secondary flow

Analysis of a finite-volume element whose cross-section spans the mixing region provides a relationship in time and space between the primary and secondary flows. The description of the mixing region is incomplete, however, since the basic profiles used previously only represent the characteristics of the jet boundary layer and not those of the secondary flow itself. In this situation an inviscid, homentropic flow assumption for the secondary flow provides closure for the mathematical representation of the mixing region.

The present analysis is predicated on a shock-free flow. However, as mentioned by Anderson [1970a,b], introduction of shocks could be explicitly introduced through discontinuities in the initial flow field.

Homentropic flow is distinguished by the absence of temporial *and* spatial gradients of entropy

$$\frac{Ds}{Dt} = \nabla s = 0 \tag{92}$$

Entropy jumps across a shock violate this condition. Nonetheless, in this work the fact that entropy is assumed uniform throughout allows the fluid flow to be described by the relation

$$\frac{P}{\rho^{\gamma}} = const \tag{93}$$

This replaces the need for the energy equation, but adherence to conservation of mass and momentum remains. The derivative of this expression yields

$$\frac{dP}{d\rho} = \frac{P\gamma}{\rho}$$

and thus

$$\left(\frac{dP}{dt}\right)_k = \left(\frac{\gamma P_e}{\rho}\right)_k \left(\frac{d\rho}{dt}\right)_k \tag{94}$$

Conservation of mass allows for the computation of the density gradient in the secondary flow, but the representation chosen here is to compute the gradient one time step after changes in the primary flow have been computed. A point function computation arises

$$\left(\frac{d\rho}{dt}\right)_k = \frac{(\rho_k)_{t+\Delta t} - (\rho_k)_t}{\Delta t} \tag{95}$$

A description of the entrained velocity derived either through a solution of the momentum equation for the secondary flow, or, as in the present work, use of a kinetic energy transfer function. The momentum equation approach is noted briefly below. Details on the kinetic energy function are given later.

i. Momentum

For an inviscid flow assumption Euler's equation represents the momentum equation for a material volume. Although previous discussions consider extention to a material volume, the assumed existance of a streamline for the homentropic flow is a valid simplification. For one-dimensional flow we have

$$\frac{\partial v}{\partial t}+\frac{\partial U}{\partial t} = -(v+U)\frac{\partial v}{\partial z}-\frac{1}{\rho}\frac{\partial P}{\partial z}$$

Finite difference approximations for the streamwise derivatives give the time derivative of velocity in terms of velocity and pressure at stations k-1, k, and $k+1$.

Finite volume initialization

Nomenclature for the virtual grid used in the finite-volume initialization is given in figure 15. Initialization of pressure, velocity, and density is based on steady-state versions of the mass, momentum, and energy equations. The assumption is made that the uniform pressure and density profiles apply. Application is discussed below.

Conservation of mass

Elimination of time derivatives in the mass conservation equation produces

$$0 = 2NWb_iZ_{1_i}-2NWb_jZ_{1_j} \tag{96}$$

where

$$Z_1 = \rho_m v_m F_1+\rho_e v_m F_2+\rho_m v_e F_3+\rho_e v_e F_4 \tag{97}$$

Now since

$$\dot{m}_1 = 2NWb_1Z_{1_1} \tag{98}$$

then the centerline density is

$$\rho_j\left\{v_m(F_1+F_2)+v_e(F_3+F_4)\right\} = \frac{\dot{m}_1}{2NWb_j} \tag{99}$$

which becomes

$$\rho_j\left\{v_m+v_e\left(\frac{F_3+F_4}{F_1+F_2}\right)\right\} = \frac{\dot{m}_1}{2NWb_j(F_1+F_2)} \tag{100}$$

Solving for density, we obtain

$$\rho_j = \frac{a}{v_m + b} \tag{101}$$

where

$$a = \frac{\dot{m}_1}{2NWb_j(F_1 + F_2)} \tag{102}$$

and

$$b = v_e\left(\frac{F_3 + F_4}{F_1 + F_2}\right) \tag{103}$$

Conservation of momentum

Computation of the jet centerline velocity derives from the momentum equation and assumes the entraned velocity is known. First, recognize the discharge momentum is

$$M_1 = A_{1P}\left(P_{1P} + \rho_{1P}v_{1P}^2\right) + A_{1S}\left(P_{1S} + \rho_{1S}v_{1S}^2\right) \tag{104}$$

and then at station k

$$M_{1_k} = 2NWb_k\left(Z_{0_k} + Z_{2_k}\right) \tag{105}$$

where

$$Z_0 = \left\{P_m E_1 + P_e E_2\right\} \tag{106}$$

$$Z_2 = \{\rho_m v_m^2 G_1 + \rho_m v_e^2 G_2 + \rho_m v_e v_m G_3 + \rho_e v_m^2 G_4 + \rho_e v_e^2 G_5 + \rho_e v_e v_m G_6\} \tag{107}$$

then

$$\frac{M_1}{2NWb_j} = p\left(E_1 + E_2\right) + \rho\left\{v_m^2\left(G_1 + G_4\right) + v_e^2\left(G_2 + G_5\right) + v_e v_m\left(G_3 + G_6\right)\right\} \tag{108}$$

Normalization yields

$$\frac{M_1}{2NWb_j(G_1+G_4)} = p\left(\frac{E_1+E_2}{G_1+G_4}\right)+\rho\left\{v_m^2+v_e^2\left(\frac{G_2+G_5}{G_1+G_4}\right)+v_e v_m\left(\frac{G_3+G_6}{G_1+G_4}\right)\right\} \tag{109}$$

which has the shorthand notation

$$\rho\left(v_m^2+v_m c+d\right)+pe = f \tag{110}$$

where

$$c = v_e\left(\frac{G_3+G_6}{G_1+G_4}\right) \tag{111a}$$

$$d = v_e^2\left(\frac{G_2+G_5}{G_1+G_4}\right) \tag{111b}$$

$$e = \left(\frac{E_1+E_2}{G_1+G_4}\right) \tag{111c}$$

$$f = \frac{M_1}{2NWb_j(G_1+G_4)} \tag{111d}$$

Conservation of energy

The steady-state result for conservation of energy is

$$\begin{aligned} 0 &= \oint p\underline{u}\cdot\underline{n}\,dA \\ &= 2NW\left\{b_k Z_{4_k}-b_j Z_{4_j}\right\} \end{aligned} \tag{112}$$

and therefore (by analogy with the conservation of mass discussion)

$$p = \frac{g}{v_m+b} \tag{113}$$

where

$$g = \frac{Z_{4_0}}{2NWb_j(F_1+F_2)} \tag{114}$$

This transformation of the thermal energy exchange is supplemented by the constant enthalpy relation applicable to homentropic flows (see earlier discussion).

Solution of the system of equations

Substitute the density and pressure representations into the simplified momentum equation so that velocity remains the only unknown

$$\frac{a}{v_m + b}\left(v_m^2 + v_m c + d\right) + \frac{ge}{v_m + b} = f \tag{115}$$

then by re-arrangement

$$v_m^2 + v_m c + d + \frac{ge}{a} = \frac{f}{a}\left(v_m + b\right) \tag{116}$$

$$v_m^2 + v_m\left(c - \frac{f}{a}\right) + d + \frac{ge}{a} - \frac{bf}{a} = 0 \tag{117}$$

$$v_m^2 + v_m B + C = 0 \tag{118}$$

This quadratic equation has the solution

$$v_m = -\frac{B}{2} \pm \frac{1}{2}\sqrt{B^2 - 4C} \tag{119}$$

where

$$\begin{aligned} B &= c - \frac{f}{a} \\ &= v_e\left(\frac{G_3 + G_6}{G_1 + G_4}\right) - \frac{M_1}{\dot{m}_1}\left(\frac{F_1 + F_2}{G_1 + G_4}\right) \end{aligned} \tag{120}$$

$$\begin{aligned} C &= d + \frac{ge}{a} - \frac{bf}{a} \\ &= v_e^2\left(\frac{G_2 + G_5}{G_1 + G_4}\right) + \frac{Z_{4,0}}{\dot{m}_1}\left(\frac{E_1 + E_2}{G_1 + G_4}\right) - v_e\frac{M_1}{\dot{m}_1}\left(\frac{F_3 + F_4}{G_1 + G_4}\right) \end{aligned} \tag{121}$$

Kinetic Energy Exchange

Analysis of the primary and secondary flow interaction has not, to this point, been completed. By themselves, the self-similar profiles close the loop for *steady-state flows*, but not *transient* ones ! This section provides an approximation for the turbulent flow kinetic energy exchange mechanism to characterize the influence of primary flow changes on the secondary flow.

Kinetic Energy Computation from Self-Similar Profiles

Kinetic energy can be computed by the integral of the product of velocity and momentum (as described in Appendix B); from this there results the scalar quantity

$$KE = \frac{1}{2}\int_s \rho v^3 dS \tag{122}$$

By substitution for the self-similar velocity profiles and with the use of a uniform density approximation, the kinetic energy becomes

$$KE = NWb\rho \int_{\xi_1}^{\xi_2} \left\{ v_o(1-\Phi) + v_m \Phi \right\}^3 d\xi \tag{123}$$

If it is assumed

$$\xi_2 \geq 1$$

then

$$KE = NWb\rho \left(\int_{\xi_1}^{1} \left\{ v_o(1-\Phi) + v_m \Phi \right\}^3 d\xi + \int_1^{\xi_2} v_o^3 d\xi \right) \tag{124}$$

Upon integration

$$KE = NWb\rho \left(v_o^3 H_1 + v_o v_m^2 H_2 + v_m v_o^2 H_3 + v_m^3 H_4 + v_o^3 H_5 \right) \tag{125}$$

where the H_i integrals are given in Appendix H.

Change in Kinetic Energy of Secondary Stream due to Mixing

Computation of the gain in secondary flow kinetic energy can be made by direct extension of the general kinetic energy relation above

$$\Delta KE = \int_{\xi}^{\xi} \rho v \left(\frac{v^2}{2} - \frac{v_o^2}{2} \right) d\xi \tag{126}$$

where ζ defines the jet boundary streamline (for which the secondary mass flow through station *i* is equal to primary mass flow through *i*). For the present discussion this dividing streamline is assumed known; Appendix L illustrates the typical approach of analysis. Expanding the equation for the change in kinetic energy yields

$$\Delta KE = NWb\rho\left\{\int_{\zeta}^{1}\left(v^3 - vv_e^2\right)d\xi + \int_{1}^{\xi}\left(v^3 - vv_e^2\right)d\xi\right\} \tag{127}$$

Consider the integration as the sum of the following four components:

$$I_a = \int_{\zeta}^{1} v^3 d\xi$$

$$= v_e^3 H_1 + v_e v_m^2 H_2 + v_m^3 H_4 \tag{128a}$$

$$I_b = \int_{1}^{\xi} v^3 d\xi$$

$$= v_e^3 H_5 \tag{128b}$$

$$I_c = \int_{\zeta}^{1} vv_e^2 d\xi$$

$$= v_m v_e^2 F_1 + v_e^3 F_3 \tag{128c}$$

$$I_d = \int_{1}^{\xi} vv_e^2 d\xi$$

$$= v_e^3 F_4 \tag{128d}$$

In sum, the change in kinetic energy of the entrained flow is

$$\Delta KE = NWb\rho\{v_e^3\left(H_1 + H_5 - F_3 - F_4\right) + v_m v_e^2\left(H_3 - F_1\right) + v_m^2 v_e H_2 + v_m^3 H_4\} \tag{129}$$

Change in Primary Flow Kinetic Energy due to Mixing

In a similar way as the change in secondary flow kinetic energy was computed, the energy loss of the primary flow is given by

$$\Delta KE = \int_{0}^{\zeta} \rho v\left(\frac{v^2}{2} - \frac{v_m^2}{2}\right)d\xi \tag{130}$$

where the limits of integration reflect interest in the domain of the primary jet cross-section.

Evaluation of the integral at station *i* yields the result

$$\Delta KE = NWb\rho\left(v_*^3 H_1 + v_* v_m^2 H_2 + v_m v_*^2 H_3 + v_m^3 H_4 - v_m^3 F_1 - v_* v_m^2 F_3\right) \tag{131}$$

Kinetic Energy Balance

Computations for a specified steady-state condition show that the change in kinetic energy due to *mixing* is not the same for the secondary flow as it is for the primary. Figure 18 illustrates some typical results (for *net* changes in kinetic energy between the input and discharge of the mixing region). In fact, the gain in kinetic energy of the secondary flow is entirely due to the mixing process, while the mixing loss of the primary flow is only a fraction of its total loss. In balance, however, the total change of kinetic energy of the primary flow is greater than that of the secondary flow.

In the works of Korst and Chow [1966] and Chow and Addy [1964] the relationship between the change in entrained flow kinetic energy and the total primary flow kinetic energy is given by

$$E_m = \frac{\Delta KE_{1S}}{\frac{1}{2}\rho_{1P} v_{1P}^3} \frac{\sigma}{z} \tag{132}$$

where a value of 12 for σ for turbulent flow provides a reasonable match between theory and experiment for low-speed flows. At higher speeds the relationship

$$\sigma = 12 + 2.758 M_{1P} \tag{133}$$

is sometimes used. The important feature of this result is that the change in secondary flow kinetic energy has the functional form

$$\Delta KE_{1S} = F\left(KE_{1P}, \frac{\sigma}{z}\right) \tag{134}$$

The difficulty with the energy transfer function described above is that it provides (by default) a quasi-steady flow approximation. It therefore cannot be used for the transient flow in its present form. To entertain local changes in primary-secondary kinetic energy in a way that does not burden the computational procedure, consider the modified function

$$\Delta KE_{1S} = \hat{F}\left(\Delta KE_{1P,m}\right) \tag{135}$$

where the subscript m denotes the loss in kinetic energy due to mixing. Numerical testing suggests that

$$(\Delta KE_{1S})^{t+\Delta t} = (\Delta KE_{1S,m})^{t+\Delta t} + C_1 \frac{\sigma^2 z}{(1+M_{1P})} (\Delta KE_{1P,m})^{t} \qquad (136)$$

This enhancement arises from the assumption that local velocity gradients in the steady flow case are typically less that the gradients experienced in the transient mode. Here, the introduction of an engineering approximation also results in the introduction of an undetermined constant, C_1. The alternative is to establish N computations of the kinetic energy exchange to coincide with the N control volumes of the mixing region; the present method permits post-processing KE information at the completion of mixing region calculations. Sample calculations indicate

$$C_1 \sim 0.95 - 1.00 \qquad (137)$$

Summary of Method

This chapter has introduced the continuity, momentum, and energy equations required for the analysis of the ejector mixing region. A quasi-steady flow assumption for the inlet and diffuser relieves us from repeating the chapter 5 discussions for those components here. The energy equation is supplemented by the kinetic energy exchange equations presented above. Figure 19 summarises the solution methodology for the unsteady flow problem. As expected, several steps are common with the steady flow solution, especially in the initialization process (recall figure 11). Some remarks are given below to highlight the assumed kinetic energy exchange process.

Communication between primary and secondary flow in the present work is based in part on kinetic energy gain by the secondary flow due to kinetic energy loss of the secondary flow. Such calculations are for the specific purpose of updating the secondary flow as time evolves (changes in the primary flow are effected through solution of the traditional momentum and energy equations for the same). Three steps are involved:

1. For a flow condition given after the primary flow has advanced forward in time, compute the jet streamline position at station N, for simplicity this station is taken to be the point of mixing region discharge.

2. Compute the entrained flow kinetic energy gain before and after the change in primary flow conditions; the difference is the net change in entrained flow kinetic energy due to changes in primary flow.

3. Update the entrained influx kinetic energy for the net change within the mixing region; extract the new secondary flow inlet velocity.

7. DISCUSSION OF RESULTS

Characteristic Test Case

In the absence of data from transient flow ejector experiments (or even from modern multi-dimensional Navier-Stokes solvers), "verification" that the proposed ejector analysis can provide reasonable thrust predictions must be left to engineering judgement. Because of this, a "familiar" ejector forcing function must be used. In the present work the system response to a step-function input is not only a characteristic transient case study, but the scenario is also coincident with typical STOVL ejector application.

For demonstration purposes the ejector system response to a step-change in primary nozzle flowrate from 18.7 to 21.85 lb_m/sec is chosen because (a) experimental steady-state data at each of these operating points is available, and (b) the 17% change in primary flowrate is well beyond a "small"-perturbation examination (this exercises the system non-linearities). Changes in primary flow stagnation temperature are taken from data given with flowrate data, but the corresponding static pressure is computed by the procedure given in Appendix J.

Calculation Results

For the mixing region finite-volume length of 0.18 ft and a characteristic mixing region velocity of 500 ft/s, the characteristic time step for computations is

$$\Delta t = \frac{0.18}{500} \cong 0.4 ms$$

To avoid infringing on this stability limit a computational time step of 0.1 ms was established; 100 time steps provided the necessary interval for examination of the step-function test case.

The empirical coefficient in the transient analysis, C_1 (required for calibration of the primary-to-secondary kinetic energy exchange mechanism), was selected to match the asyptotic transient thrust prediction with the quasi-steady value at the new set point; satisfying this condition required

$$C_1 = 0.97$$

Figure 20 illustrates the predicted ejector thrust profile for this coefficient. It appears the 2 millisecond residence time of the flow (elapsed time for primary nozzle flow to reach the diffuser exit plane) is slightly less than the 3 millisecond interval for the thrust to reach a new maximum. Oscillations in thrust after that point appear to settle in about 5 milliseconds.

An unexpected feature of the thrust profile is the dip in thrust immediately following the step-change in primary nozzle efflux. Examination of the field variable profiles reveals this is not a numerical problem, but that the increase in static pressure associated with the instantaneous change in driving flow temporarily impedes the secondary flow. After a short period, the secondary flow kinetic energy builds (commesurate with the increase in primary flow energy) to overcome this effect, then continues in the intuitively expected manner.

Remarks

A distinctive second-order flavor is displayed by the predicted thrust profile; under a second-order assumption the ejector test case has approximately a 0.75 damping ratio and a natural frequency on the order of 300 Hz. Although the results seem reasonable, it is necessary to conduct more extensive computational tests before conclusions about the order or linearity (about the perturbation) of the system can be made. The purpose here is to establish the routine is operational and that it can in fact provide reasonable results between two steady-state conditions.

The strongest criticizim of the proposed method of analysis probably lies within the entrained flow prediction by kinetic energy exchange; the one-dimensional flow limitation has required the traditional theoretical analysis of the problem to be modified and an empirical coefficient introduced. This may mitigate the robust nature of the simulation approach and require fine-tuning for a specific ejector configuration. Once this has been established, however, the simulation permits characterization of the transient ejector behavior very quickly, for a wide spectrum of operating conditions. If it determined the ejector time constants are "small enough" so as to be neglected (relative to time constants for other propulsion system components) then a quasi-steady flow assumption for the ejector mixing-region may be valid.

8. CONCLUSION

Assumption Highlights

It should remain clear the intent of the proposed finite volume method of analysis is to meet the combined requirements of

1. Thrust prediction for *real-time* simulation,
2. A *predictive* fluid-dynamic methodology, and
3. Characterization of *turbulent* flow.

As a result of the assumptions and compromises that must be made to reach these goals, two empirical constants have been introduced. The result is a simulation detailed enough to allow a rational introduction of experimental data in the simulation, while at the same time being of a simple nature; this is anticipated to provide a realistic candidate for real-time simulation. Several assumptions made with this goal in mind (and with significant impact on the algorithm structure) are worth repeating:

1. Primary nozzle and all free-stream conditions are known as a function of time.
2. Quasi-steady flow conditions exist at the inlet and diffuser.
3. Entrained flow velocity predictions are adequately given by the proposed kinetic energy exchange mechanism.

Exploration of a step-function test case reveals that items 2 and 3 appear not to have compromised the fundamental description of ejector physics.

Closing Remarks

The method of analysis for the description of transient ejector characteristics provides reasonable results for the single test case considered. As such, the method can be concluded as viable if the specific intent of development is kept in mind. An operational computer program has been based on the equations presented. Application of the method to a broad class of ejector configurations and operating parameters will require exploration into the sensitivity of the two empirical coefficients introduced in the course of the analysis.

As more detailed experimental and theoretical treatment on the theory of turblent mixing evolve, it remains to make practical application of those results to the ejector analysis. It remains that the basic turbulent flow control volume approach is an excellent vehicle on which to test new (or modified versions of the present) method of turbulent mixing characterization.

Solutions to some of the equations described in this work have, due to the limited time available, been solved iteratively. There is considerable opportunity to decrease the execution time of the method by replacing the iterative rotuines with analytic solutions. Such solutions may be available in future work through application of, for instance, the MACSYMA symbolic manipulator.

REFERENCES

Abramovich,G.N. (1963), The theory of turbulent jets, MIT Press.

Addy,A.L., J.C.Dutton, and C.D.Mikkelsen (1981), Ejector-diffuser theory and experiments," Report No. UILU-ENG-82-4001, Department of Mechanical and Industrial Engineering,University of Illinois at Urbana-Champaign, Ill.

Addy,A.L. and Mikkelsen,C.D. (1974), "An investigation of gas dynamic flow problems in chemical laser systems," Report No. UILU-ENG-74-4009, Department of Mechanical and Industrial Engineering, University of Illinois at Urbana-Champaign, Ill.

Alperin, M. and J. Wu (1983a), "Thrust augmenting ejectors, I," AIAA Journal, V.21, Oct, pp.1428-1436.

Alperin, M. and J. Wu (1983b), "Thrust augmenting ejectors,II," AIAA Journal, V.21, Dec, pp.1698-1706.

Anderson, B.H. (1974a), "Assessment of an analytical procedure for predicting supersonic ejector nozzle performance," NASA TN D-7601.

Anderson, B.H. (1974b), "Computer program for calculating the flow field of supersonic ejector nozzles," NASA TN D-7602.

Anderson, J.D. (1970a), "A time-dependent analysis for vibrational and chemical non-equilibrium nozzle flows," AIAA Journal, V.8, No.3, pp.545-550.

Anderson, J.D. (1970b), "A time-dependent solution of nonequilibrium nozzle flows - A sequal," AIAA Journal, V.8, No.12, pp.2280-2282.

Bernal, L. and V.Sarohia (1983), "Entrainment and mixing in thrust augmenting ejectors," AIAA 83-0172

Bevilaqua, P.M. (1974), "Evaluation of hypermixing for thrust augmenting ejectors," J. Aircraft, V.11, No.6, pp.348-354.

Bevilaqua, P.M. (1984), "Advances in ejector thrust augmentation," AIAA Paper 84-2425.

Braden, R.P., K.S.Nagarja, and H.J.P.VanOhain (1982), Proceedings: Ejector Workshop for Aerospace Applications, AFWAL-TR-82-3059.

Drummond, C.K. (1985), "Numerical analysis of mass transfer from a sphere in an oscillatory flow," Ph.D Thesis, Syracuse University, 1985.

Drummond, C.K. and F.A.Lyman (1986), "Numerical Analysis of secondary streaming in the vicinity of a sphere," Forum on Unsteady Flows, ASME FED, V.39.

Dutton, J.C. and B.F.Carroll (1983), "Optimized ejector-diffuser design procedure for natural gas vapor recovery, "ASME Journal of Energy Resources Technology, V.105, No.3, pp.388-393.

Dutton, J.C. and B.F. Carroll (1986), "Optimal supersonic ejector designs," ASME Transactions, Journal of Fluids Engineering. V.108, December 1986, pp.414-420.

Fabri, J. and R.Siestrunck (1958), "Supersonic air ejectors, "Advances in Applied Mechanics, Vol.V, Academic Press, pp.1-34.

Hedges, K.R. and P.G.Hill (1974), "Compressible flow ejectors, Part I - Development of a Finite-Diference flow model," ASME Paper No.74-FE-1. Also, Transactions of the ASME, Journal of Fluids Engineering, September, pp.272-281.

Hussain, A.M. (1981), "Role of coherent structures in turbulent shear flows," Proc. Indian Acad. Sci. (Engg. Sci.), Vol.4, Pt.2, pp.129-175.

Kentfield,J.A.C. (1978), "Prediction of performance of low pressure ratio thrust augmenting ejectors," Journal of Aircraft, V.15, pp.849-856.

Knott, P.G. and D.N.Cundy (1986), "Installation aerodynamics of ejectors in combat aircraft," Aeronautical Journal, V.90, December, pp.410-413.

Koening, D.G., F.Stoll, and K.Aoyagi (1981), "Application of thrusting ejectors to tactical aircraft having vertical lift and short-field capability," AIAA Paper 81-2629.

Korst, H.H. and W.L.Chow (1966), "Non-isoenergetic turbulent jet mixing between two compressible streams at constant pressure," NASA CR-419.

Krothapalli, A., D. Baganoff, and K. Karamcheti (1980), "Development and structure of a rectangular jet in a multiple jet configuration," AIAA Journal, V.18, No.8, pp.945-950.

Liepmann,H.W. (1979), "The rise and fall of ideas in turbulence," American Scientist, V.67, pp.221-228.

Lund,T.S., D.A.Tavella, and L.Roberts (1986), "Analysis of interacting dual lifting ejector systems," AIAA Paper 86-0478.

Mikkelsen, C.D., M.R.Sandberg, and A.L.Addy (1976), "Theoretical and experimental analysis of the constant area, supersonic - supersonic ejector," Report UILU-ENG-76-4003, Department of Mechanical and Industrial Engineering, University of Illinois at Urbana-Champaign.

Miller, D.R. and E.W. Comings (1957), "Static Pressure distribution in the free turbulent jet", JFM, pp.1-16.

Minardi, J.E. (1982), "Characteristics of high performance ejectors," Proceedings: Ejector Workshop for Aerospace Applications, pp.179-279.

Minardi, J.E. (1982), "Compressible flow ejector analysis with application to energy conversion and thrust augmentation," AIAA Paper 82-0133.

Qian,H., M.Zhang, and G.Ye (1984), "A method for calculating the performance of ejector nozzles," Journal of Engineering Thermophysics, V.5, February, pp.47-50.

Salter,G.E. (1975), "Method for analysis of V/Stol aircraft ejectors," Journal of Aircraft, V.12, pp.974-978.

Seldner,K., J.R.Mihaloew, and R.J.Blaha (1972),"Generalized simulation technique for turbo-jet engine system analysis," NASA TN-D-6610.

Shen,H., E.Dong, T.Shyur, and M.Kee (1981), "The sweep finite element method for calculating the flow field and performance of supersonic ejector nozzles," Proceedings: Fifth International Symposium on Air Breathing Engines.

Tavella,D. and L.Roberts (1984), "A simple viscous-inviscid aerodynamic analysis of two-dimensional ejectors," AIAA Paper 84-0281.

Thompson,P.A. (1972), Compressible Fluid Dynamics, New York: McGraw-Hill.

BIBLIOGRAPHY

Abramovich,G.N. (1963), The theory of turbulent jets, MIT Press.

Addy,A.L., J.C.Dutton, and C.D.Mikkelsen (1981), Ejector-diffuser theory and experiments," Report No. UILU-ENG-82-4001, Department of Mechanical and Industrial Engineering,University of Illinois at Urbana-Champaign, Ill.

Addy,A.L. and Mikkelsen,C.D. (1974), "An investigation of gas dynamic flow problems in chemical laser systems," Report No. UILU-ENG-74-4009, Department of Mechanical and Industrial Engineering, University of Illinois at Urbana-Champaign, Ill.

Alperin, M. and J. Wu (1983a), "Thrust augmenting ejectors, I," AIAA Journal, V.21, Oct, pp.1428-1436.

Alperin, M. and J. Wu (1983b), "Thrust augmenting ejectors,II," AIAA Journal, V.21, Dec, pp.1698-1706.

Anderson, B.H. (1974a), "Assessment of an analytical procedure for predicting supersonic ejector nozzle performance," NASA TN D-7601.

Anderson, B.H. (1974b), "Computer program for calculating the flow field of supersonic ejector nozzles," NASA TN D-7602.

Anderson, J.D. (1970a), "A time-dependent analysis for vibrational and chemical non-equilibrium nozzle flows," AIAA Journal, V.8, No.3, pp.545-550.

Anderson, J.D. (1970b), "A time-dependent solution of nonequilibrium nozzle flows - A sequal," AIAA Journal, V.8, No.12, pp.2280-2282.

Anderson, J.D. (1976): Gasdynamic lasers: An Introduction. Academic Press

Banks, D.W. and G.M. Gatlin (1986), "Longitudinal and lateral aerodynamic data from tests of an advanced STOVL fighter employing a powered lift ejector," NASA TM 87672.

Batterton, P.G. and B. J. Blaha (1987), "NASA supersonic STOVL technology program," NASA TM 100227.

Beard, B.B. and W.H.Foley (1982), "An engine trade study for a supersonic STOVL fighter/attack aircraft," NASA CR-166304.

Beheim, M.A., B.H.Anderson, J.S.Clark, B.W.Corson, L.E.Stitt,and F.A.Wilcox (1970), "Supersonic exhaust nozzles," in Aircraft Propulsion, NASA SP-259, pp.233-282.

Berg, D.F. (1982), "F101 DFE preliminary study: Transient performance customer deck - User's manual," GE-R82AEB507.

Bernal, L. and V.Sarohia (1983), "Entrainment and mixing in thrust augmenting ejectors," AIAA 83-0172

Bernstein, A., C.Hevenor, and W.Heiser (1967), "Compound-compressible nozzle flow," AIAA Paper 66-663; also: J. Appl. Mechanics, V.34, No.3, Sept.1967, pp.548-554.

Bevilaqua, P.M. (1974), "Evaluation of hypermixing for thrust augmenting ejectors," J. Aircraft, V.11, No.6, pp.348-354.

Bevilaqua, P.M. (1984), "Advances in ejector thrust augmentation," AIAA Paper 84-2425.

Bodden,D.S., D.W.Whatley, and R.K.Douglas (1987),"E-7 STOVL aircraft low speed flight control system," AIAA Paper 87-2903.

Braden, R.P., K.S.Nagarja, and H.J.P.VanOhain (1982), Proceedings: Ejector Workshop for Aerospace Applications, AFWAL-TR-82-3059.

Bresnahan, D.L. (1968), "Experimental investigation of a 10-degree conical turbojet plug nozzle with iris primary and translating shroud at Mach numbers from 0 to 2.0," NASA TM X-1709.

Brown, E.F. (1968), "Compressible flow through convergent conical nozzles with emphasis on the transonic region," Ph.D Thesis, University of Illinois.

Cantwell,B.J.(1986),"Viscous starting jets," Journal of Fluid Mechanics, V.173, pp.159-189.

Carroll,B.F. and J.C.Dutton (1985), "CAEOPT2: A computer program for supersonic ejector optimization," Report No. ULIU-ENG-85-4006, Department of Mechanical and Industrial Engineering, University of Illinois at Urbana-Champaign.

Chandrasekhara, M.S., A. Krothapalli, and D. Baganoff (1987), "Mixing characteristics of a supersonic multiple jet ejector," AIAA Paper 87-0248.

Chandrasekhara, M.S., A. Krothapalli, and D. Baganoff (1987), "Similarity of ejector wall-pressure distributions" AIAA Journal, V.25, No. 9, pp.1266 - 1268.

Cheng, L. (1988), "CFD efforts @ BMA in support of STOVL technology development," Presentation to NASA/Lewis, 30 March 1988.

Chow, W.L. and A.L.Addy (1964), "Interaction between primary and secondary streams of supersonic ejector systems and performance characteristics," AIAA J., V.2, No.4, pp.686-695.

Chow,W.L. and P.S.Yeh (1965), "Characteristics of ejector systems nonconstant area shrouds," AIAA Journal, V.3, No.3, pp.525-527.

Collins, D.J. and M.F.Platzer (1982), "Experimental investigation of oscillating subsonic jets," Proceedings: Ejector Workshop for Aerospace Applications, pp.463-474.

Crane,L.J.(1957), "The laminar and turbulent mixing of jets of compressible fluid. Part II: The mixing of two semi-infinte streams," JFM, V.2, pp.81-92.

Dahm, W.J. and P.E. Dimotakis (1987), "Measurements of entrainment and mixing in turbulent jets," AIAA Journal, V.25, No.9, pp. 1215-1223.

DeJoode,A.D. and Patankar,S.V. (1978), "Prediction of three dimensional turbulent jet mixing in an ejector," AIAA Journal, V.16, No.2, February, pp.145-150.

Deleo,R.V., R.E.Rose, and R.S.Dant (1962), "An experimental investigation of the use of supersonic driving jets for ejector pumps," ASME Journal of Engineering for Power, V.84, pp.204-212.

Droste, C.S. (1988), "A case study the F-16 fly-by-wire flight control system," AIAA Case Study.

Drummond, C.K. (1985), "Numerical analysis of mass transfer from a sphere in an oscillatory flow," Ph.D Thesis, Syracuse University, 1985.

Drummond, C.K. and F.A.Lyman (1986), "Numerical Analysis of secondary streaming in the vicinity of a sphere," Forum on Unsteady Flows, ASME FED, V.39.

Dutton, J.C., C.D.Mikkelsen, and A.L.Addy (1982), "A theoretical and experimental investigation of the constant area supersonic - supersonic ejector," AIAA Journal, V.20, No.10, pp.1392-1400.

Dutton, J.C. and B.F.Carroll (1983), "Optimized ejector-diffuser design procedure for natural gas vapor recovery, "ASME Journal of Energy Resources Technology, V.105, No.3, pp.388-393.

Dutton, J.C. and B.F. Carroll (1986), "Optimal supersonic ejector designs," ASME Transactions, Journal of Fluids Engineering, V.108, December 1986, pp.414-420.

Elbanna, H., S. Gahin and M.I.I.Rashed (1983), "Investigation of two plane parallel jets," AIAA Journal, V.21, No.7, pp.986-991.

Elgin, J. (1988), "Control mode analysis," Presentation to NASA/Lewis, March 16 at GE Aircraft Engine Group.

Emanuel, G. (1976), "Optimum performance for a single-stage gaseous ejector," AIAA Journal, V.14, No.9, pp.1292-1296.

Emanuel, G. (1982), "Comparison of one-dimensional solutions with Fabri theory for ejectors," Acta Mechanica, V.44, No.3-4, pp.187-200.

Fabri,T. and J. Paulon (1958), "Theory and experiments on supersonic air-to-air ejectors," NACA TM 1410.

Fabri, J. and R.Siestrunck (1958), "Supersonic air ejectors, "Advances in Applied Mechanics, Vol.V, Academic Press, pp.1-34.

Fisher, S.A. (1981), "Thrust augmenting ejectors for high pressure ratio propulsive jets," 7th Austrailian Conference on Hydraulics and Fluid Mechanics, Brisbane, Australia, August 18-22, 1980.

Foa, J.V. (1982), "Considerations on steady- and nonsteady-flow ejectors," Proceedings: Ejector Workshop for Aerospace Applications, pp.659-698.

Foa, J.V. and C.A.Garris (1984), "Cryptosteady modes of energy exchange," Mechanical Engineering, V.106, Nov., pp.68-75.

Foley, W.H., A.E.Sheridan, and C.H.Smith (1982), "Study of aerodynamic technology for single-cruise-engine V/STOVL fighter/attack aircraft," NASA CR-166268.

Fozard, J.W. (1978), "The jet V/STOL Harrier," AIAA Case Study.

Franke, M.E. and G.Unnever (1985), "Performance characteristics of rectangular and circular thrust augmenting ejectors," AIAA Paper 85-1344.

Franklin,J.A. and S.A.Englland (1987),"E-7A Aero and Propulsion Model," Unpublished.

Garland, D.B. (1987), "Specification for tests of the full-scale single-sided ejector for the Spey/E7 model at Lewis Research Center, NASA," DeHavilland Aircraft Company, DHC-DRIE 87-1.

Garland, D.B. (1987), "Development of lift ejectors for STOVL combat aircraft," AIAA Paper 87-2324.

Goff,J.A. and C.H.Coogan (1942), "Some two-dimensional aspects of the ejector problem," Journal of Applied Mechanics, V.9, No.4, pp A151-A154.

Greathouse, W.K. and D.P.Hollister (1953), "Air-flow and thrust characteristics of several cylindrical cooling-air ejectors with a primary to secondary temperature ratio of 1.0," NACA RM E52L24.

Grohs,G. and G.Emanuel (1976), "Gas dynamics of supersonic mixing lasers," in the Handbook of Cemical Lasers, John Wiley & Sons, pp.263-388.

Habib,M.A. and J.H.Whitelaw (1979),"Velocity characteristics of a confined coaxial jet," Journal of Fluids Engineering, V.103, pp.605-608.

Hardy, J.M. and H.Lacombe (1967), "Supersonic bypass nozzles - computing methods," Rev. Francaise de Mechanique, 4th qtr, pp.49-59.

Hart, C.E. (1971), "Function generation subprograms for use in digital simulations," NASA-TM-X-71526.

Hassinger, S.H. (1978), "Ejector optimization," Report AFFDL- TR-78-23, Air Force Flight Dynamics Laboratory, Wright-Patterson Air Force Base, Ohio.

Hassinger, S.H. (1984), "A new method for calculating duct flows," AIAA Journal, V.22, January, pp.141-143.

Hedges, K.R. and P.G.Hill (1974), "Compressible flow ejectors, Part I - Development of a Finite-Diference flow model," ASME Paper No.74-FE-1. Also, Transactions of the ASME, Journal of Fluids Engineering, September, pp.272-281.

Heiser, W.H. (1967), "Thrust augmentation", Journal of Engineering for Power, pp.75-82.

Hickman, K.E., P.G.Hill, and G.B.Gilbert (1972), "Analysis and testing of compressible flow ejectors with variable area mixing tubes," ASME Journal of Basic Engineering, V.94, pp.407-416.

Hoh, R. and S.R. Sturmer (1987), "Handling qualities criteria for STOL landings," STI Paper 407.

Howe,R.M. (1986), Dynamics of real-time simulation, ADI, Inc.

Hussain, A.M. (1981), "Role of coherent structures in turbulent shear flows," Proc. Indian Acad. Sci. (Engg. Sci.), Vol.4, Pt.2, pp.129-175.

Iob, M. (1987), "An investigation of some simple models for the F/A-18 flight dynamics," Australian DoD AR-004-513.

Iwaniw,M.A. and A. Pollard (1983), "Multiple jet mixing in a rectangular duct - Center plane behavior," ASME Paper 83-FE-35.

Johnson, J.D. (1966), "An analytical and experimental investigation of ejector performance for nonsteady flow conditions," College of Engineering, Clemson University., Engineering Experiment Station Bulletin 107, July.

Keenen, J.H. and E.P.Nuemann (1982), "A simple air ejector," Journal of Applied Mechanics, V.9, No.2, pp.A75-A81.

Kentfield,J.A.C. (1978), "Prediction of performance of low pressure ratio thrust augmenting ejectors," Journal of Aircraft, V.15, pp.849-856.

Khare,J.M. (1973),"An analytical and experimental investigation of an unsteady flow ejector," University of Calgary, Mechanical Engineering Department, Rept.53.

Khare,J.M. and J.A.C.Kentfield (1978),"A simple apparatus for the experimental study of non-steady flow thrust-augmenting ejector configurations," Workshop on Thrust Augmenting Ejectors, June 1978.

Knott, P.G. and D.N.Cundy (1986), "Installation aerodynamics of ejectors in combat aircraft," Aeronautical Journal, V.90, December, pp.410-413.

Kochendorfer, F.D. and M.D.Rousso (1951), "Performance characteristics of aircraft cooling ejectors having short cylindrical shrouds," NACA RM E51E01.

Koening, D.G., F.Stoll, and K.Aoyagi (1981), "Application of thrusting ejectors to tactical aircraft having vertical lift and short-field capability," AIAA Paper 81-2629.

Korst, H.H. and W.L.Chow (1966), "Non-isoenergetic turbulent jet mixing between two compressible streams at constant pressure," NASA CR-419.

Krothapalli, A., D. Baganoff, and K. Karamcheti (1980), "Development and structure of a rectangular jet in a multiple jet configuration," AIAA Journal, V.18, No.8, pp.945-950.

Krothapalli, A., L.VanDominelen, and K.Karancheti (1985), "The influence of forward flight on thrust augmenting ejectors,"AIAA Paper 85-1589.

Kuhlman, J.M. (1987), "Variation of entrainment in annular jets," AIAA Journal, V.25, No.3, pp.373-379.

Lewis, W.G.E and F.W.Armstrong (1970), "Some experiments on two-stream propelling nozzles for supersonic aircraft," ICAS Paper 70-48.

Liepmann,H.W. (1979), "The rise and fall of ideas in turbulence," American Scientist, V.67, pp.221-228.

Loth, J.L. (1966), "Theoretical optimization of staged ejector systems, Part I," Report AEDC-TR-66-2.

Loth, J.L. (1968), "Theoretical optimization of staged ejector systems, Part II," Report AEDC-TR-68-80.

Luidens,R., R.Plencner, W.Haller, and A.Glassman (1984), "Supersonic STOVL ejector aircraft from a propulsion point of view," NASA TM-83641.

Lund,T.S., D.A.Tavella, and L.Roberts (1986), "Analysis of interacting dual lifting ejector systems," AIAA Paper 86-0478.

Maphet,J.A. and W.T.McKenzie (1958), "Internal performance of several cylindrical and divergent shroud ejector nozzles with exit diameter ratios of 1.11, 1.19, 1.27, 1.35, 1.43, 1.53,and 1.65," Report FZA-4-341 General Dynamics/Convair.

Marsters, G.F. (1977), "Interaction of two plane parallel jets," AIAA Journal, V.15, No.12, pp.1756-1762.

Matsuo, K., H.Mochizuki, K.Sasaguchi, and Y.Kiyotki (1982), "Investigation of supersonic air ejectors II - Effects of throat-area-ratio on ejector performance," JSME Bulletin, V.25, December, pp.1898-1905.

McLachlan,B.G., A.Krothapalli, K.Nagaraja (1984), "Flow structure within a heated rectangular jet ejector," AIAA Paper 84-0571.

McRuer, D. (1980), "Human dynamics in man-machine systems," Automatica, V.16, pp. 237-253.

McRuer,D., Ashkenas,I., and Graham,D. (1973), Aircraft dynamics and automatic control, Princeton University Press.

McRuer, D. and H. Jex (1967), "A review of quasi-linear pilot models," IEE Transactions on Human Factors in Electronics, No.3, pp.231-239.

Mihaloew, J. R. (1988), "Flight propulsion control integration for V/STOL aircraft," NASA TM-100226.

Mikkelsen, C.D., M.R.Sandberg, and A.L.Addy (1976), "Theoretical and experimental analysis of the constant area, supersonic - supersonic ejector," Report UILU-ENG-76-4003, Department of Mechanical and Industrial Engineering, University of Illinois at Urbana-Champaign.

Miller, D.R. and E.W. Comings (1957), "Static Pressure distribution in the free turbulent jet", JFM, pp.1-16.

Miller, D.R. and E.W. Comings (1960), "Force-momentum fields in dual-jet flow," JFM, V.7, pp.237-256.

Miller, R.J. and R.D. Hackney (1976), "F100 multivariable control system engine models/design criteria," AFAPL-TR-76-74.

Minardi, J.E. (1982), "Characteristics of high performance ejectors," Proceedings: Ejector Workshop for Aerospace Applications, pp.179-279.

Minardi, J.E. (1982), "Compressible flow ejector analysis with application to energy conversion and thrust augmentation," AIAA Paper 82-0133.

Mitchell, D.G. and J.M. Morgan (1987), "A flight investigation of helicopters low-speed response requirements," STI Paper 402.

Narayaman, M.A. and S.A. Raghu (1982), "An experimental study on the mixing of two-dimensional jets," Proceedings: Ejector Workshop for Aerospace Applications, pp.383-405.

Neiders, G.K., A.S.Goldstien, and J.E.Davidson, "Evaluation of prototype digital flight control algorithms in hardware-in-the-loop environment," Proceedings of Digital Avionics Systems, IEEE, pp.547-554.

Nelson, D.P. and D.L.Bresnahan (1983), "Ejector nozzle test results at simulated flight conditions for an advanced supersonic transport propulsion system," AIAA Paper 83-1287.

Parikitt,P.G. and R.J.Moffat (1982), "Resonant entrainment of a confined pulsed jet," ASME Transactions, Journal of Fluids Engineering, V.104, December, pp.482-488.

Patankar, S.U. and Spalding, D.B. (1972), "A calculation procedure for heat mass, and momentum transfer in three-dimensional parabolic flows," Int. J. Heat Mass Transfer, V.15, pp.1787-1806.

Paynter, H.M. (1985), "Representation of measured ejector characteristics by a simple Eulerian bond graph models," Transactions of the ASME, Journal of Dynamic Systems, Measurement, and Control, V.107, December, pp.258-261.

Petrie,H.L. (1980), "An experimental and theoretical investigation of multiple ducted streams with a periodic or a steady supersonic driven flow," M.S. Thesis, Department of Mechanical and Industrial Engineering, University of Illinois at Urbana-Champaign.

Petrie, H.L. and A.L.Addy (1982), "An investigation of planar, two-dimensional ejectors with periodic or steady supersonic driver flow," Proceedings: Ejector Workshop for Aerospace Applications, pp.475-492.

Petrie,H.L., A.L.Addy, and J.C.Dutton (1985), "Multiple ducted streams with a periodic or steady supersonic driven flow," AIAA Journal, V.23, December, pp.1851-1852.

Porter,J.L. and R.A.Squyers (1981), "A summary/overview of ejector augmentation theory and performance," ATC Report No. R-91100/9CR-47A, Vought Corporation Advanced Technology Center, Dallas, Texas. Also, USAF Technical Report No. R-91100-9CR-47, April 1981, Volumes I and II.

Pratt & Whitney Aircraft (1968), "Users manual for the general ejector nozzle deck," Report PWA-3465.

Qian,H., M.Zhang, and G.Ye (1984), "A method for calculating the performance of ejector nozzles," Journal of Engineering Thermophysics, V.5, February, pp.47-50.

Quinn, B. (1973), "Compact ejector thrust augmentation," J. Aircraft, V.16, No.8, pp.481-486.

Rizzi,A. and B.Engquist (1987),"Selected topics in the theory and practice of computational fluid mechanics," Journal of Computational Physics, V.72, No.1, pp.1-69.

Rojek,F.W. (1986),"Development of a mathematical model that simulates the longitudinal, and lateral-directional response of the F/A-18 for the study of flight control reconfiguration," M.S.Thesis, Naval Postgraduate School.

Runstadler, P.W., F.X.Dolan, and R.C.Dean (1975), "Diffuser data book," 1st Ed., Creare Technical Information Service, Hanover, New Hampshire, pp.1-88.

SAE (1984), "V/STOL: An update and introduction," SAE SP-591.

Salter,G.E. (1975), "Method for analysis of V/Stol aircraft ejectors," Journal of Aircraft, V.12, pp.974-978.

Saminich,N.E. and S.C.Huntly (1969), "Thrust and pumping characteristics of cylindrical ejectors using afterburning turbojet gas generator," NASA TM X-52565.

Sayer, R.A. (1961), "The flow due to a two-dimensional jet issuing parallel to a flat plate," JFM, V.9, pp.543-561.

Sawyer, R.A. (1963), "Two-dimensional reattaching jet flows including the effects of curvature on entrainment," JFM, V.17, pp481-498.

Schum,E.F., J.H.Dehart, and P.M.Bevilaqua (1982), "Ejector nozzle development," 13th Congress on International Council of the Aeronautical Sciences & AIAA Aircraft Systems and Technology Conference, Seattle, WA, August 22-27, V1 of Proceedings (A82-40876 20-01), pp.410-417.

Schrewsbury,G.D. and J.R.Jones (1968), "Static performance of an auxiliary inlet ejector nozzle for supersonic cruise aircraft," NASA TM X-1653.

Seldner,K., J.R.Mihaloew, and R.J.Blaha (1972),"Generalized simulation technique for turbo-jet engine system analysis," NASA TN-D-6610.

Shen,H., E.Dong, T.Shyur, and M.Kee (1981), "The sweep finite element method for calculating the flow field and performance of supersonic ejector nozzles," Proceedings: Fifth International Symposium on Air Breathing Engines.

Stratford,B.S. and G.S.Beavers (1961), "The calculation of compressible turbulent boundary layer in an arbitrary pressure gradient - a correlation of certain previous methods," Rept R&M-3207, Aeronautical Research Council, Great Britan.

Sully, P.R. and D.C. Whittley (1987), "The synthesis of ejector lift / vectored thrust for STOVL," AIAA Paper 87-2378.

Sweetman, B. (1988), "ASTOVL requirements begin to take shape," Interavia, V.3, pp.261-264.

Tavella,D. and L.Roberts (1984), "A simple viscous-inviscid aerodynamic analysis of two-dimensional ejectors," AIAA Paper 84-0281.

Thompson,P.A. (1972), Compressible Fluid Dynamics, New York: McGraw-Hill.

Toulmay,F. (1984), "Internal aerodynamics of infared suppressors for helicopter engines," 40th Annual Forum of the American Helicopter Society, Arlington, VA, May 16-18.

Turner, J.S. (1986), "Turbulent entrainment: the development of the entrainment assumption, and its application to geophysical flows," Journal of Fluid Mechanics, V.173, pp.431-471.

Vavra, M.H. (1960), Aero-thermodynamics and flow in turbomachines, New York: Wiley and Sons.

VonGlaun, U.H. (1986), "Plume characteristics of single-stream and dual-flow conventional and inverted profile nozzles at equal thrust." NASA TM-87323

VonGlaun, U.H. (1987), "Two-dimensional nozzle plume characteristics," NASA TM-89812.

VonGlaun, U.H. (1987), "Secondary stream and excitation effects of two-dimensional plume characteristics," NASA TM-89813.

Vogt, W.G., M.H.Mickle, M.Zipf, S.Kucuk (1987), "Research activities at the University of Pittsburgh, School of Electrical Engineering," Presentation to NASA/Lewis, December.

VonKarman, T (1949),"Theoretical remarks on thrust augmentation," Contributions to Applied Mechanics.

Wacholder,E and J.Dayan (1984), "Application of the adjoint sensitivity method to the analysis of a supersonic ejector,"Transactions of the ASME, Journal of Fluids Engineering, V.106, December, pp.425-429.

Whittley,D.C., and F.L.Gilbertson (1984), "Recent developments in ejector design for V/STOL aircraft," SAE Paper 841498 (in SAE-SP-591).

Wood, J.J. (1982), "Non-recoverable stall transient engine model: Volume dynamic simulation," GE M&AETA Memo, Jan. 13 (P).

Yang,T., T.Jiang, D.R.Pitts, and F.Ntone (1984), "An investigation of high performance, short thrust augmenting ejectors," ASME Paper 84-WA/FE-10.

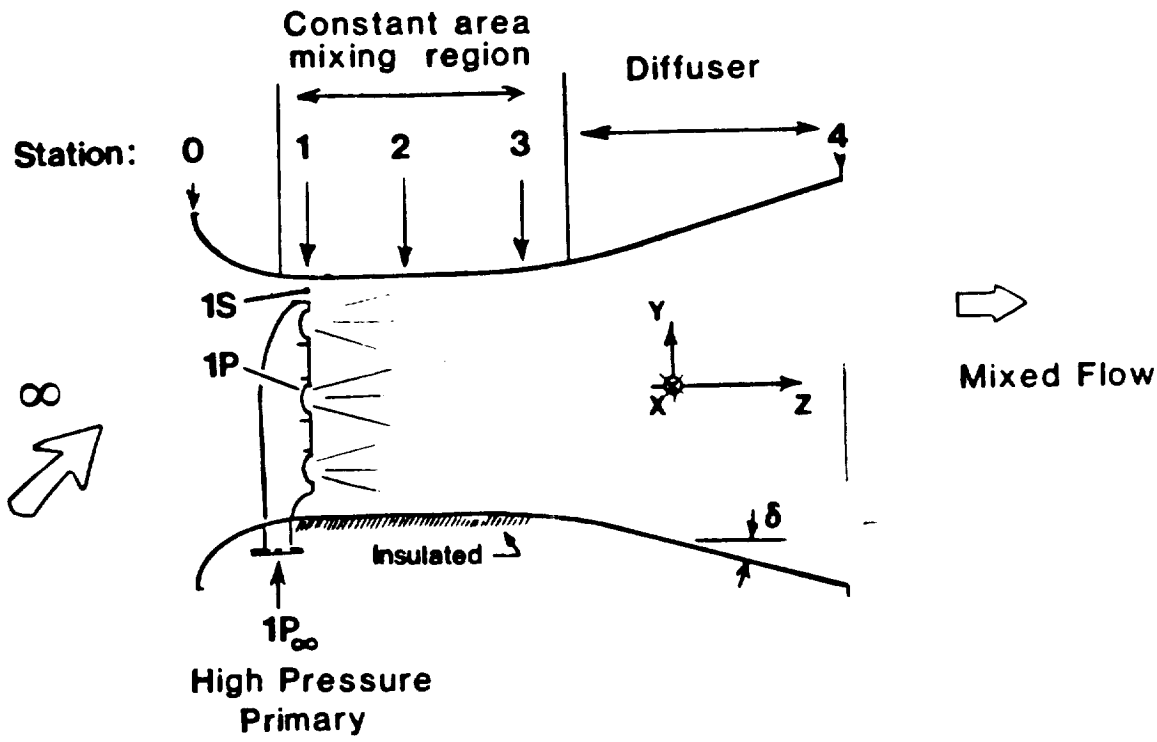

Figure 1. Generic Ejector Configuration

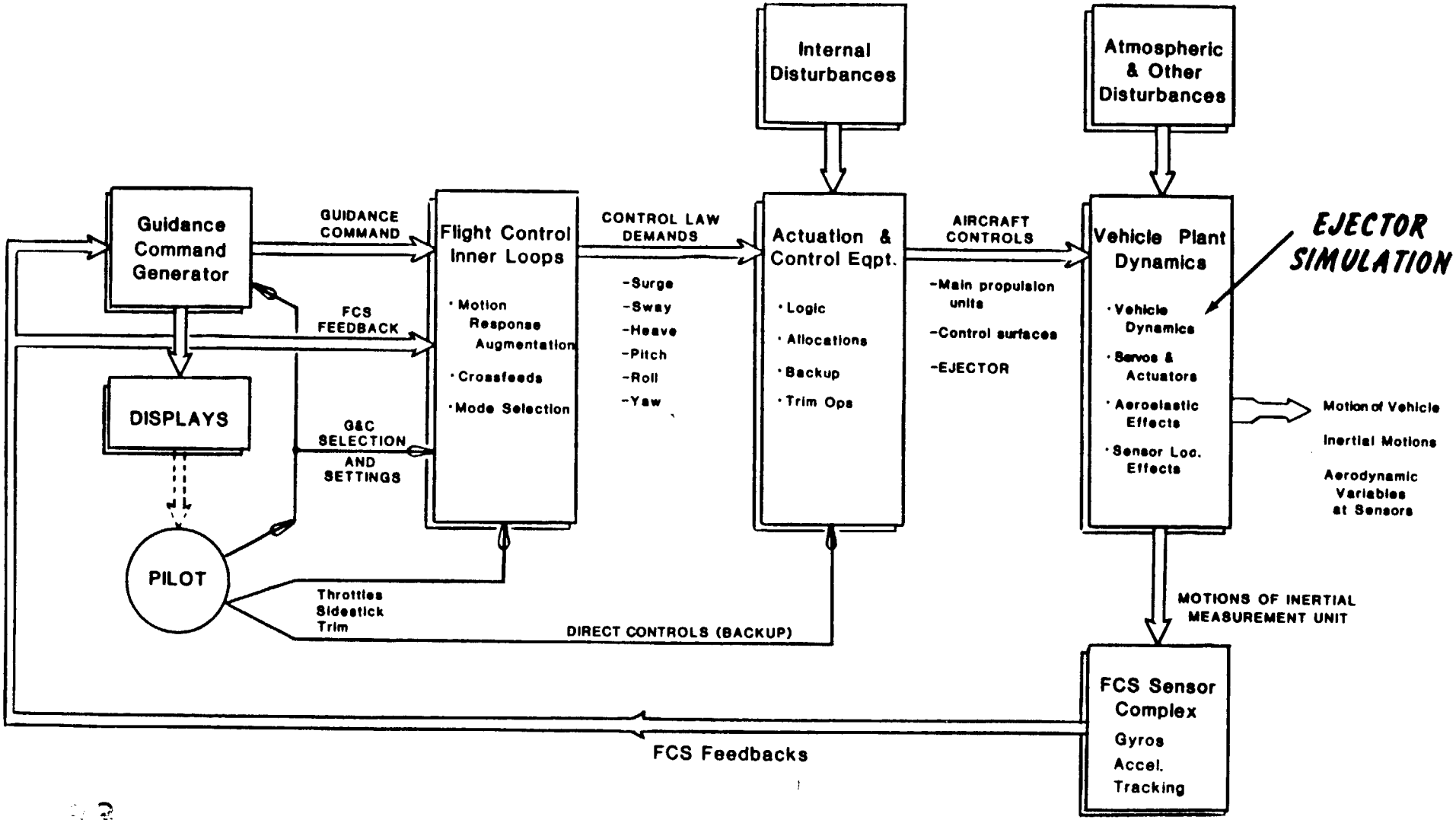

Figure 2. Generic Vehicle Flight Control Architecture and Controls

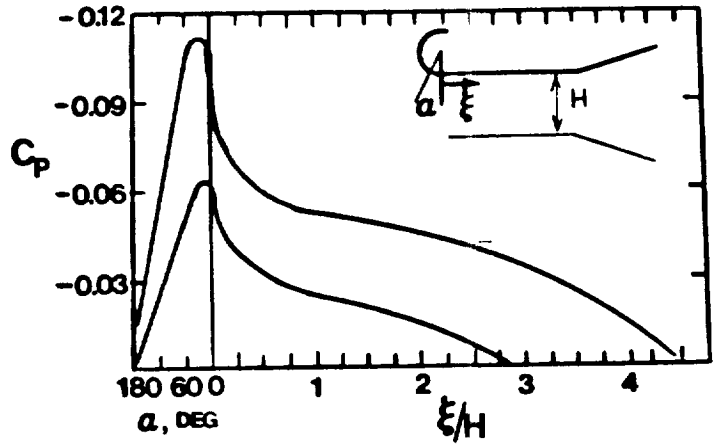

Figure 3. Typical Ejector Wall Pressure Distribution

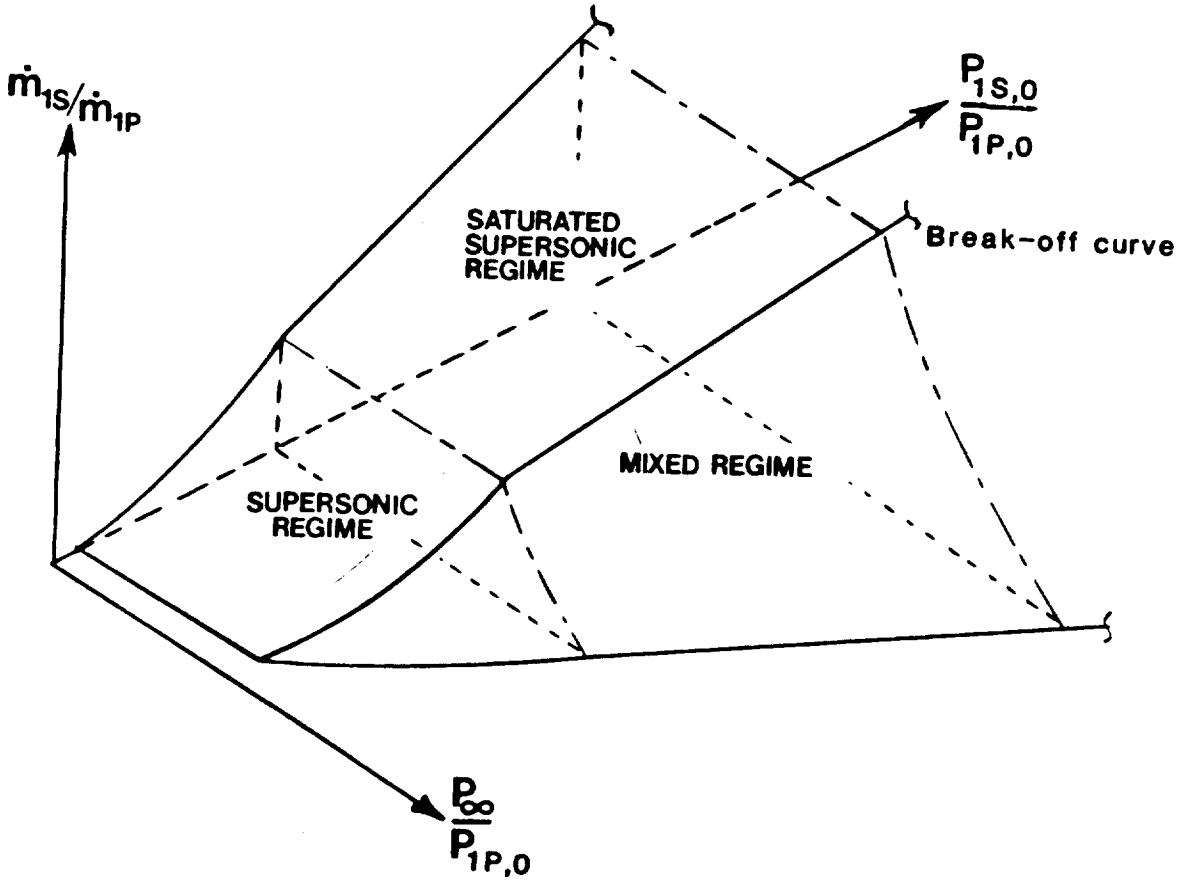

Figure 4. Mass Flow Characteristic Surfaces

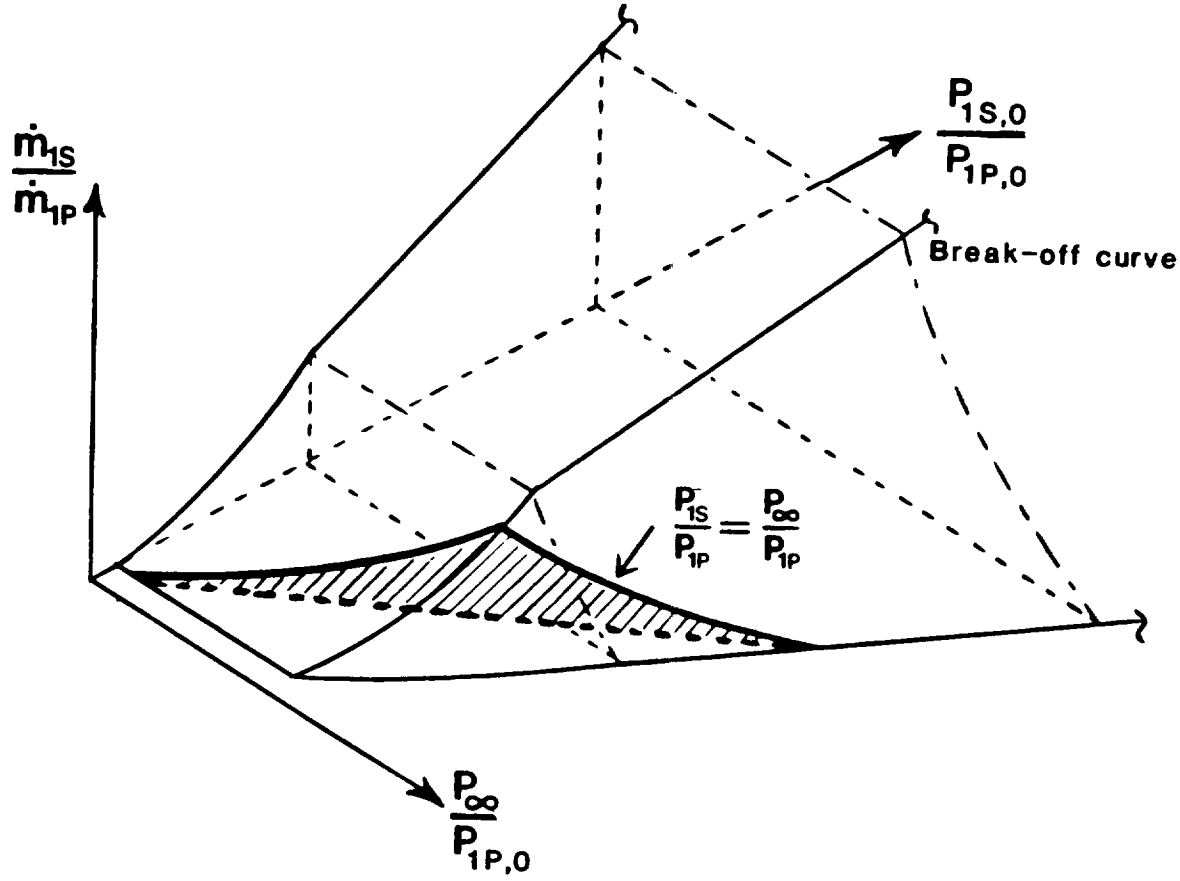

Figure 5. Thrust Augmentation Profile

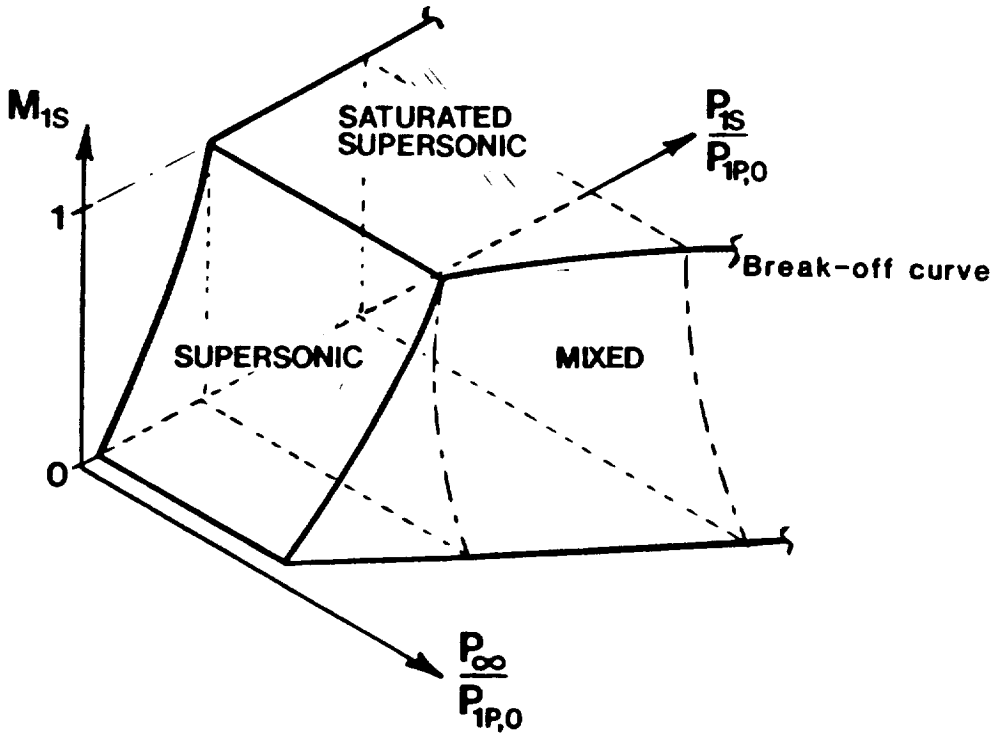

Figure 6. Secondary Mass Flow Characteristics

(a) Arbitrary control volume

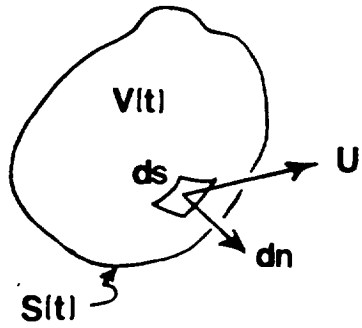

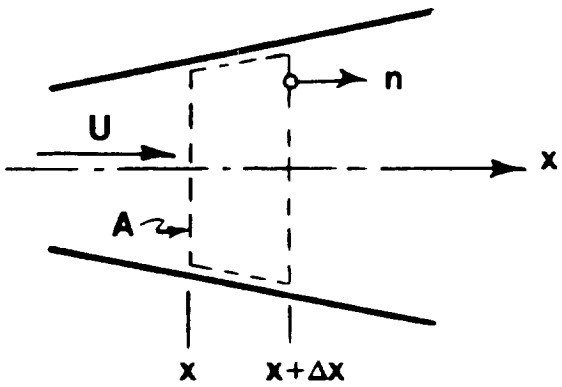

(b) simplified duct control volume

Figure 7. Nomenclature for Arbitrary Control Volume

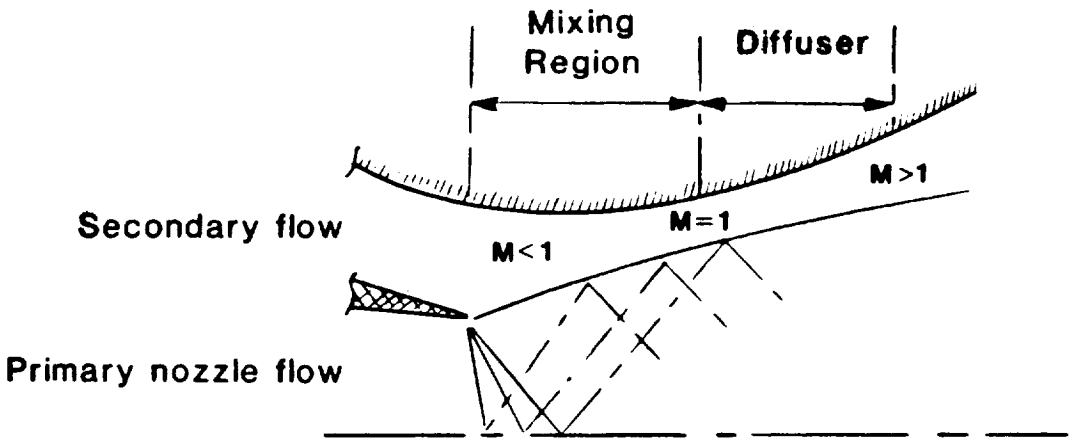

(a) High secondary flowrate

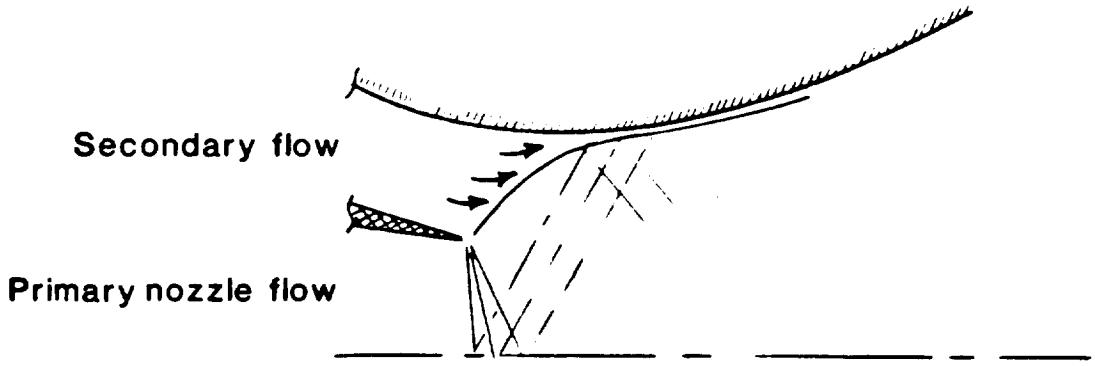

(b) Low secondary flowrate

Figure 8. Flow Model for High and Low Secondary Flow Rates

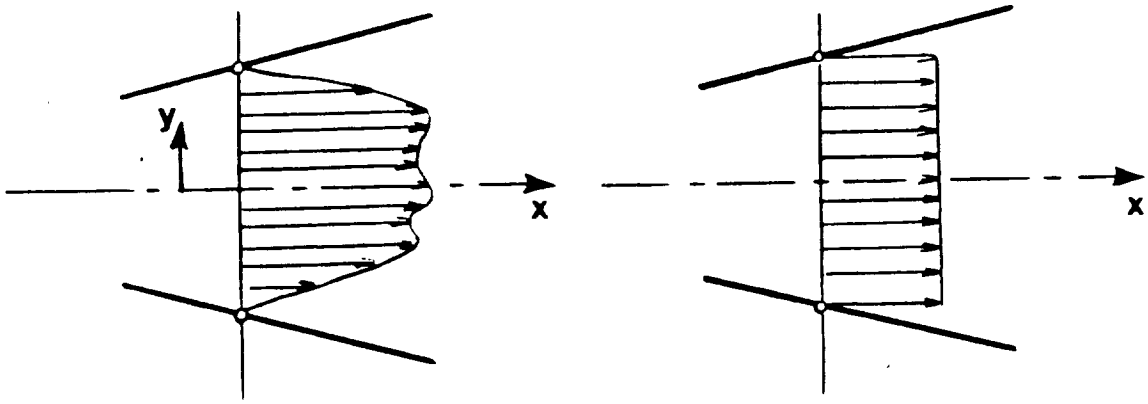

(a) Real flow field

(b) Assumed flow field

Figure 9. Transverse Velocity Distribution

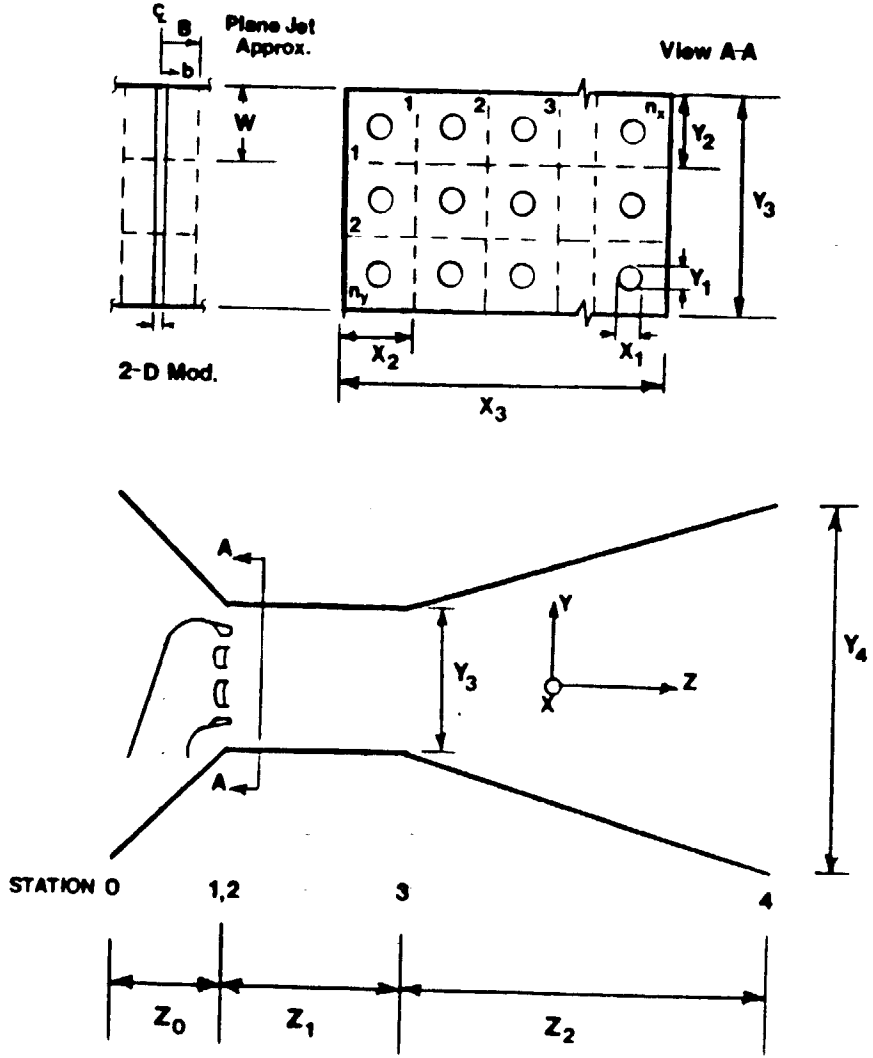

Station Geometric Data for Test Case

Characteristic Dimensions, *ft*			
Station	X	Y	Z
0	9.333	1.875	0.900
1	0.108	0.108	0.900
2	0.778	0.347	-
3	9.333	1.042	2.917
4	9.333	1.875	-

Incremental Volume and Area, Mixing Region

$dA = Wdx$

$dV = Wdxdz = z_1 Wdx = z_1 A$

Scale Factors, Mixing Region

n_x , number of units in the x-direction

n_y , number of units in the y-direction

$N = n_x n_y$, scale factor for an incremental volume and areas

Configuration

12 nozzles in a duct of 112" width; 3 orafices per nozzle

$n_x = 12$

$n_y = 3$

$N = 36$

Figure 10 Control Volume Nomenclature for the Ejector

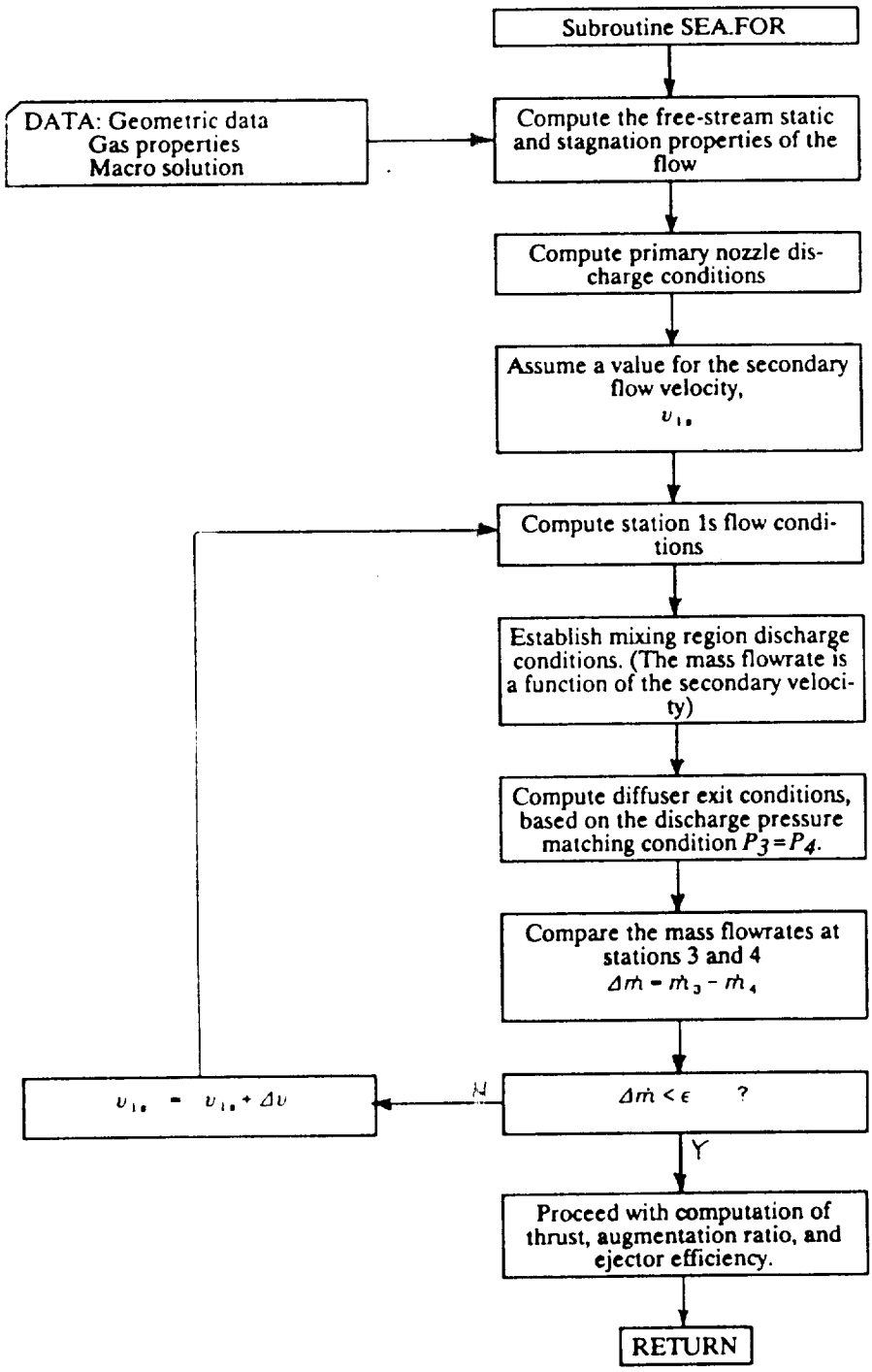

Figure 11. Steady Flow Solution Procedure

Property variations as a function of Temperature, taken from Faires (1938)

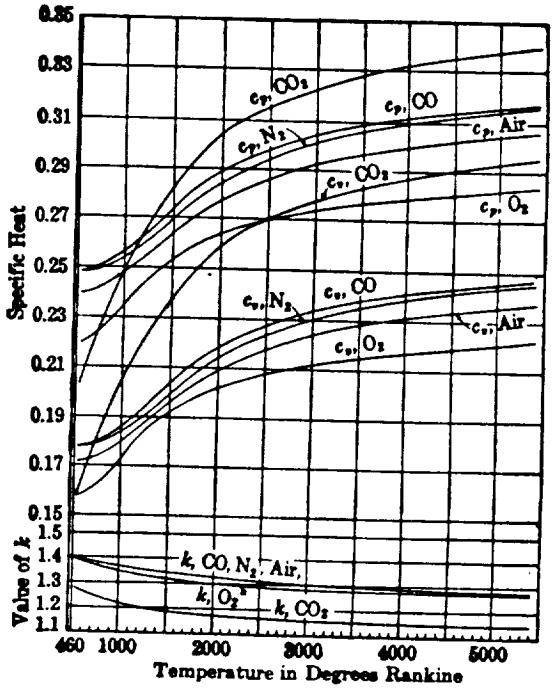

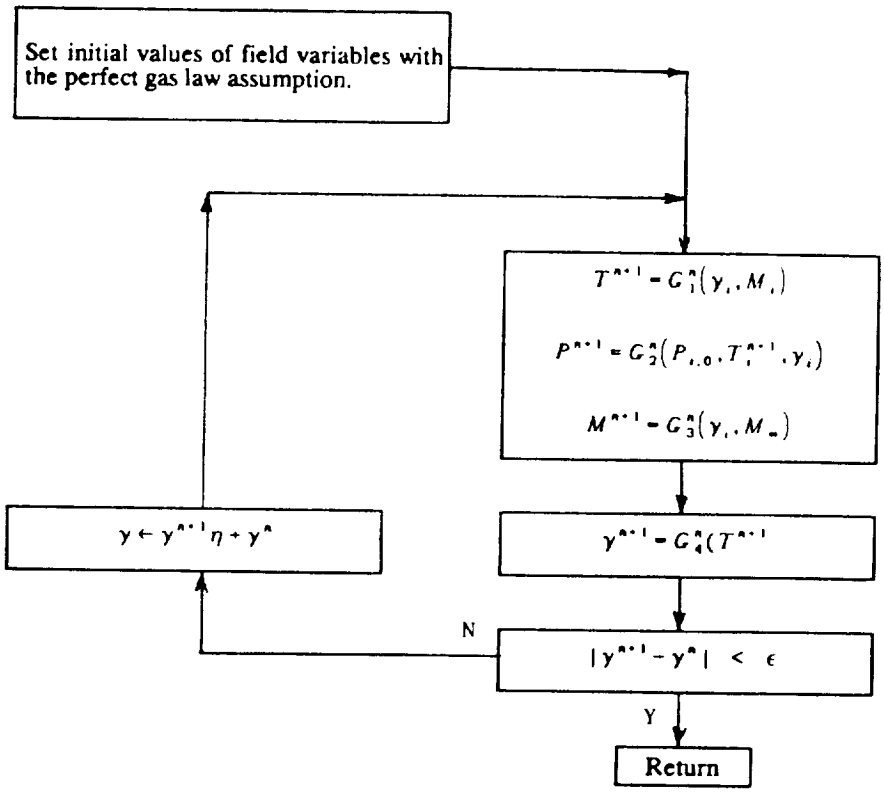

Algorithm for computations

Figure 12. Algorithm to Accommodate an Ideal Gas Assumption

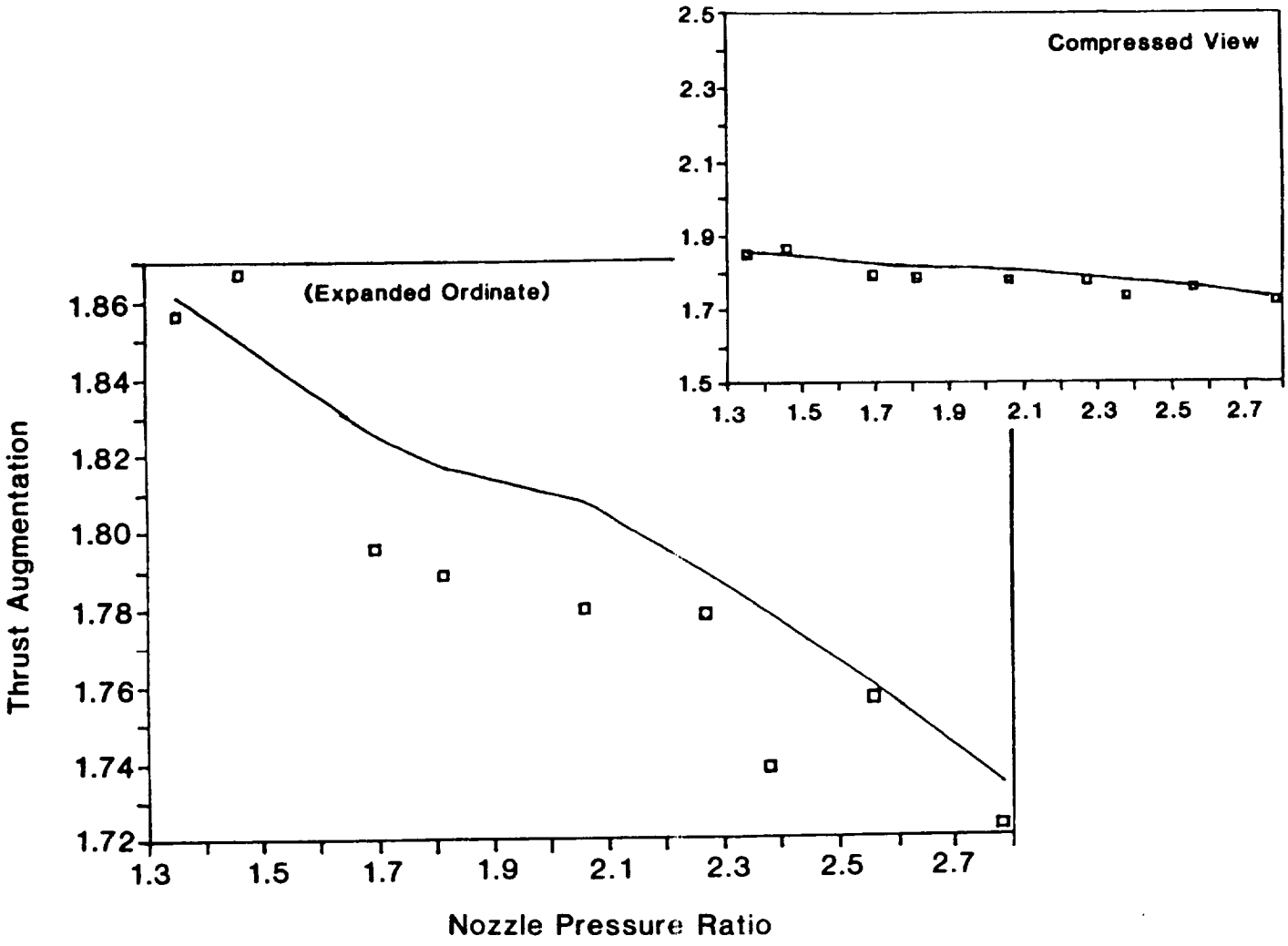

Figure 13. Results from Steady Flow Test Case

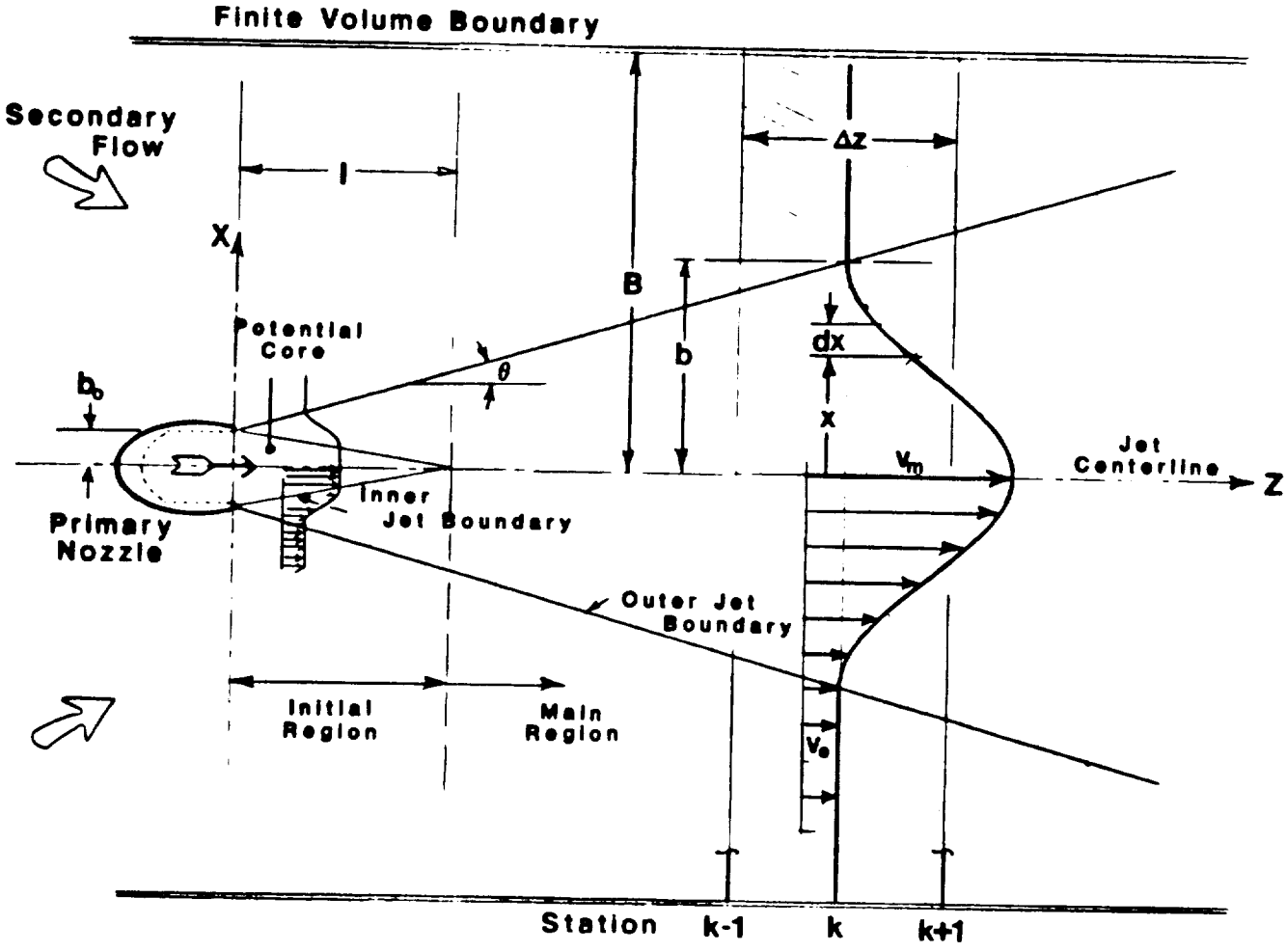

Figure 14. Nomenclature for Finite Volume Analysis

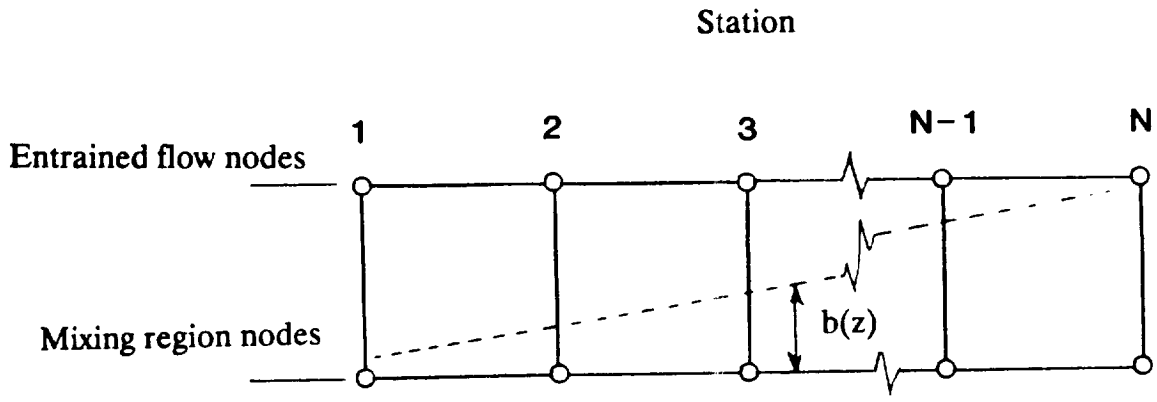

Figure 15. Virtual Grid for Finite Volumes

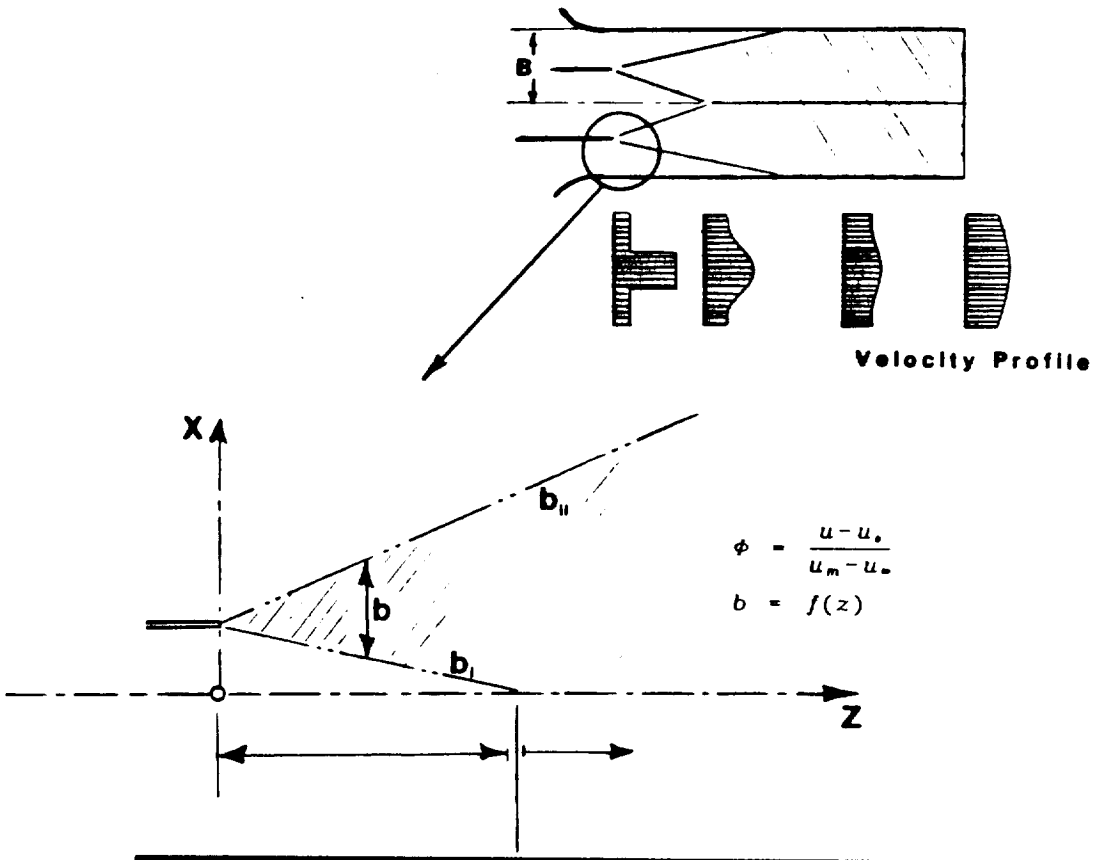

Region I	Region II
$\Phi_0 = \left(1-\eta^{1.5}\right)^2$	$\Phi_0 = \left(1-\xi^{1.5}\right)^2$
$\eta = \frac{x-b_I}{b_{II}-b_I} = \frac{x-b_I}{b}$	$\xi = \frac{x}{b_{II}} = \frac{x}{b}$
$\Phi = \left\{\begin{matrix} 1, \eta_0 < \eta < 0 \\ \Phi_0, 0 \le \eta \le 1 \\ 0, 1 < \eta \le \hat{\eta} \end{matrix}\right\}$	$\Phi = \left\{\begin{matrix} \Phi_0, 0 \le \xi \le 1 \\ 0, 1 < \xi \le \hat{\xi} \end{matrix}\right\}$
$\frac{d\eta}{dx} = \frac{1}{b}, \quad \eta_0 = -\frac{b_I}{b}, \quad \hat{\eta} = \frac{B-b_I}{b}$	$\frac{d\xi}{dx} = \frac{1}{b}, \quad \hat{\xi} = \frac{B}{b}$

Figure 16. Jet Flow Pattern Approximation

All data and figures taken from Krothapolli et al (1980)

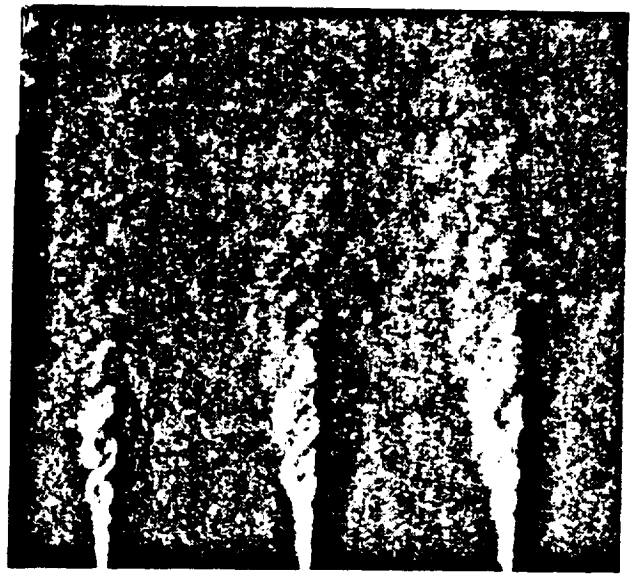

Schlieren picture of a multiple free jet.

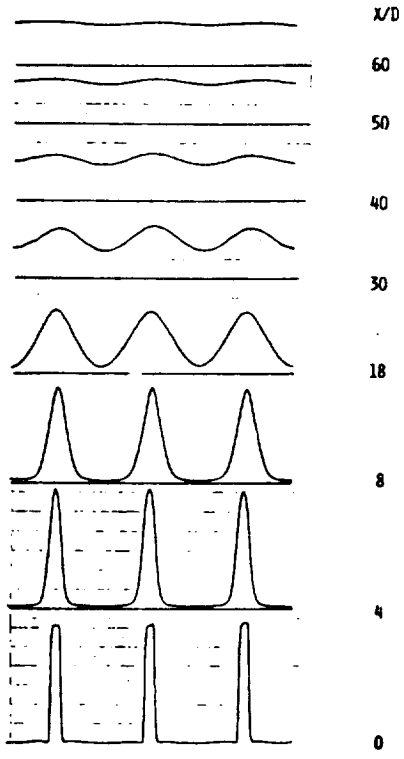

Velocity profiles

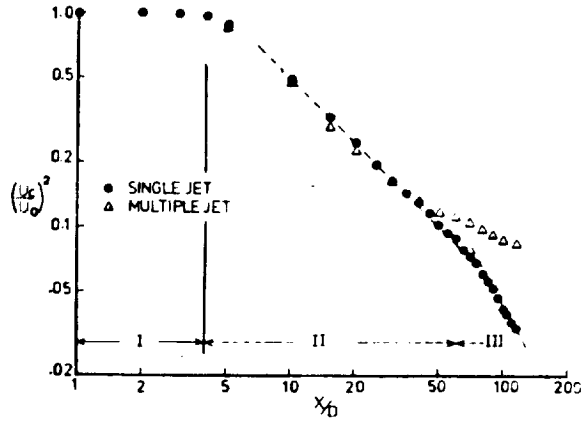

Centerline velocity decay

Figure 17. Axial Velocity Decay

```
      BALANCE

FIELD VARIABLE SPECIFICATIONS:

   V1S    =  303.97000   RHO1S =      .06898
   V1P    =  860.20000   RHO1P =      .06049
   VE     =  303.97000   RHO   =      .06757
   VM     =  473.20000   RHO   =      .06757

GEOMETRIC SPECIFICATIONS:

   B      =      .13425
   BO     =        .0168100
   BSTAR  =        .0281333
   BMAX   =        .3900000
   A1S    =       9.3238000
   A1P    =        .4199800

KINETIC ENERGY BUDGET

   TOTAL INFLUX KE:       17116507.383
      PRIMARY:              8084624.157
      SECONDARY:            9031883.227
      RATIO OF 1P/1S:              .895

   TOTAL DISCHARGE KE:    12708543.375
      PRIMARY:
          KE FLUX:          2323197.145
          CHANGE:           5761427.011
          MIXING LOSS:     -125825.306
       SECONDARY:
          KE FLUX:         10385346.230
          CHANGE:          -1353463.003
          MIXING GAIN:      1353480.284
```

Figure 18. Typical Kinetic Energy Budget

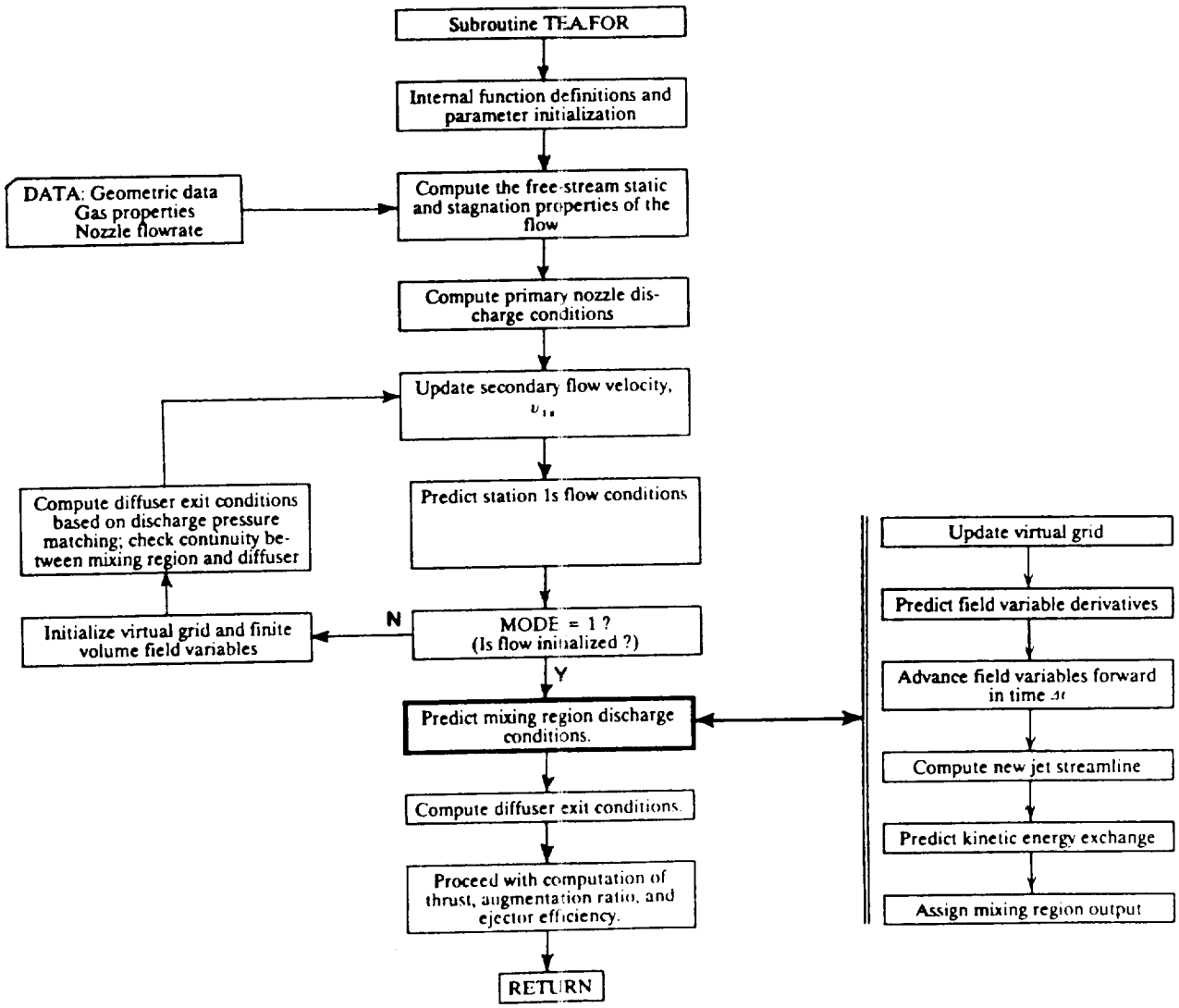

Figure 19. Unsteady Flow Solution Procedure

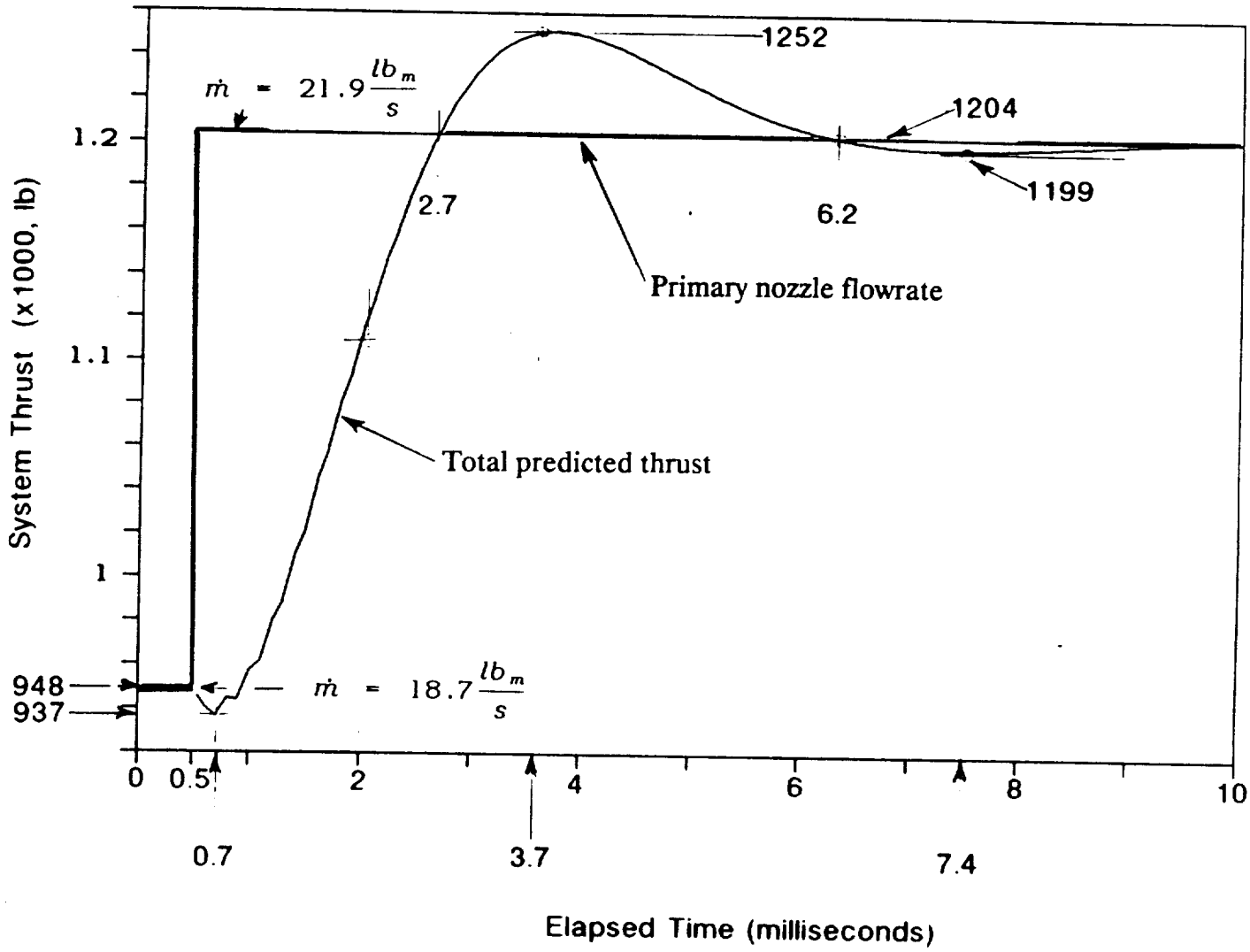

Figure 20. Results from Transient Flow Test Case

Appendix A

Development of the Integral Equations

Overview

A material volume of $V(t)$ and surface $S(t)$ can be described by four laws of motion:

1. **Conservation of Mass:** Based on continuity conditions, this is a statement that the material volume is of constant mass.

2. **Balance of Linear Momentum:** Newton's second law provides that the rate of change of momentum is equal to the sum of body and surface forces.

3. **Balance of Energy:** The first law of thermodynamics describes the balance of internal plus kinetic energy, the rate at which work is being performed, and the rate at which heat is transferred.

4. **Creation of Entropy:** The second law of thermodynamics dictates which of the energy transport processes (that the first law provides) that are acceptable; the rate of entropy creation is balanced by the sum of the rate of increase of entropy and that transported through the material surface.

These laws are not derivable from a set of more primitive laws and are essentially axioms supported by experimental work.

In the sections to follow the development of the control volume equations is given for an arbitrary control volume with a uniform (but time dependent) motion in space.

Continuity

Conservation of mass for a *material* volume takes the form

$$\frac{d}{dt}\int_V \rho\, dV = 0 \qquad (A.1)$$

where d/dt is the total derivative. From Reynolds' transport theorem

$$\frac{d}{dt}\int_V \rho\, dV = \int_V \frac{\partial \rho}{\partial t} dV + \oint_S \rho \underline{u} \cdot \underline{n}\, dA \qquad (A.2)$$

Reynolds' theorem can also be applied to a *control* volume defined by a region Ω and surface Γ,

$$\frac{d}{dt}\int_\Omega \rho\, dV = \int_\Omega \frac{\partial \rho}{\partial t} dV + \oint_\Gamma \rho \underline{U} \cdot \underline{n}\, dA \qquad (A.3)$$

where $\underline{U}$ defines the surface velocity of the control volume, related to the absolute velocity by

$$\underline{v} = \underline{u} - \underline{U} \qquad (A.4)$$

Except for the total derivative terms, integrals over the region Ω are identical to those chosen to be instantaneously coincidental with the (arbitrary) region V; in other words

$$\int_V \frac{\partial \rho}{\partial t} dV = \int_\Omega \frac{\partial \rho}{\partial t} dV \qquad (A.5)$$

$$\frac{d}{dt}\int_V \rho\, dV \neq \frac{d}{dt}\int_\Omega \rho\, dV \qquad (A.6)$$

but through substitution

$$\frac{d}{dt}\int_\Omega \rho\, dV = \frac{d}{dt}\int_V \rho\, dV - \oint_\Gamma \rho \underline{u}\cdot\underline{n} dA + \oint_\Gamma \rho \underline{U}\cdot\underline{n} dA \qquad (A.7)$$

so now

$$\frac{d}{dt}\int_\Omega \rho\, dV + \oint_\Gamma \rho(\underline{u}-\underline{U})\cdot\underline{n} dA = 0 \qquad (A.8)$$

Momentum

The net body force and surface forces acting on the material volume is balanced by the rate of change of the material volume momentum

$$\frac{d}{dt}\int_V \rho \underline{u} dV = \int_V \rho \underline{g} dV + \oint_S \underline{n}\cdot\underline{\hat{S}} dA \qquad (A.8)$$

here, **g** is identified as the specific gravitational force; the general fluid stress tensor, $\underline{\hat{S}}$, can be decomposed into a "pressure stress" and a "viscous stress" (deviatoric stress) tensor

$$\underline{\hat{S}} = -p\underline{\hat{I}} + \underline{S}' \qquad (A.9)$$

To obtain the momentum balance for a control volume, Reynolds' transport theorem is first applied to the total derivative for a material volume

$$\frac{d}{dt}\int_V \rho \underline{u} dV = \int_V \frac{\partial}{\partial t}(\rho \underline{u}) dV + \oint_S \rho \underline{u}(\underline{u}\cdot\underline{n}) dA \qquad (A.10)$$

and also to the control volume

$$\frac{d}{dt}\int_{\Omega}\rho\underline{u}dV = \int_{\Omega}\frac{\partial}{\partial t}(\rho\underline{u})dV + \oint_{S}\rho\underline{u}(\underline{U}\cdot\underline{n})dA \qquad (A.11)$$

where, again, we note the use of $\underline{U}$ in the latter. Once the arbitrary material volume is extended to coincide with the control volume

$$\frac{d}{dt}\int_{V}\rho\underline{u}dV = \frac{d}{dt}\int_{\Omega}\rho\underline{u}dV + \oint\rho\underline{u}(\underline{u}\cdot\underline{n})dA - \oint\rho\underline{u}(\underline{U}\cdot\underline{n})dA \quad (A.12)$$

It is now evident that

$$\frac{d}{dt}\int_{\Omega}\rho\underline{u}dV = -\oint_{\Gamma}\rho\underline{u}(\underline{u}-\underline{U})\cdot\underline{n}dA + \int_{\Omega}\rho\underline{g}dV + \oint_{\Gamma}\underline{n}\cdot\underline{\hat{S}}dA \quad (A.13)$$

and therefore

$$\frac{d}{dt}\int_{\Omega}\rho\underline{u}dV = -\oint_{\Gamma}\rho\underline{u}(\underline{u}-\underline{U})\cdot\underline{n}dA + \int_{\Omega}\rho\underline{g}dV - \oint_{\Gamma}\underline{n}\cdot(p\underline{\hat{I}})dA + \oint_{\Gamma}\underline{n}\cdot\underline{S}'dA \qquad (A.14)$$

Energy

Because textbooks and the literature are often inconsistent in the use of the term "energy equation", some clarification is worthwhile so that the present work is interpreted correctly. Obviously, an energy-conversion law must account for all forms of energy within and across the control volume. Confusion often arises since a continuous flow of mass across a control volume admits two independent energy equations. In one case, the **mechanical power equation** is derived from the product of the Navier-Stokes equation and the particle velocity; this gives the so-called balance of mechanical power or transport equation for kinetic energy. The other case involves the first law of thermodynamics and is the **general power equation**, or, as viewed here, the **general energy equation**. It can be shown that the **heat equation** is the difference of the mechanical and general power equations; in the present work the heat equation can be transformed into a statement of the entropy balance and will be covered in Section A.5.

With the first law of thermodynamics in mind, the energy per unit volume of a fluid is the sum of the specific internal energy, e, and the specific kinetic energy, $u^2/2$. For a material volume this energy is balanced by the energy due to heat and work; the general power equation is therefore

$$\frac{d}{dt}\int_{V}\rho\left(e+\frac{u^2}{2}\right)dV = \int_{V}\rho\underline{g}\cdot\underline{u}dV + \oint_{S}\underline{u}\cdot(\underline{n}\cdot\underline{\hat{S}})dA - \oint_{S}\underline{q}\cdot\underline{n}dA \qquad (A.15)$$

Employing the logic used earlier in the extension of the material volume to a control volume

$$\frac{d}{dt}\int_V \rho\left(e+\frac{u^2}{2}\right)dV = \frac{d}{dt}\int_\Omega \rho\left(e+\frac{u^2}{2}\right)dV + \oint_\Gamma \rho\left(e+\frac{u^2}{2}\right)(\underline{u}-\underline{U})\cdot\underline{n}\,dA \tag{A.16}$$

so that

$$\frac{d}{dt}\int_V \rho\left(e+\frac{1}{2}u^2\right)dV = \int_\Omega \rho\underline{g}\cdot\underline{u}\,dV + \oint_\Gamma \underline{u}\cdot(\underline{n}\cdot\underline{\hat{S}})dA - \oint_\Omega \underline{q}\cdot\underline{n}\,dA - \oint_\Gamma \rho\left(e+\frac{1}{2}u^2\right)(\underline{u}-\underline{U})\cdot\underline{n}\,dA \tag{A.17}$$

From the definition of the stress tensor we expand the stress term:

$$\oint_\Gamma \underline{u}\cdot(\underline{n}\cdot\underline{\hat{S}})dA = \oint_\Gamma \underline{u}\cdot(\underline{n}\cdot\underline{S}')dA - \oint_\Gamma p\underline{n}\cdot\underline{u}\,dA \tag{A.18}$$

and since the enthalpy is defined as

$$h = e + \frac{p}{\rho} \tag{A.19}$$

then

$$\frac{d}{dt}\int_\Omega \rho\left(h+\frac{u^2}{2}-\frac{p}{\rho}\right)dV = -\oint_\Gamma \rho\left(h+\frac{u^2}{2}-\frac{p}{\rho}\right)(\underline{u}-\underline{U})\cdot\underline{n}\,dA + \int_\Gamma \rho\underline{g}\cdot\underline{u}\,dV + \oint_\Gamma \underline{u}\cdot(\underline{n}\cdot\underline{S}')dA - \oint_\Gamma p\underline{n}\cdot\underline{u}\,dA - \oint_\Gamma \underline{q}\cdot\underline{n}\,dA \tag{A.20}$$

It is quite useful to assume the heat equivalent to the work of viscous forces to be immediately transferred to the region where the forces occur. No part of that energy is transmitted to the surroundings so its presence becomes nested within the other forms of energy the governing equations provide a balance for. Furthermore, if gravitational effects are neglected and like terms in the energy equation are eliminated, the energy equation becomes

$$\frac{d}{dt}\int_{\Omega}\rho\left(h+\frac{u^2}{2}-\frac{p}{\rho}\right)dV \;=\; -\oint_{\Gamma}p\underline{U}\cdot\underline{n}dA \;-\; \oint_{\Gamma}\rho\left(h+\frac{u^2}{2}\right)(\underline{u}-\underline{U})\cdot\underline{n}dA \tag{A.21}$$

Alternate Energy Equation

In the absence of dissipative effects, an adiabatic ejector representation of the *heat equation* is

$$\frac{d}{dt}\int_{V}\rho e dV \;=\; -\oint_{S}p\underline{u}\cdot\underline{n}dA \tag{A.22}$$

Apply Reynold's transport theorem to the total derivative for a material volume

$$\frac{d}{dt}\int_{V}(\rho e)dV \;=\; \int_{V}\frac{\partial}{\partial t}(\rho e)dV \;+\; \oint_{S}\rho e(\underline{u}\cdot\underline{n})dA \tag{A.23}$$

and also to the control volume

$$\frac{d}{dt}\int_{\Omega}(\rho e)dV \;=\; \int_{\Omega}\frac{\partial}{\partial t}(\rho e)dV \;+\; \oint_{\Gamma}\rho e(\underline{u}\cdot\underline{n})dA \tag{A.24}$$

then

$$\frac{d}{dt}\int_{V}(\rho e)dV \;=\; \frac{d}{dt}\int_{\Omega}(\rho e)dV \;+\; \oint_{S}\rho e(\underline{u}-\underline{U})\cdot\underline{n}dA \tag{A.25}$$

and

$$\frac{d}{dt}\int_{\Omega}(\rho e)dV \;=\; -\oint_{S}\rho e(\underline{u}-\underline{U})\cdot\underline{n}dA \;+\; \oint_{S}p(\underline{u}\cdot\underline{n})dA \tag{A.26}$$

Since the enthalpy is defined as

$$h \;=\; e \;+\; \frac{p}{\rho} \tag{A.27}$$

then by rearrangement and substitution

$$\frac{d}{dt}\int_{\Omega}\rho\left(h-\frac{p}{\rho}\right)dV = -\oint_{S}\rho\left(h-\frac{p}{\rho}\right)(\underline{u}-\underline{U})\cdot\underline{n}dA - \oint_{S}p\underline{u}\cdot\underline{n}dA$$

$$= -\oint_{S}\rho h\underline{v}\cdot\underline{n} - \oint_{S}p\underline{U}\cdot\underline{n}dA \qquad (A.28)$$

An interesting observation extends from the steady-flow zero-reference velocity simplification; the result is

$$0 = -\oint_{S}\rho h\underline{u}\cdot\underline{n}dA \qquad (A.29)$$

which is simply a statement of *conservation of heat content* between two streams that mix. Compare equations A.28 and A.21.

Introduction of the ideal gas approximation into the heat equation yields

$$\frac{d}{dt}\int_{\Omega}\rho\left(c_pT-\frac{p}{\rho}\right)dV = -\oint\rho c_pT\underline{v}\cdot\underline{n}dA - \oint_{S}p\underline{U}\cdot\underline{n}dA \qquad (A.30)$$

Now, from the relations

$$p = \rho RT$$

$$c_p = \frac{\gamma}{\gamma-1}R$$

then

$$\frac{d}{dt}\int_{\Omega}\left(p\frac{\gamma}{\gamma-1}-p\right)dV = -\oint_{S}p\frac{\gamma}{\gamma-1}\underline{v}\cdot\underline{n}dA - \oint_{S}p\underline{U}\cdot\underline{n}dA \qquad (A.31)$$

which simplifies to

$$\frac{d}{dt}\int_{\Omega}\left\{\frac{p}{\gamma-1}\right\}dV = -\oint_{S}p\frac{\gamma}{\gamma-1}\underline{v}\cdot\underline{n}dA - \oint_{S}p\underline{U}\cdot\underline{n}dA \qquad (A.32)$$

and if the specific heat ratio is constant

$$\frac{d}{dt}\int_{\Omega}pdV = -\oint_{S}p\gamma\underline{v}\cdot\underline{n}dA - (\gamma-1)\oint_{S}p\underline{U}\cdot\underline{n}dA \qquad (A.33)$$

In the finite volume analysis of the present work this form of the heat equation is more convenient (than the general power equation) because of the absence of the cube of velocity.

Entropy

Creation of entropy in a material volume is given by the balance of the rate of increase of entropy and the entropy flux across the surface and, by definition, is a positive quantity,

$$\frac{d}{dt}\int_V \rho s dV + \oint_S \frac{1}{T}\underline{q}\cdot\underline{n}dA \geq 0 \qquad (A.34)$$

where the entropy flux has been identified as the quotient of the heat flux and temperature of transport (this can be shown; see for instance, Appendix B). Reynolds' transport theorem is again drawn on to provide the extention of a material volume to a control volume with local surface velocity $\underline{U}$; the result is

$$\frac{d}{dt}\int_\Omega \rho s dV + \oint_\Gamma \rho s(\underline{u}-\underline{U})\cdot\underline{n}dA - \oint_\Gamma \frac{1}{T}\underline{q}\cdot\underline{n}dA \geq 0 \qquad (A.35)$$

An interesting analytic excursion (see Appendix B) shows the production of entropy is given by viscous dissipation and thermal effects

$$\frac{Ds}{Dt} + \frac{1}{\rho}\nabla\cdot\left(\frac{q}{T}\right) = \frac{1}{\rho T}\psi + \frac{\kappa}{\rho}\left(\frac{\nabla T}{T}\right)^2 \geq 0 \qquad (A.36)$$

where the viscous dissipation is defined as

$$\psi = (\underline{S}'\cdot\nabla)\cdot\underline{u} \qquad (A.37)$$

It is evident that if the entropy balance is non-zero the result must be positive since the production terms are proportional to the *square* of temperature and velocity gradients.

Appendix B

Derivation of the Heat Equation

Overview

It is understood that the *mechanical power equation* is given by the product of the Navier Stokes equation and velocity, and that the *general power equation* is formed by application of the first law of thermodynamics to a control volume. Here, an integral form of the *heat equation* is derived as the difference between the integral forms of the mechanical power and general power equations.

Mechanical Power Equation

For an infinitesimal fluid volume the product of velocity and the Navier Stokes equation yields

$$\rho \underline{u} \cdot \frac{d\underline{u}}{dt} = \rho \underline{u} \cdot \underline{g} + \underline{u} \cdot (\nabla \cdot \underline{S}) \qquad (B.1)$$

where the general stress tensor is composed of normal (pressure) and viscous components

$$\underline{S} = -p\underline{I} + \underline{S}' \qquad (B.2)$$

If gravitational effects are ignored and the total derivative written in explicit form, the mechanical power equation becomes

$$\rho \underline{u} \cdot \frac{d\underline{u}}{dt} + \underline{\rho} \cdot \{(\underline{u} \cdot \nabla)\underline{u}\} = -(\underline{u} \cdot \nabla)p + \underline{u} \cdot (\nabla \cdot \underline{S}) \qquad (B.3)$$

Expanding the first term

$$\rho \underline{u} \cdot \frac{\partial \underline{u}}{\partial t} = \frac{\partial}{\partial t}\left(\frac{\rho u^2}{2}\right) - \frac{u^2}{2}\frac{\partial u}{\partial t} \qquad (B.4)$$

then the convective flux term becomes

$$\rho \underline{u} \cdot \{(\underline{u} \cdot \nabla)\underline{u}\} = (\underline{u} \cdot \nabla)\left(\rho \frac{u^2}{2}\right) - \frac{u^2}{2}(\underline{u} \cdot \nabla)\rho \qquad (B.5)$$

and combining with the mechanical power equation results in

$$\frac{\partial}{\partial t}\left(\rho \frac{u^2}{2}\right) - \frac{u^2}{2}\left(\frac{\partial \rho}{\partial t} + (\underline{u} \cdot \nabla)\rho\right) = -(\underline{u} \cdot \nabla)\left(\rho \frac{u^2}{2} + p\right) + \underline{u} \cdot (\nabla \cdot \underline{S}') \qquad (B.6)$$

From the general form of the continuity equation

$$-\frac{u^2}{2}\frac{\partial \rho}{\partial t} = \rho\frac{u^2}{2}\nabla\cdot\underline{u}+\frac{u^2}{2}(\underline{u}\cdot\nabla)\rho \qquad (B.7)$$

and also from the relation

$$\nabla\cdot\left\{\underline{u}\left(\rho\frac{u^2}{2}\right)\right\} = (\underline{u}\cdot\nabla)\left(\rho\frac{u^2}{2}\right)+\rho\frac{u^2}{2}(\nabla\cdot\underline{u}) \qquad (B.8)$$

then

$$\frac{\partial}{\partial t}\left(\rho\frac{u^2}{2}\right) = \left\{-\rho\frac{u^2}{2}\nabla\cdot\underline{u}-\frac{u^2}{2}(\underline{u}\cdot\nabla)\rho\right\}+\frac{u^2}{2}(\underline{u}\cdot\nabla)\rho$$
$$-\nabla\cdot\left\{\underline{u}\left(\rho\frac{u^2}{2}\right)\right\}+\rho\frac{u^2}{2}(\nabla\cdot\underline{u})-(\underline{u}\cdot\nabla)p+\underline{u}\cdot(\nabla\cdot\underline{S}') \qquad (B.9)$$

this can be reduced to

$$\frac{\partial}{\partial t}\left(\rho\frac{u^2}{2}\right) = -\nabla\cdot\left\{\underline{u}\left(\rho\frac{u^2}{2}\right)\right\}-(\underline{u}\cdot\nabla)p+\underline{u}\cdot(\nabla\cdot\underline{S}') \qquad (B.10)$$

which, when integrated over a material volume V, yields

$$\int_V\frac{\partial}{\partial t}\left(\rho\frac{u^2}{2}\right)dV = -\oint_S\underline{n}\cdot\left\{\underline{u}\left(\rho\frac{u^2}{2}\right)\right\}dS-\int_V\underline{u}\cdot(\nabla p-\nabla\cdot\underline{S}')dV \qquad (B.11)$$

This is the desired result; it is a statement that the integrated kinetic energy inside the material volume will change if work has been done (due to pressure forces or viscous stresses within the control volume) or there is a net flux of kinetic energy.

General Power Equation

The first law of thermodynamics for a system has been shown to be

$$\frac{d}{dt}\int_V\rho\left(e+\frac{u^2}{2}\right)dV = \int_V\rho\underline{g}>\underline{u}dV+\oint_S\underline{u}\cdot(\underline{n}\cdot\underline{S})dA-\oint_S\underline{q}\cdot\underline{n}dA \qquad (B.12)$$

If the gravitational effect is ignored and Reynolds' transport theorem applied to the total derivative,

$$\int_V \frac{d}{dt}\left\{\rho\left(e+\frac{u^2}{2}\right)\right\}dV = -\oint_S \rho\left(e+\frac{u^2}{2}\right)\underline{u}\cdot\underline{n}dA + \oint_S \underline{n}\cdot(\underline{u}\cdot\underline{S})dA - \oint_S \underline{q}\cdot\underline{n}dA \tag{B.13}$$

which can conveniently be written

$$\int_V \frac{\partial}{\partial t}\left(\rho\frac{u^2}{2}\right)dV + \int_V \frac{\partial}{\partial t}(\rho e)dV = -\oint_S \left(\rho\frac{u^2}{2}\right)\underline{n}\cdot\underline{u}dA - \oint_S \rho e\underline{n}\cdot\underline{u}dA + \int_V \nabla\cdot(\underline{U}\cdot\underline{S})dV - \int_V \nabla\cdot\underline{q}dA \tag{B.14}$$

Now, since

$$\nabla\cdot(\underline{u}\cdot\underline{S}) = \underline{u}\cdot(\nabla\cdot\underline{S}' - \underline{u}\cdot\nabla P + \phi - P(\underline{n}\cdot\nabla)\underline{u} \tag{B.15}$$

then

$$\int_V \frac{\partial}{\partial t}\left(\rho\frac{u^2}{2}\right)dV + \int_V \frac{\partial}{\partial t}(\rho e)dV = -\oint_S \left(\rho\frac{u^2}{2}\right)\underline{n}\cdot\underline{u}dA - \oint_S \rho e\underline{n}\cdot\underline{u}dA + \int_V \{\underline{u}\cdot(\nabla\cdot\underline{S}') + \phi - \underline{u}\cdot\nabla P\}dV - \int_V \nabla\cdot\underline{q}dV - \int_V P\underline{n}\cdot(\nabla\cdot\underline{u})dV \tag{B.16}$$

This is the desired form; it is evident we can identify the mechanical power equation within the general power equation.

Heat Equation

Recall that the heat equation is formed as the difference of the mechanical power and general power equations; for the form of these equations as derived above, the result is

$$\int_V \frac{\partial}{\partial t}(\rho e)dV = -\oint_S \rho e\underline{n}\cdot\underline{u}dA + \int_V \phi dV - \int_V \nabla\cdot\underline{q}dV - \int_V p\underline{n}\cdot(\nabla\cdot\underline{u})dV \tag{B.17}$$

or simply

$$\frac{d}{dt}\int_V \rho e\, dV = \int_V \{\phi - \nabla \cdot \underline{q} - P\nabla \cdot \underline{u}\}\, dV \qquad (B.18)$$

An important form of Reynolds' transport theorem provides that

$$\frac{d}{dt}\rho X\, dV = \int_V \rho \frac{DX}{Dt}\, dV \qquad (B.19)$$

and therefore

$$\int_V \left\{ \rho \frac{\epsilon}{Dt} + \nabla \cdot \underline{q} - \phi + P\nabla \cdot \underline{u} \right\} dV = 0 \qquad (B.20)$$

so for an arbitrary material volume

$$\rho \frac{e}{Dt} + P\nabla \cdot \underline{u} = \phi - \nabla \cdot \underline{q} \qquad (B.21)$$

Introduce

$$\frac{1}{\nu}\frac{D\rho}{Dt} = \nabla \cdot \underline{u} \qquad (B.22)$$

$$T\frac{Ds}{Dt} = \frac{\epsilon}{Dt} + P\frac{D\rho}{Dt} \qquad (B.23)$$

so

$$\rho\left\{ T\frac{Ds}{Dt} - P\frac{D\rho}{Dt} \right\} + \rho P\frac{D\rho}{Dt} = \rho T\frac{Ds}{Dt}$$

$$= \phi - \nabla \cdot \underline{q} \qquad (B.24)$$

Recognize that

$$\underline{q} = -\kappa \nabla T \qquad (B.25)$$

and

$$\nabla \cdot \left\{ \frac{\kappa \nabla T}{T} \right\} = -\frac{\kappa}{T^2} + \frac{1}{T}\nabla \cdot (\kappa \nabla T) \qquad (B.26)$$

so

$$\frac{Ds}{Dt} = \frac{\phi}{\rho T} + \frac{T}{\rho T}\left\{\nabla\cdot\left(\frac{\kappa\nabla T}{T}\right)+\frac{\kappa}{T^2}(\nabla T)^2\right\} \qquad (B.27)$$

$$\frac{Ds}{Dt}-\nabla\cdot\left\{\frac{\kappa\nabla T}{T}\right\} = \frac{\phi}{\rho T}+\frac{\kappa}{\rho}\left(\frac{\nabla T}{T}\right)^2 \qquad (B.28)$$

The terms on the right-hand-side represent the square of velocity and temperature gradients and are therfore always positive; this forms the basis for the second law. Clearly

$$\frac{Ds}{Dt} - \nabla\cdot\left\{\frac{\kappa\nabla T}{T}\right\} \geq 0 \qquad (B.29)$$

and since

$$\frac{q}{T} = -\frac{\kappa\nabla T}{T} \qquad (B.30)$$

we finally obtain

$$\frac{Ds}{Dt} + \nabla\cdot\left(\frac{q}{T}\right) \geq 0 \qquad (B.31)$$

Appendix C

Steady-State Nozzle Coefficient

Flow coefficient

At an (isolated) ejector nozzle exit the steady-state mass flowrate is, for a uniform flow, given by

$$\dot{m} = \rho u A \qquad (C.1)$$

Of interest here is a more convenient form of this relation which introduces stagnation field variables and the flow coefficient, Φ.

Stagnation conditions are incorporated by the product

$$\dot{m} = \rho_0 c_0 A \left\{ \frac{\rho}{\rho_0} \frac{u}{c} \frac{c}{c_0} \right\} \qquad (C.2)$$

and identify the flow coefficient

$$\dot{m} = \rho_0 c_0 A \Phi \qquad (C.3)$$

The flow coefficient can be expressed in terms of the Mach number

$$\Phi = M \frac{\rho}{\rho_0} \frac{c}{c_0} \qquad (C.4)$$

but a more convenient relation uses

$$M \frac{c}{c_0} = \frac{u}{c_0} \qquad (C.5)$$

so the expression for the flow coefficient becomes

$$\Phi = \left\{ \frac{\rho}{\rho_0} \right\} \left(\frac{2}{\gamma - 1} \left\{ 1 - \left(\frac{P}{P_0} \right)^{\frac{\gamma - 1}{\gamma}} \right\} \right)^{\frac{1}{2}} \qquad (C.6)$$

To complete the desired form of the flow coefficient we recognize the isentropic pressure ratio

$$\frac{\rho_1}{\rho_0} = \left(\frac{P_1}{P_0} \right)^{\frac{1}{\gamma}} \qquad (C.7)$$

and therefore

$$\Phi = \left(\frac{P_1}{P_0}\right)^{\frac{1}{\gamma}}\left(\frac{2}{\gamma-1}\left\{1-\left(\frac{P_1}{P_0}\right)^{\frac{\gamma-1}{\gamma}}\right\}\right)^{\frac{1}{2}} \qquad (C.8)$$

As a final step, introduce

$$\left(\frac{P}{P_0}\right)^{\frac{1}{\gamma}} = \left(\frac{c}{c_0}\right)^{\frac{2}{\gamma-1}} \qquad (C.9)$$

so that

$$\Phi = \left(\frac{c_1}{c_0}\right)^{\frac{2}{\gamma-1}}\left(\frac{2}{\gamma-1}\left\{1-\left(\frac{P_1}{P_0}\right)^{\frac{\gamma-1}{\gamma}}\right\}\right)^{\frac{1}{2}} \qquad (C.10)$$

Aerodynamic choking

Channel flow is considered aerodynamically choked if the *normalized* mass flow rate through a section reached a maximum. Because the fluid stagnation properties are assumed constant, the flow function has the functional form

$$\Phi = f\left(\frac{c_1}{c_0}\right) \qquad (C.11)$$

(and represents the functional form of the normalized mass flow rate).

If Φ is a maximum so must also its square; we obtain the condition for choking that

$$\frac{d(\Phi^2)}{d(\beta^2)} = 0 \qquad (C.12)$$

where

$$\beta = \left(\frac{c_1}{c_0}\right)^2 \qquad (C.13)$$

The square of the flow function is now

$$\Phi^2 = \beta^{\frac{2}{\gamma-1}}\left(\frac{2}{\gamma-1}\{1-\beta\}\right) \qquad (C.14)$$

which simplifies to

$$\Phi^2 = \frac{2}{\gamma-1}\beta^{\frac{2}{\gamma-1}} - \frac{2}{\gamma-1}\beta^{\frac{\gamma+1}{\gamma-1}} \qquad (C.15)$$

and the derivative is

$$\frac{d(\Phi^2)}{d\beta} = 0 = \frac{2}{\gamma-1}\beta^{\frac{2}{\gamma-1}-1}\left\{\frac{2}{\gamma-1} - \frac{\gamma+1}{\gamma-1}\beta\right\} \qquad (C.16)$$

Since

$$\beta \neq 0 \qquad (C.17)$$

then it is clear

$$\frac{\gamma+1}{\gamma-1}\beta = \frac{2}{\gamma-1} \qquad (C.18)$$

and therefore the condition of aerodynamically choked flow is that

$$\beta = \frac{2}{\gamma+1} \qquad (C.19)$$

or

$$\left(\frac{c_1}{c_2}\right)^2 = \frac{2}{\gamma+1} \qquad (C.20)$$

$$\frac{P_1}{P_0} = \left(\frac{2}{\gamma+1}\right)^{\frac{\gamma}{\gamma-1}} \qquad (C.21)$$

When this result is compared with the expression for the local Mach number we find the trivial result that sonic conditions are reached when the flow is choked.

Summary

Steady-state mass flowrate through the primary nozzle of the ejector is given by

$$\dot{m}_1 = \rho_0 c_0 A_1 \Phi$$

where

$$\Phi = \left(\frac{1}{NPR}\right)^{\frac{1}{\gamma}} \left(\frac{2}{\gamma - 1}\left\{1 - \left(\frac{1}{NPR}\right)^{\frac{\gamma - 1}{\gamma}}\right\}\right)^{\frac{1}{2}} \qquad NPR < \left(\frac{\gamma + 1}{2}\right)^{\frac{\gamma}{\gamma - 1}}$$

$$\Phi = \left(\frac{2}{\gamma + 1}\right)^{\frac{\gamma + 1}{2(\gamma - 1)}} \qquad NPR \geq \left(\frac{\gamma + 1}{2}\right)^{\frac{\gamma}{\gamma - 1}}$$

Appendix D

Alternate Mass Flowrate Equations

Summary of Relations

The literature reflects the use of several different forms of the mass flowrate equation; the most common are gathered below:

$$\dot{m} = \rho c A \left(\frac{P_0}{P}\right)^{\gamma-1/2\gamma} \left\{\frac{2}{\gamma-1}\left(1-\left(\frac{P}{P_0}\right)^{\gamma-1/\gamma}\right)\right\}^{1/2} \qquad (D.1)$$

$$\dot{m} = \rho A \left\{\frac{2\gamma R T_0}{\gamma-1}\left(1-\left(\frac{P}{P_0}\right)^{\gamma-1/\gamma}\right)\right\}^{1/2} \qquad (D.2)$$

$$\dot{m} = \frac{A P_0}{\sqrt{T_0}}\left(\frac{P}{P_0}\right)^{1/\gamma} \left\{\frac{2\gamma}{R(\gamma-1)}\left(1-\left(\frac{P}{P_0}\right)^{\gamma-1/\gamma}\right)\right\}^{1/2} \qquad (D.3)$$

For the present work, the mass flowrate equation is that given by the derivation in Appendix G:

$$\dot{m} = \frac{P A}{\sqrt{R T_0}} f_6(\gamma, M) \qquad (D.4)$$

Appendix E

Change in Entropy due to Mixing

Overview

In situations where multiple solutions for the Mach numbercan be extracted from the momentum equation, the "correct" answer is quite often given by that whose circumstances are in collaboration with the second law of thermodynamics. For a steady-state flow, the form of the second law takes on a convenient form and is derived below for interest and the completeness of this report.

Derivation

For an ideal gas, Gibbs' relation gives that

$$dS = C_P \frac{dT}{T} - R \frac{dP}{P} \qquad (E.1)$$

If the gas is thermally and calorically perfect, then

$$C_P = \frac{\gamma}{\gamma - 1} R = const \qquad (E.2)$$

and integration of the previous result gives

$$\frac{S_1 - S_0}{R} = \frac{\gamma}{\gamma - 1} \ln\left(\frac{T_1}{T_0}\right) - \ln\left(\frac{P_1}{P_0}\right) \qquad (E.3)$$

Consider steady-state, steady-flow as an example; the integral entropy balance yields

$$\int_\Gamma \rho s \underline{u} \cdot \underline{n} dA \geq 0 \qquad (E.4)$$

so from the definition

$$\frac{d\dot{m}}{dA} = -\rho \underline{u} \cdot \underline{n} \qquad (E.5)$$

then

$$-\int_\Gamma S d\dot{m} \geq 0 \qquad (E.6)$$

For one-dimensional flow

$$-S_{P1}\dot{m}_{P1} - S_{S1}\dot{m}_{S1} + S_2\dot{m}_2 \geq 0 \qquad (E.7)$$

we obtain

$$\frac{\Delta S}{\dot{m}_{P1}} = -S_{P1} - S_{S1}\frac{\dot{m}_{S1}}{\dot{m}_{P1}} + S_2\frac{\dot{m}_2}{\dot{m}_{P1}} \geq 0 \qquad (E.8)$$

Because

$$\dot{m}_{S1} = \dot{m}_2 - \dot{m}_{P1} \qquad (E.9)$$

then

$$\frac{\Delta S}{\dot{m}_{P1}} = -S_{P1} - S_{S1}\left(\frac{\dot{m}_2}{\dot{m}_{P1}} - 1\right) + S_2\frac{\dot{m}_2}{\dot{m}_{P1}} \geq 0 \qquad (E.10)$$

and so

$$\frac{\Delta S}{\dot{m}_{P1}} = -(S_{P1} - S_{S1}) + \frac{\dot{m}_2}{\dot{m}_{P1}}(S_2 - S_{S1}) \geq 0 \qquad (E.11)$$

By application of the ideal gas relation

$$\frac{\Delta S}{R\dot{m}_{P1}} = -\left(\left\{\frac{\gamma}{\gamma-1}\ln\left(\frac{T_{P1}}{T_{S1}}\right)\right\} - \ln\left(\frac{P_{P1}}{P_{S1}}\right)\right) + \frac{\dot{m}_2}{\dot{m}_{P1}}\left(\left\{\frac{\gamma}{\gamma-1}\ln\left(\frac{T_2}{T_{S1}}\right)\right\} - \ln\left(\frac{P_2}{P_{S1}}\right)\right)$$

which simplifies to the form

$$\frac{\Delta S}{R\dot{m}_{P1}} = \frac{\gamma}{\gamma-1}\ln\left(\frac{T_{S1}}{T_{P1}}\right) + \frac{\gamma}{\gamma-1}\left(\frac{\dot{m}_2}{\dot{m}_{P1}}\right)\ln\left(\frac{T_2}{T_{S1}}\right) - \frac{\dot{m}_2}{\dot{m}_{P1}}\ln\left(\frac{P_2}{P_{P1}}\right)$$

This can be re-arranged in terms of the mass entrainment ratio

$$\frac{\Delta S}{R\dot{m}_{P1}} = \frac{\gamma}{\gamma-1}\ln\left(\frac{T_{S1}}{T_{P1}}\right) + \frac{\gamma}{\gamma-1}\ln\left(\frac{T_2}{T_{S1}}\right) + \frac{\gamma}{\gamma-1}\left(\frac{\dot{m}_{S1}}{\dot{m}_{P1}}\right)\ln\left(\frac{T_2}{T_{S1}}\right) - \frac{\dot{m}_2}{\dot{m}_{P1}}\ln\left(\frac{P_2}{P_{P1}}\right)$$

$$\frac{\Delta S}{R\dot{m}_{P1}} = \frac{\gamma}{\gamma-1}\ln\left(\frac{T_2}{T_{P1}}\right) + \frac{\gamma}{\gamma-1}\left(\frac{\dot{m}_{S1}}{\dot{m}_{P1}}\right)\ln\left(\frac{T_2}{T_{S1}}\right) - \frac{\dot{m}_2}{\dot{m}_{P1}}\ln\left(\frac{P_2}{P_{P1}}\right) \qquad (E.12)$$

Introducing the entrainment ratio

$$\mu = \frac{\dot{m}_{S1}}{\dot{m}_{P1}} \qquad (E.13)$$

then we have the desired result

$$\frac{\Delta S}{R\dot{m}_{P1}} = \frac{\gamma}{\gamma-1}\ln\left(\frac{T_2}{T_{P1}}\right) + \frac{\mu\gamma}{\gamma-1}\ln\left(\frac{T_2}{T_{S1}}\right) - (1+\mu)\ln\left(\frac{P_2}{P_{P1}}\right) \qquad (E.14)$$

Appendix F

Mixed Flow Fluid Properties

Basic Relations

Fluid properties for the mixed flow can be estimated through application of Dalton's law of partial pressures to an ideal mixing process. We summarize for convenience here relations extracted from the works of, for instance, Addy et.al.[1981] or Minardi[1982].

The specific heat is given by

$$C_{p,MR} = C_{p,P}\left(\frac{1}{1+\mu}\right)\left\{1+\mu\frac{C_{p,S}}{C_{p,P}}\right\} \qquad (F.1)$$

where the specific heat is related to the gas constant by

$$C_p = \frac{\gamma}{(\gamma-1)}R \qquad (F.2)$$

The equivalent molecular weight is given by a similar relation

$$M_{MR} = M_P(1+\mu)\left\{1+\mu\frac{M_P}{M_S}\right\} \qquad (F.3)$$

The specific heat ratio is

$$\frac{1}{\gamma_{MR}} = 1 - \left\{\frac{\gamma_P-1}{\gamma_P}\right\}\frac{1+\mu\frac{M_P}{M_S}}{1+\mu\frac{\gamma_S}{\gamma_P}\frac{(\gamma_P-1)}{(\gamma_S-1)}\frac{M_P}{M_S}} \qquad (F.4)$$

Appendix G

Flow Functions

Overview

Manipulation of equations is simplified (and the potential for errors reduced) when commonly occuring expressions are introduced as functions. In this appendix five expressions with physical significance are derived; they are:

1. Steady flow stagnation temperature ratio
2. Steady flow isentropic pressure ratio
3. Steady flow isentropic velocity ratio
4. Steady state isentropic area ratio
5. Mass flow function

Steady flow stagnation temperature ratio

For a steady inviscid flow with negligible body forces the energy equation for a streamline is

$$h + \frac{u^2}{2} = h_0 \qquad (G.1)$$

where h_0 is the stagnation enthalpy. This equation *does not* imply the flow is isentropic, only that there is negligible heat transfer across the control surface. Introduce a perfect gas so that

$$h = c_p T + const \qquad (G.2)$$

$$Pv = RT \qquad (G.3)$$

where P is the thermodynamic (static) pressure; also

$$c_p = \gamma R/(\gamma - 1) \qquad (G.4)$$

$$c^2 = (\partial P/\partial \rho)_s = \gamma(\partial P/\partial v)_T = \gamma RT \qquad (G.5)$$

where c_p is the specific heat at constant pressure and c is the speed of sound. These results provide

$$c_p T + \frac{u^2}{2} = c_p T_0 \qquad (G.6)$$

$$\frac{c_p T}{c^2} + \frac{1}{2}\frac{u^2}{c^2} = \frac{c_p T_0}{c^2} \qquad (G.7)$$

so that

$$\frac{T_0}{T} = 1 + \frac{1}{2}\frac{u^2 c^2}{c^2 c_p T}$$

$$= 1 + \frac{1}{2} M^2 \frac{\gamma R T}{\gamma R}(\gamma - 1)\frac{1}{T}$$

$$= 1 + \frac{\gamma - 1}{2} M^2 \qquad (G.8)$$

In functional form this is written as

$$\frac{T_0}{T} = f_2(\gamma, M) \qquad (G.9)$$

Note that no specific assumption of isentropic flow was made.

Steady flow isentropic pressure ratio

In a steady isentropic flow there exists a convenient relation between temperature and pressure

$$\frac{T_0}{T} = \left(\frac{P_0}{P}\right)^{\left(\frac{\gamma-1}{\gamma}\right)} \qquad (G.10)$$

and thus

$$\frac{P_0}{P} = \left\{1 + \frac{\gamma - 1}{2} M^2\right\}^{\frac{\gamma}{\gamma-1}} \qquad (G.11)$$

so

$$\frac{P_0}{P} = \{f_1(\gamma, M)\}^{\frac{\gamma}{\gamma-1}} = f_3(\gamma, M) \qquad (G.12)$$

Steady flow isentropic velocity ratio

It is useful in the analysis of choked flow to invert the isentropic pressure ratio equation so that

$$\frac{u}{c} = \sqrt{\frac{2}{\gamma - 1}\left\{\left(\frac{P_0}{P}\right)^{\gamma - 1/\gamma} - 1\right\}} \qquad (G.13)$$

this can be rearranged to yield

$$\frac{u}{c} = \left(\frac{P_0}{P}\right)^{\gamma - 1/2\gamma}\sqrt{\frac{2}{\gamma - 1}\left\{1 - \left(\frac{P}{P_0}\right)^{\gamma - 1/\gamma}\right\}} \qquad (G.14)$$

A characteristic pressure ratio is that given by the quotient of the stagnation pressure and the static pressure,

$$NPR = \frac{P_0}{P} \qquad (G.15)$$

and we recognize that, as a general rule, $P < P_0$, then $NPR > 1$. The isentropic velocity ratio is now

$$\frac{u}{c} = (NPR)^{\gamma - 1/2\gamma}\sqrt{\frac{2}{\gamma - 1}\left\{1 - \left(\frac{1}{NPR}\right)^{\gamma - 1/\gamma}\right\}}$$

$$= f_4(\gamma, NPR) \qquad (G.16)$$

Since the speed of sound can be written as a function of the nozzle pressure ratio,

$$\frac{c}{c_0} = \left(\frac{P}{P_0}\right)^{\frac{\gamma - 1}{2\gamma}} \qquad (G.17)$$

then an alternate expression is

$$\frac{u}{c_0} = \sqrt{\frac{2}{\gamma - 1}\left\{1 - (NPR)^{\frac{\gamma}{\gamma - 1}}\right\}} \qquad (G.18)$$

Steady-state isentropic area ratio

For a steady-state flow the condition of conservation of mass yields the mass flux ratio

$$\frac{A}{A^*} = \frac{\rho_* u_*}{\rho u} \qquad (G.19)$$

where an asterisk denotes sonic conditions. From this ratio

$$\frac{\rho_* u_*}{\rho u} = \frac{\rho_* c_*}{\rho_0 c_0}\frac{1}{M}\frac{\rho_0 c_0}{\rho c}$$

$$= \left(\frac{2}{\gamma+1}\right)^{1/\gamma-1}\frac{1}{M}\sqrt{\frac{2}{\gamma+1}}\left(1+\frac{\gamma-1}{2}M^2\right)^{1/\gamma-1}\sqrt{1+\frac{\gamma-1}{2}M^2}$$

$$= \frac{1}{M}\left(\frac{2}{\gamma+1}\right)^{\left(\frac{\gamma+1}{2(\gamma-1)}\right)}\left(1+\frac{\gamma-1}{2}M^2\right)^{\left(\frac{\gamma+1}{2(\gamma-1)}\right)}$$

$$= \frac{1}{M}\left\{\left(\frac{2}{\gamma+1}\right)\left(1+\frac{\gamma-1}{2}M^2\right)\right\}^{\left(\frac{\gamma+1}{2(\gamma-1)}\right)}$$

$$= f_5(\gamma, M) \qquad (G.20)$$

Mass flow function

From the definition of the mass flow rate

$$\dot{m} = \rho v A = \frac{v A P}{R T} \qquad (G.21)$$

then

$$\frac{\dot{m}}{P A} = \frac{v}{R T} = \frac{v}{R}\frac{1}{T_0}\frac{T_0}{T}$$

$$= \frac{1}{R T_0}\frac{T_0}{T}\frac{v}{c_0}c_0$$

$$= \sqrt{\frac{\gamma}{R T_0}}\frac{T_0}{T}\frac{v}{c_0} \qquad (G.22)$$

Since the velocity is given by

$$v = Mc$$

then

$$\frac{\dot{m}}{P A} = M\sqrt{\frac{\gamma}{R T_0}}\frac{T_0}{T}\frac{c}{c_0} \qquad (G.23)$$

and the temperature ratio

$$\frac{T_0}{T} = 1 + \frac{\gamma - 1}{2} M^2 \qquad (G.24)$$

$$\frac{c_0}{c} = \sqrt{\frac{T_0}{T}} \qquad (G.25)$$

leads to the result

$$\frac{\dot{m}}{PA} = M\sqrt{\frac{\gamma}{RT_0}}\sqrt{1 + \frac{\gamma - 1}{2} M^2}$$

$$= \sqrt{\frac{1}{RT_0}}\left(M\sqrt{\gamma\left(1 + \frac{\gamma - 1}{2} M^2\right)}\right)$$

$$= \sqrt{\frac{1}{RT_0}} f_6(\gamma, M) \qquad (G.26)$$

Summary

Five dimensionless functions have been derived, each associated with a specific nondimensional physical meaning derived above; they are:

$$f_2 = 1 + \frac{\gamma - 1}{2} M^2$$

$$f_3 = \left\{1 + \frac{\gamma - 1}{2} M^2\right\}^{\gamma/\gamma - 1}$$

$$f_4 = \left(\frac{P_0}{P}\right)^{\gamma - 1/2\gamma} \sqrt{\frac{2}{\gamma - 1}\left\{1 - \left(\frac{P}{P_0}\right)^{\gamma - 1/\gamma}\right\}}$$

$$f_5 = \frac{1}{M}\left\{\left(\frac{2}{\gamma + 1}\right)\left(1 + \frac{\gamma - 1}{2} M^2\right)\right\}^{\left(\frac{\gamma + 1}{2(\gamma - 1)}\right)}$$

$$f_6 = M\sqrt{\gamma\left(1 + \frac{\gamma - 1}{2} M^2\right)}$$

Appendix H

Integrals of Self-Similar Profiles

Introduction

Specific assumptions for the dimensionless form of the self-similar temperature and velocity profiles will avoid cumbersum numerical integration schemes in the final analysis (and in the computer code). This appendix provides an assumed form of the various profiles for the present work and the results of integrations of them. Some of the more difficult integrals have been explored with the MACSYMA symbolic manipulator on the NASA/Lewis Vax.

If we consider the jet expansion characteristics of Figure H.1, then it is evident two expressions should be constructed for each self-similar profile, one for Region I and the other for Region II. The basic form of the non-dimensional profiles are given by:

$$\Phi(\xi) = \begin{cases} (1-\xi^{1.5})^2 & ; \quad 0 \le \xi < 1, \quad \hat{\xi} > 1 \\ 0 & ; \quad 1 \le \xi \le \hat{\xi}, \quad \hat{\xi} > 1 \\ (1-\xi^{1.5})^2 & ; \quad 0 \le \xi \le \hat{\xi}, \quad \hat{\xi} < 1 \end{cases} \tag{H.1}$$

$$\Lambda(\xi) = \begin{cases} 1; & 0 \le \xi < \xi^*, \quad \hat{\xi} > 1 \\ 0; & \xi^* \le \xi \le \hat{\xi}, \quad \hat{\xi} > 1 \\ 1; & 0 \le \xi \le \hat{\xi}, \quad \hat{\xi} < 1 \end{cases} \tag{H.2}$$

Application to integrals incorporating these profiles are given in the sections that follow. For the case of analysis in the present work it is assumed that

$$\xi^* = 1. \tag{H.3}$$

Basic f_i Integrals

Several of the velocity integrals are common to many of the self-similar profile integrals, so it simplifies the presentation to summarize them. First, set

$$f_1 = (1-\xi^{1.5})^2 \tag{H.4}$$

from which

$$\int f_1 d\xi = +0.25\xi^4 - 0.8\xi^{2.5} + \xi \tag{H.5}$$

$$\int (1-f_1) d\xi = -0.25\xi^4 + 0.8\xi^{2.5} \tag{H.6}$$

$$\int f_1^2 d\xi = \frac{110\xi^7 - 560\xi^{5.5} + 1155\xi^4 - 1232\xi^{2.5} + 770\xi}{770} \qquad (H.7)$$

$$\int (1 - f_1)^2 d\xi = \frac{11\xi^7 - 56\xi^{5.5} + 77\xi^4}{77} \qquad (H.8)$$

$$\int (f_1 - f_1^2) d\xi = - \frac{220\xi^7 - 1120\xi^{5.5} + 1925\xi^4 - 1232\xi^{2.5}}{1540} \qquad (H.9)$$

E_i Integrals

Integral evaluation distinguishes between Region I and Region II values, difference residing within the limits of integration in each case. Figure H.1 illustrates the variables used.

Region II coefficients

$$E_1 = \int_0^{\xi} \Lambda d\xi = \int_0^1 (1) d\xi + \int_1^{\xi} (0) d\xi = 1 \qquad (H.10)$$

$$E_2 = \int_0^{\xi} (1 - \Lambda) d\xi = \int_0^1 (0) d\xi + \int_0^{\xi} (1) d\xi = \xi - 1 \qquad (H.11)$$

Case where b > B

$$E_1 = \int_0^{\xi} (1) d\xi = \hat{\xi} \qquad (H.12)$$

$$E_2 = \int_0^{\xi} (0) d\xi = 0 \qquad (H.13)$$

Region I coefficients

In region I b is always less than B, but account of the potential core region requires a modification of the lower limit of integration (see figure H.1)

$$E_1 = \int_{\eta_0}^{\hat{\eta}} \Lambda d\xi = 1 - \eta_0 \qquad (H.14)$$

$$E_2 = \int_{\eta_0}^{\hat{\eta}} (1 - \Lambda) d\xi = \hat{\eta} - 1 \qquad (H.15)$$

F_i Integrals

Region II coefficients

$$F_1 = \int_0^{\xi} \Lambda \Phi d\xi = \int_0^1 (1)(f_1)d\xi + \int_1^{\xi} (0)d\xi$$

$$= +0.25(1)^4 - 0.8(1)^{2.5} + 1$$

$$= 0.45 \qquad (H.16)$$

$$F_2 = \int_0^{\xi} (1-\Lambda)\Phi d\xi = \int_0^1 (0)(f_1)d\xi + \int_1^{\xi} (0)(0)d\xi$$

$$= 0 \qquad (H.17)$$

Hereafter, elimination of the integrals of '0' can be made by inspection.

$$F_3 = \int_0^{\xi} \Lambda(1-\Phi)d\xi = \int_0^1 (1-f_1)d\xi$$

$$= -0.25(1)^4 + 0.8(1)^{2.5}$$

$$= 1 - F_1 = 0.55 \qquad (H.18)$$

$$F_4 = \int^{\xi} (1-\Lambda)(1-\Phi)d\xi = \int_0^{\xi} (1)d\xi = \xi - 1 \qquad (H.19)$$

Region I coefficients

$$F_1 = \int_{\eta_0}^0 (1)(1)d\eta$$

$$= \{-\eta_0\} + \{1 - 0.8(1)^{2.5} + 0.25(1)^4\} + \{0\}$$

$$= -\eta_0 + 0.45 \qquad (H.20)$$

$$F_2 = 0 \qquad (H.21)$$

$$F_3 = \int_0^1 (1)(1-f_1)d\eta$$

$$= 0.8(1)^{2.5} - 0.25(1)^4$$

$$= 0.55 \qquad (H.22)$$

$$F_4 = \int_1^{\hat{\eta}} (1)(1)d\xi = \hat{\eta} - 1 \qquad (H.23)$$

G_i Integrals

Region II coefficients

$$G_1 = \int_0^{\xi} \Lambda \Phi^2 d\xi = \int_0^1 \Lambda \Phi^2 d\xi$$

$$= \frac{110(1)^7 - 560(1)^{5.5} + 1155(1)^4 - 1232(1)^{2.5} + 770\,1}{770}$$

$$= \frac{243}{770} = \frac{486}{1540} \qquad (H.24)$$

$$G_2 = \int_0^{\xi} \Lambda (1-\Phi)^2 d\xi = \int_0^1 (1-\Phi)^2 d\xi$$

$$= \frac{11(1)^7 - 56(1)^{5.5} + 77(1)^4}{77} = \frac{320}{770} = \frac{640}{1540} \qquad (H.25)$$

$$G_3 = 2\int_0^{\xi} \Lambda (\Phi - \Phi^2) d\xi = 2\int_0^1 (\Phi - \Phi^2) d\xi$$

$$= -2\left\{ \frac{220(1)^7 - 1120(1)^{5.5} + 1925(1)^4 - 1232(1)^{2.5}}{1540} \right\} = \frac{414}{1540}$$

$$(H.26)$$

$$G_4 = 0 \qquad (H.27)$$

$$G_5 = \int_0^{\xi} (1-\Lambda)(1-\Phi)^2 d\xi = \int_1^{\xi} (1) d\xi = (\xi - 1) \qquad (H.28)$$

$$G_6 = 0 \qquad (H.29)$$

Region I coefficients

$$G_1 = \int_{\eta_0}^{0}(1)d\eta + \int_0^1 \Phi^2 d\eta = -\eta_0 + \frac{243}{770} \qquad (H.30)$$

$$G_2 = \int_0^1 (1-\Phi)^2 d\eta = \frac{320}{770} \qquad (H.31)$$

$$G_3 = 2\int_0^1 (\Phi - \Phi^2)d\eta = \frac{414}{1540} \qquad (H.32)$$

$$G_4 = 0 \qquad (H.33)$$

$$G_5 = \int_1^{\hat{\eta}}(1)d\eta = \hat{\eta} - 1 \qquad (H.34)$$

$$G_6 = 0 \qquad (H.35)$$

H_i Integrals

Presentation of the H_i integrals is given in terms of an arbitrary upper limit to the integration; this relates to their use in the kinetic energy analysis of Section 5.

Region I coefficients

$$H_1 = \int_0^{\xi} \Lambda(1-\Phi)^3 d\xi = \int_0^{\xi^*}$$

$$= -\{1309\xi^{*10} - 9240\xi^{*8.5} + 22440\xi^{*7} - 19040\xi^{*5.5}\}/13090 \qquad (H.36)$$

$$H_2 = \int_0^{\xi} 2\Lambda(\Phi^2 - \Phi^3)d\xi = 2\int_0^{\xi^*}(\Phi^2 - \Phi^3)d\xi$$

$$= -\{374\xi^{*10} - 2640\xi^{*8.5} + 7480\xi^{*7}$$

$$- 10880\xi^{*5.5} + 8415\xi^{*4} - 2992\xi^{*2.5}\}/1870 \qquad (H.37)$$

$$H_3 = \int_0^{\xi} \Lambda(3\Phi - 6\Phi^2 + 3\Phi^3)d\xi = \int_0^{\xi^*} \Lambda(3\Phi - 6\Phi^2 + 3\Phi^3)d\xi$$

$$= \{3927\xi^{*10} - 27720\xi^{*8.5} + 72930\xi^{*7} - 85680\xi^{*5.5} + 39270\xi^{*4}\}/13090 \quad (H.38)$$

$$H_4 = \int_0^{\xi} \Lambda\Phi^3 d\xi = \int_0^{\xi^*} \Phi^3 d\xi$$

$$= \{2618\xi^{*10} - 18480\xi^{*8.5} + 56100\xi^{*7} - 95200\xi^{*5.5} + 98175\xi^{*4} - 62832\xi^{*2.5} + 26180\xi^{*}\}/26180 \quad (H.39)$$

$$H_5 = \int_0^{\xi} (1-\Lambda)(1-\Phi)^3 d\xi = \int_{\xi^*}^{1} (1-\Phi)^3 d\xi + \int_1^{\xi} (1)d\xi$$

$$= (\xi - 1) + \left(\frac{4531}{13090} - H_1\right) \quad (H.40)$$

$$H_6 = 2\int_0^{\xi} (1-\Lambda)(\Phi^2 - \Phi^3)d\xi = 2\int_{\xi^*}^{1} (\Phi^2 - \Phi^3)d\xi$$

$$= \left(\frac{243}{1870} - H_2\right) \quad (H.41)$$

$$H_7 = \int_{\xi^*}^{1} (3\Phi - 6\Phi^2 + 3\Phi^3)d\xi = \left(\frac{2727}{13090} - H_3\right) \quad (H.42)$$

$$H_8 = \int_{\xi^*}^{1} \Phi^3 d\xi = \left(\frac{6561}{26180} + H_4\right) \quad (H.43)$$

Region II coefficients

$$H_1 = \int_0^{\xi} \Lambda(1-\Phi)^3 d\xi = \int_0^{\xi} \Lambda(1-\Phi)^3 d\xi$$

$$= -\{1309\xi^{10} - 9240\xi^{8.5} + 22440\xi^{7} - 19040\xi^{5.5}\}/13090 \quad (H.44)$$

$$H_2 = \int_0^{\xi} 2\Lambda(\Phi^2 - \Phi^3)d\xi$$

$$= -\{374\xi^{10} - 2640\xi^{8.5} + 7480\xi^{7}$$

$$-10880\xi^{5.5} + 8415\xi^{4} - 2992\xi^{2.5}\}/1870 \qquad (H.45)$$

$$H_3 = \int_0^{\xi} \Lambda(3\Phi - 6\Phi^2 + 3\Phi^3)d\xi$$

$$= \{3927\xi^{10} - 27720\xi^{8.5}$$

$$+72930\xi^{7} - 85680\xi^{5.5} + 39270\xi^{4}\}/13090 \qquad (H.46)$$

$$H_4 = \int_0^{\xi} \Lambda\Phi^3 d\xi$$

$$= \{2618\xi^{10} - 18480\xi^{8.5}$$

$$+56100\xi^{7} - 95200\xi^{5.5} + 98175\xi^{4} - 62832\xi^{2.5} + 26180\xi\}/26180$$

$$(H.47)$$

$$H_5 = 0 \qquad (H.48)$$

$$H_6 = 0 \qquad (H.49)$$

$$H_7 = 0 \qquad (H.50)$$

$$H_8 = 0 \qquad (H.51)$$

Figure H.1 Non-dimensional Mixing Region Profiles

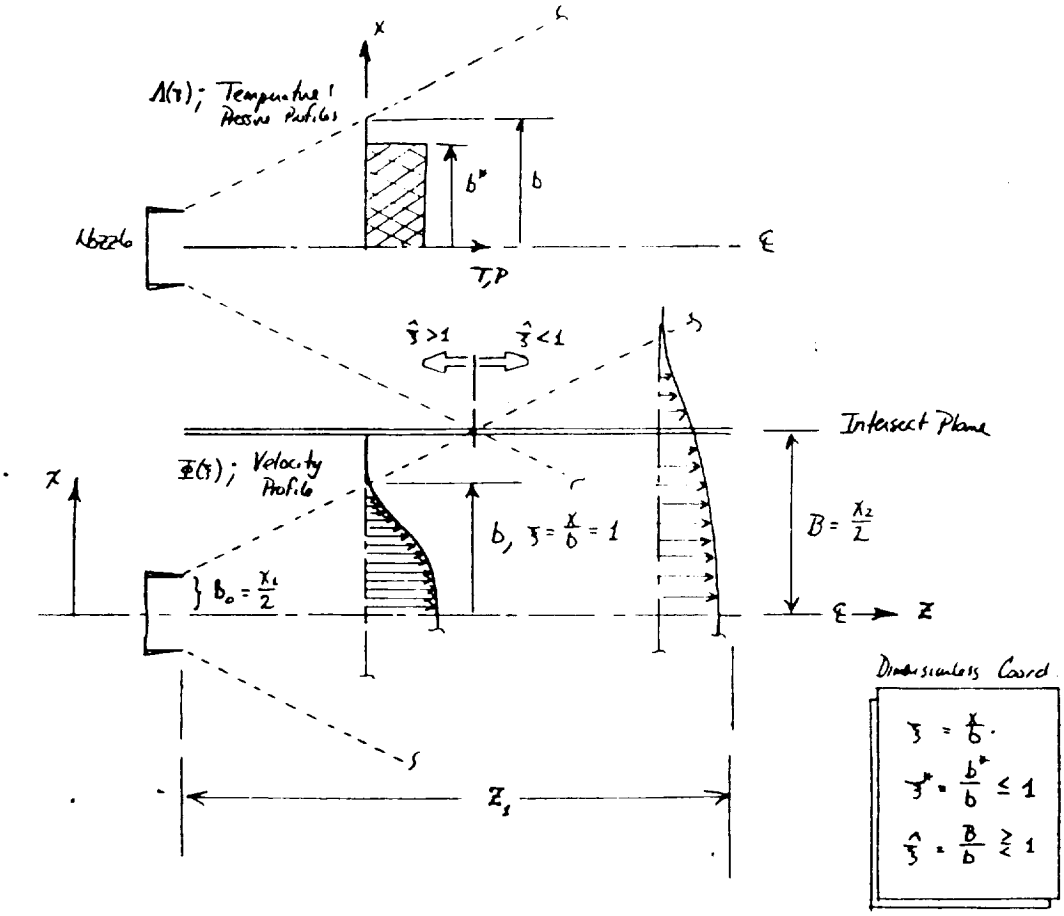

$$\Phi(\xi) = \begin{cases} \left(1-\xi^{1.5}\right)^2 & ; \quad 0 \le \xi < 1, \quad \hat{\xi} > 1 \\ 0 & ; \quad 1 \le \xi \le \hat{\xi}, \quad \hat{\xi} > 1 \\ \left(1-\xi^{1.5}\right)^2 & ; \quad 0 \le \xi \le \hat{\xi}, \quad \hat{\xi} < 1 \end{cases}$$

$$\Lambda(\xi) = \begin{cases} 1; & 0 \le \xi < \xi^*, \quad \hat{\xi} > 1 \\ 0; & \xi^* \le \xi \le \hat{\xi}, \quad \hat{\xi} > 1 \\ 1; & 0 \le \xi \le \hat{\xi}, \quad \hat{\xi} < 1 \end{cases}$$

Appendix I

Remark on System of Units

Introduction

Few applications of engineering analyses appear exempt from the need to clarify the system of units involved in calculations. Typically, confusion extends from translating back and forth between force, mass, and pressure; the usual remark is that a "consistent" system of units must be used in analysis. In the present work the *Engineering English* system of units is used.

This appendix is intended to summarize the 6 systems of units commonly used in engineering analyses so that no confusion will exist over the definition of Engineering English system for the present work. The difference in each system of units can be described by first identifying the fundamental units in each case, then categorizing each system by observing:

- the magnitude of the fundamental units,

- the choice of the physical nature of the fundamental units

- the choice in the number of fundamental units

The *magnitude* of the fundamental units originates from the metric and English systems. Because metric units are established primarily by international conferences, English units are related to them by several convenient conversion factors. Conversion factors exist within the different English systems and reflects the varied historical development of the overall system.

All the systems include length and time as defined quantities - the *physical nature* of the fundamental units indicates whether mass, force, or both are defined within the system. In an *absolute* (also known as physical) system the mass has a defined fundamental unit and force units are derived on the basis of Newton's second law. An absolute system is one for which measurements made in terms of the fundamental units are independent of the location of the measurements. In the *gravitational* system, however, a standard weight (standard force) is defined and mass units are derived. Note in either of these systems only three defined units, known as primary units, are required to define the system, with all remaining quantities derived (secondary units). The *engineering* system of units in unique in that both mass and force are defined. In this case the total number of primary units is four and consistency of units is provided by the introduction of a universal constant in Newton's second law.

From the three general systems described above, six specific systems of units can be identified; the *absolute MKS, absolute CGS, metric gravitational, English gravitational, absolute English,* and *engineering English*. In each case force, mass, length, and time are related by newtons second law

$$F = k(ma)$$

where k is a constant. A discussion of each system follows.

Absolute MKS

Also referred to as the International System (SI), mass, length, and time are defined by units of kilograms (*kg*), meters (*M*), and seconds (*s*), respectively. The unit of force is a Newton (*N*). A *1 Newton* force will give a mass of *1 kg* an acceleration of *1 m/s*^{2}. This system is the most popular Metric system and was adopted for international use by the Ninth International Congress on Weights and Measures in 1948.

Absolute CGS

This absolute system is very similar to the absolute MKS system. The unit of mass is defined as the gram (g), the unit of length is the centimeter (cm). Force units are derived and given in dynes - no abbreviated symbol - where 1 dyne = 1 g cm/s^2.

Metric gravitational

Since weights are measured by the force of attraction that a given mass experiences, a standard weight for the metric gravitational system is defined with the introduction of a standard gravitational constant g_c. The unit of mass, the kilogram-mass (kgm), is derived. Using the meter for units of length and the second for time, the kilogram-force (kgf) is a defined standard weight for the attractional force exerted on 1 kg mass by the earth where the gravitational constant has a standard value of $g_c = 9.80665$. Note a total of three defined units and one derived.

English gravitational

Making use of the foot and second that is common to all English systems of units, the English gravitational system differs from the absolute system in the same way the metric graviational does. That is, the unit of force is defined as pound-force (lbf) and the unit of mass is derived as the slug - no abbreviated name. From Newton's second law we obtain 1 slug = 1 lbf s^2/ft. When a force of 1 lbf is applied to a mass of 1 slug it will yield an acceleration of 1 ft/s^2.

Absolute English

This system is also based on three defined fundamental units; feet (ft), seconds (s), and pound-mass (lbm). The units of force are derives as the poundal, where 1 poundal = 1 lbm.ft/s^2.

Engineering English

This system is based on *four* fundamental units for length, force, time, and mass. As before, the units of length and time are feet and seconds respectively, but the unit of force is the lbf and the unit of mass is the lbm. Compatability of units is provided by the introduction of an English gravitational constant g_c into Newton's law. *This is the system used in the present work* !

$$F = m\frac{a}{g_c}$$

where g_c = 32.174 lbm ft/lbf s^2. So for this system, rather than a unit force imparting a unit acceleration to a unit mass, a unit force causes a unit mass to accelerate with a value equal to the gravitational constant. It should be noted that the constant g_c is numerically but not dimensionally equal to the standard gravitational acceleration g. Two problems arise that often lead to confusion with this system: (a) g_c is often thought of as g, implying the problem depends on terrestrial graviation when it may not, and (b) the ratio g/g_c obtained by setting $a=g$ in Newton's law is often approximated as unity and discarded, leaving the appearance that the problem is not a function of gravitational effects where it might indeed be an important part.

Conversion Between Systems

The present work uses the Engineering English system of units. A summary of the "hierarchy" of the systems in given in Table I.1. Comparison of the MKS and Engineering English units for quanities of key interest are given in Table I.2. More detailed conversions between the various systems are provided in Table I.3.

Illustrative Calculations

Some illustrative calculations may seem trivial, but are quite illustrative in following the presence (or absence) of g_c when, for instance, the details of the computer program are being traced.

Gas Constant The gas constant for air at "standard" conditions can be computed from

$$R = \overline{R}/M$$

where

$$\overline{R} = 49,720 \left\{ \frac{ft^2}{R\,s^2}\frac{lb_m}{lb_{mole}} \right\}$$

$$M = 28.98 \left\{ \frac{lb_m}{lb_{mole}} \right\}$$

Now

$$R = \frac{49,720}{28.98} \left\{ \frac{ft^2}{s^2\,R}\frac{lb_m}{lb_{mole}}\frac{lb_{mole}}{lb_m} \right\}$$

$$= 1715.66 \frac{ft^2}{s^2 R}$$

Specific Heat For calculations in the computer programs the specific heat at constant pressure is given by

$$c_p = \frac{\gamma}{\gamma - 1} R$$

so for the data of the previous calculation and a specific heat ratio of 1.4

$$c_p = \frac{1.4}{1.4 - 1} 1715.66 = 6004.81 \frac{ft^2}{s^2 R}$$

but this does not immediately conjure the "0.24" value one might expect. That value is obtained by conversion of units

$$c_p = 6004.81 \frac{ft^2}{s^2 R} \frac{1}{778.6} \frac{Btu}{lb_f ft} \frac{1}{g_c} \frac{lb_f s^2}{lb_m ft}$$

$$= 0.24 \frac{Btu}{lb_m R}$$

Sound Speed For an ideal gas approximation the speed of sound is given by

$$c = \sqrt{\gamma R T}$$

so for the data

$$\gamma = 1.4$$
$$T = 759.67 \quad R$$
$$R = 1715.66 \quad ft^2 / R s^2$$

then

$$c = \sqrt{1.4(759.67)(1715.66)} \quad \left\{ \sqrt{\frac{ft^2}{s^2 R} R} \right\}$$

$$= 1350.80 ft/s$$

Gas Density Consider an ideal gas at a pressure of 4233.6 lb_f/ft^2 and a temperature of 300 *F*; the density is determined from

$$\rho = P/RT$$

$$= \frac{4233.6}{1715.66(759.67)} \left\{ \frac{lb_f/ft^2}{(ft^2/s^2R)R} \right\}$$

$$= 0.0032483 \ \frac{lb_f s^2}{ft^4}$$

To be in a consistent Engineering English system of units the factor of g_c must not be dropped

$$\rho = (P/RT)g_c$$

$$= 0.0032483(32.174) \left\{ \frac{lb_f s^2}{ft^4} \frac{lb_m ft}{lb_f s^2} \right\}$$

$$= 0.1045 \ \frac{lb_m}{ft^3}$$

Of course, in the English *gravitational* system the *derived* mass is the slug

$$1 \ slug = 1 \ \frac{lb_f s^2}{ft}$$

so the first result is immediately recognized as

$$\rho = 0.0032483 \ \frac{slugs}{ft^3}$$

Stagnation Pressure The stagnation pressure for a 300 *F* gas flow with a 150 *ft/s* velocity and 4233.6 lb_f/ft^2 static pressure can be computed from

$$P_0 = P + \frac{\rho u^2}{2}$$

so

$$P_0 = 4233.60 \left\{ \frac{lb_f}{ft^2} \right\} + \frac{0.1045(150)^2}{2} \left\{ \frac{lb_m}{ft^2} \frac{ft^2}{s^2} \right\}$$

$$P_0 = 4233.60\left\{\frac{lb_f}{ft^2}\right\} + 1175.63\left\{\frac{lb_m}{ft-s^2}\right\}$$

and the inconsistency in units resulting from the ommission of g_c; correcting the density, then

$$P_0 = P + \frac{\rho u^2}{2g_c}$$

$$= 4233.60 + \frac{1175.63}{32.174}\left\{\frac{lb_f}{ft^2}\right\}$$

$$= 4270.14 \frac{lb_f}{ft^2}$$

Note that computations in the Gravitational English system do not, by default, require an explicit inclusion of a numerical value for g_C since it is unity.

Stagnation Temperature Correction of the density for stagnation temperature calculations is done the same as in the stagnation pressure case

$$T_0 = T + \frac{u^2}{2c_p}$$

Kinetic Energy of the Flow This quantity has the units of work since the "mass" in this case is a flowrate term

$$KE = \frac{\dot{m}u^2}{2}$$

$$= \frac{1}{2}\frac{\rho}{g_c}v^3 A \left\{\frac{lb_f ft}{s}\right\}$$

Table I.1 Unit Systems Hierarchy

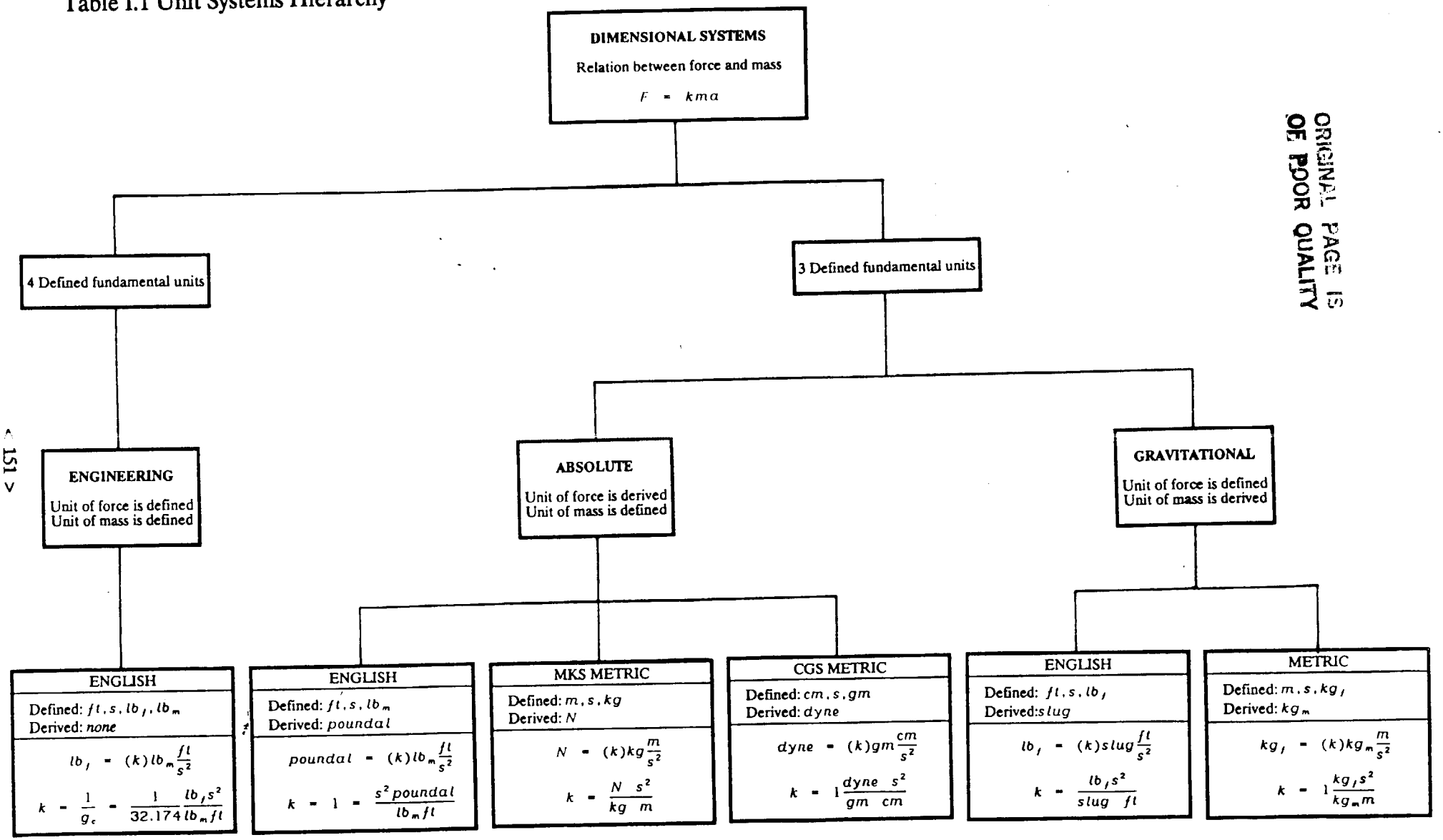

$1\,lb_m = 0.453592\,kg$ $\quad$ $1\,lb_f = 4.448\,N$

$1\,slug = 32.174\,lb_m$ $\quad$ $1\,ft = 0.3048\,m$

Table I.2 Summary of Engineering and MKS Systems

Quantity	*symbol*	*English*	*MKS*
Length	L	ft	m
Time	t	s	s
Mass	m	lb_m	kg
Force	F	lb or lb_f	N
Density	ρ	lb_m/ft^3	kg/m^3
Dynamic Viscosity	μ	$lb_f\text{-}s/ft^2$	Ns/m^2
Kinematic Viscosity	ν	ft^2/s	m^2/s
Pressure	P	lb_f/ft^2	N/m^2
Work, Energy	W	$lb_f\text{-}ft$	$N\text{-}m$
Power	$\dot{W}$	$lb_f\text{-}ft/s$	$N\text{-}m/s$

Note:

$$g_c = 32.174 \frac{lb_m ft}{lb_f s^2} = 1 \frac{kg - m}{N - s^2}$$

Table I.3 Conversion Factors

Pressure

To obtain → / Multiply by ↓ Number in Table	N/m^2	atm	$\frac{lbf}{in^2}$	$\frac{kgf}{cm^2}$
N/m^2, Pa	1	9.8692×10^{-6}	1.4504×10^{-4}	1.0197×10^{-4}
atm(760 mmHg)	10135	1	14.696	1.0332
bar	10^5	0.98692	14.504	1.0197
dyne/cm^2(microbar)	0.1	9.8692×10^{-7}	1.4504×10^{-5}	1.0197×10^{-6}
lbf/in^2, psi	6894.8	0.068046	1	0.070307
lbf/ft^2, psf	47.880	4.7254×10^{-4}	6.9444×10^{-3}	4.8824×10^{-4}
kgf/cm^2	98066.5	0.96784	14.223	1
mm HG @ 0°C (32°F)	133.32	0.001316	0.019337	0.0013595
mm HG @ 20°C (68°F)	132.84	0.0013110	0.019267	0.0013546
in HG @ 0°C (32°F)	3386.4	0.033421	0.49115	0.034532
in HG @ 20°C (68°F)	3374.1	0.03330	0.48937	0.034407

Dynamic viscosity

To obtain → / Multiply by ↓ Number in Table	$\frac{N\,S}{m^2}$ = $\frac{kg}{m\,s}$	$\frac{g}{cm\,s}$ = $\frac{dyne\,s}{cm^2}$	$\frac{lbm}{ft\,s}$ = $\frac{poundal\,s}{ft^2}$	$\frac{lbf\,s}{ft^2}$ = $\frac{slug}{ft\,s}$
$N\,s/m^2$	1	10	0.67197	0.020885
g/cm s(poise)	0.1	1	0.067197	0.0020885
centipoise	0.001	0.01	6.7197×10^{-4}	2.0885×10^{-5}
kg/m hr	2.7778×10^{-4}	0.0027778	1.8667×10^{-4}	5.8015×10^{-6}
lbm/ft s	1.4882	14.882	1	0.031081
lbm/ft hr	4.1338×10^{-4}	0.0041338	2.7778×10^{-4}	8.6336×10^{-6}
slug/ft s	47.880	478.80	32.174	1
slug/ft hr	0.013300	0.13300	0.0089372	2.7778×10^{-4}
lbm/in s	17.858	178.58	12	0.37297
lbm/in hr	0.0049605	0.049605	0.0033333	1.0360×10^{-4}
slug/in hr	0.15960	1.5960	0.10725	0.0033333
lbf s/in^2(Regn)	6894.7	68947.0	4633.1	144

Kinematic viscosity

To obtain → / Multiply by ↓ Number in Table	$\frac{m^2}{s}$	$\frac{cm^2}{s}$	$\frac{ft^2}{s}$	$\frac{in^2}{s}$
m^2/s	1	10^4	10.764	1550.0
cm^2/s(stroke)	10^{-4}	1	0.0010764	0.1550
centistroke	10^{-6}	0.01	1.0764×10^{-5}	0.001550
m^2/hr	2.7778×10^{-4}	2.7778	2.990×10^{-3}	0.43056
ft^2/s	0.09290304	929.0304	1	144
ft^2/hr	2.58064×10^{-5}	0.258064	2.7778×10^{-4}	0.04
in^2/s	6.4516×10^{-4}	6.4516	6.9444×10^{-3}	1
in^2/hr	1.7921×10^{-8}	1.7921×10^{-3}	1.9290×10^{-6}	2.7778×10^{-4}

Temperature

°F = 9/5 °C + 32
°R = °F + 459.69
°K = °C + 273.16
°R = 9/5 °K

Work & Energy

1 Btu = 778.16 lbf ft
1 Btu = 1055 J
1 Kcal = 4182 J
1 lbf ft = 1.356 J
1 Btu = 252 cal

Appendix J

Computation of Nozzle Exit Static Pressure

Introduction

Instrument data for the primary nozzle flow conditions has been assumed to be for mass flowrate, stagnation temperature, and static pressure. From this information the velocity, static temperature, and static pressure for the primary nozzle can be computed. However, if *stagnation* pressure is given rather than *static* pressure the analysis for primary nozzle conditions (given in the main body of this report) must be modified; the details for this are given below.

Derivation

The nozzle pressure ratio can be given by

$$\frac{P_0}{P} = \left(1 - \frac{\gamma - 1}{2} M^2\right)^{\gamma/(\gamma-1)}$$

so the Mach number is

$$M = \sqrt{\frac{2}{\gamma - 1}\left\{\left(\frac{P_0}{P}\right)^{\gamma-1/\gamma} - 1\right\}}$$

Combine this result with the modified mass flow-rate expressions of Appendix D to obtain

$$\frac{W}{A} = P_0\sqrt{\frac{1}{RT_0}\frac{2\gamma}{\gamma-1}\left\{\left(\frac{P_0}{P}\right)^{\gamma-1/\gamma} - 1\right\}^{1/2}\left(\frac{P_0}{P}\right)^{-\gamma+1/2\gamma}}$$

and after re-arrangement

$$\left(\frac{W}{A}\right)^2 \frac{\gamma - 1}{2\gamma}\frac{RT_0}{P_0^2} = \left(\frac{P_0}{P}\right)^{-\frac{2}{\gamma}} - \left(\frac{P_0}{P}\right)^{-\frac{\gamma+1}{\gamma}}$$

If the stagnation pressure, stagnation temperature, and mass flowrate are known, then this equation contains only the pressure ratio as an unknown; in polynomial form

$$\left(\frac{P}{P_0}\right)^{\frac{2}{\gamma}} - \left(\frac{P}{P_0}\right)^{\frac{\gamma+1}{\gamma}} - \left(\frac{W}{A}\right)^2 \frac{\gamma - 1}{2\gamma}\frac{RT_0}{P_0^2} = 0$$

Solution

The root of the equation above provides the solution for the nozzle pressure ratio and, since the stagnation pressure is known, the static pressure computes directly therefrom. Because this is not an ordinary polynomial which benefits from a simple analytic solution, a numerical approach is reccommended. Figure J.1 provides a listing and sample calculation for the APL computer program that provides this service.

Figure J.1 APL Solution Approach for Static Pressure

```
      ∇NSP[□]∇
[0]   NSP
[1]   ''
[2]   'ESTIMATE OF NOZZLE EXIT STATIC PRESSURE' ⍪ ''
[3]   '   ...INPUT DATA...'
[4]   '   PO      = ',(10 4 ⍕PO),' LBF/FT2'
[5]   '   TO      = ',(10 4 ⍕TO),' °R'
[6]   '   A       =  ',(10 4 ⍕A),' FT2'
[7]   '   GAMMA   = ',(10 4 ⍕GAMMA
[8]   '   R       =  ',(10 4 ⍕R),' FT-LBF/LBM-°R'
[9]   '   MDOT    = ',(10 4 ⍕MDOT),' LBM/S'
[10]  P←NEWTON 2000.1E¯6
[11]  '   ...RESULT...'
[12]  '   P       = ',(10 4 ⍕P),' LBF/FT2'

      ∇NEWTON[□]∇
[0]   Z←NEWTON X
[1]   ⍝
[2]   ⍝     NEWTONS METHOD FOR ROOT-FINDING
[3]   ⍝
[4]   ⍝        INPUT : X - VECTOR OF INITIAL GUESS AND ERROR BOUND
[5]   ⍝        OUTPUT: Z - ROOT OF THE FUNCTION 'ZERO'
[6]   ⍝
[7]   ⍝     NOTE: THE EXTERNALLY DEFINED FUNCTION 'ZERO' MUST
[8]   ⍝           RESIDE THE USER'S ACTIVE WORKSPACE.
[9]   ⍝
[10]  CT←0 ⋄ Z←X[2]+Z1←X[1]
[11]  Y←Y1←ZERO Z
[12]  L0:DX←Y[2]××Y××1÷Z-Z1
[13]  →L1×⍳0<Y×W←ZERO Z+DX
[14]  →0
[15]  L1:Y←ZERO Z←(Z1←Z)-(Y1×DX)÷W←Y1←Y
[16]  →L0×⍳70>CT←CT+(Y)≠Y1
[17]  'DIVERGING'
[18]  →0

      ∇ZERO[□]∇
[0]   Z←ZERO X
[1]   C1←(X÷PO)*2÷G
[2]   C2←(X÷PO)*(G+1)÷G
[3]   C3←((MDOT÷A)*2)×(G-1)×R×TO÷(2×32.174×G×PO*2)
[4]   Z←(C1-C2)-C3


      NSP

ESTIMATE OF NOZZLE EXIT STATIC PRESSURE

   ...INPUT DATA...
   PO      =  2799.9000 LBF/FT2
   TO      =   769.7000 °R
   A       =      .4200 FT2
   GAMMA   =    1.4000
   R       =   53.3039 FT-LBF/LBM-°R
   MDOT    =   18.7000 LBM/S
   ...RESULT...
   P       =  2219.7800 LBF/FT2
```

Appendix K

Overview of some PLF ejector data

Some geometric and instrumentation data

In the evaluation of the methods of analysis outlined in the text, it is necessary to have data with which to compare theoretical predictions. Information on some past NASA/Lewis PLF ejector tests have been made available to the present work. Figure 1 summarizes some geometric and instrumentation data believed to apply to the DeHaviland ejector tests conducted at the NASA/Lewis PLF facility.

Knowledge of the type of test data to be collected is fundamental in shaping the input requirements of practical computer programs. For the present work the requirements developed in the text (see chapter 5 of the text) have been based on the type of information one might expect from the PLF.

The general geometric characteristics of the DeHaviland ejector are also shown in figure 1. Use of this data has guided the geometric data requirements for the analysis as illustrated in Figure 11 of the text.

Some performance data

Performance data used for comparison with the theoretical predictions is shown in Table 1 - 3. The nomenclature for the computer printouts is defined (to a limited extent) in Figure 1.

Figure K.1 Some Geometric and Thermodynamic Ejector Information

Ⓐ Location of Ejector on Thrust Rig

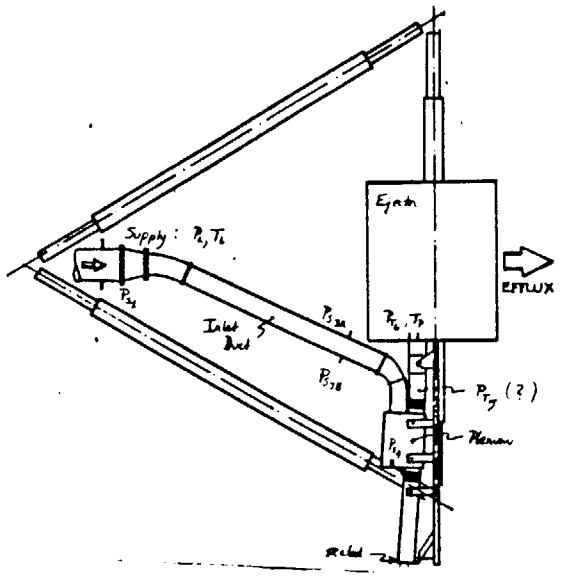

Air Supply Conditions

P_{s_L}	PSL	line pressure
T_L	TL	line temperature
P_L		(also line)
P_{TM}/P_A		operating pressure ratio

Model Pressures

$P_{s_{IN}}$, $P_{s_{TH}}$	duct inlet
P_{s_P}	plenum wall
P_{T_D}	ejector duct
$P_{T_{N_{01}}} - P_{T_{N_{12}}}$	ejector nozzle release pressures

Lewis Vendor Meter

P_V	PV	upstream pressure
ΔP_V	DELV	differential pressure
T_V	TV	upstream temperature

Ejector Exit Rakes

$P_{T_{E_{01}}} - P_{T_{E_{22}}}$	total pressure at ejector exit, 1 deg at same
$T_{E_{01}} - T_{E_{05}}$	

T - total
S - static

Inlet Duct Conditions

- Average duct inlet static pressure: $P_{s_{IN}} = \frac{1}{2}(P_{s_{IN}} + P_{s_{TH}})$
- Inlet duct pressure ratio: $P_{T_{IN}} / P_{s_{IN}} = \eta_1$ measured !
- Inlet duct Mach number: M_{IN}

$P_{T_{IN}} = P_{s_{IN}} \eta_1$

$Q_{IN} = \frac{1}{2} \gamma P_{s_{IN}} M_{IN}^2$

Pressure Losses

$\Delta P_{s_P} = P_{T_{IN}} - P_{s_P}$

$\Delta P_{T_D} = P_{T_{IN}} - P_{T_D}$

- Plenum exit total pressure: $P_{T_P} = P_{T_{IN}} - Q_{IN}\left\{\frac{\Delta P_{T_5}}{\Delta P_{IN}}\right\}$ → 0.96

XX Point 5 is a computed station that is the plenum exit

Ⓑ Thrust Computations

1. Isentropic ejector nozzle thrust

- Below choking, $NPR \le \left(\frac{\gamma+1}{2}\right)^{\gamma/\gamma-1}$

$$X_I = \frac{W\sqrt{T_D}}{g}\left\{\frac{2\gamma R}{\gamma-1}\left[1-\left(\frac{1}{NPR}\right)^{\frac{\gamma-1}{\gamma}}\right]\right\}^{1/2}$$

- Above choking, $NPR > \left(\frac{\gamma+1}{2}\right)^{\gamma/\gamma-1}$

$$X_I = \frac{W\sqrt{T_D}}{g}\sqrt{2}\left\{\frac{(\gamma+1)-\left[\left(\frac{\gamma+1}{2}\right)^{\gamma/\gamma-1}/NPR\right]}{\sqrt{2\gamma(\gamma+1)}}\right\}$$

2. Net (isentropic) thrust augmentation ratio

$$\phi_{NET} = \frac{X_M}{X_I}$$

X_M - measured ejector thrust from load cell

Need: NPR - average ejector nozzle pressure ratio
T_D - ejector duct temperature

Ⓒ Ejector Profile

- Rectangular Configuration
- 12 Nozzles

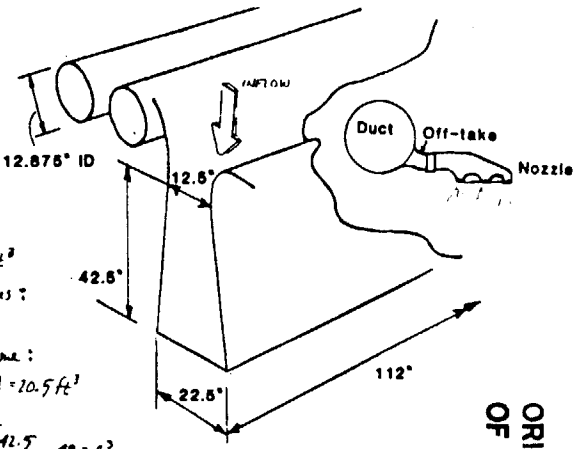

- Ejector duct volume: $112" \times 12.875" = 2.44\ ft^3$
- Ejector Nozzles + off-takes: $0.15\ ft^3$ each
- Total Duct / Nozzle Volume: $(2 \times 3.44) + (2 \times 12 \times 0.15) = 10.5\ ft^3$
- Ejector Diffuser Volume: $112 \times \left(\frac{17.5+22.5}{2}\right) = \frac{12.5}{1728} = 48.2\ ft^3$

Ejector Inlet Volume $\approx 112 \times 15 \times \frac{10}{1728} = 9.7\ ft^3$

Ⓓ Ejector Measurements and Computations

Averaged Ejector Stats

- Average ejector nozzle exit total pressure: $P_{T_{EJ}} = \frac{1}{12}\sum_{i=1}^{12} P_{T_{N_i}}$
- Average ejector nozzle pressure ratio: $NPR = P_{T_D} / P_A$

Note:
1. Ejector pressure drop calculation includes the pressure drop of the supply duct
2. No correction for adiabatic assumption

Ejector Nozzle Pressure Data

- Nozzle release pressures: $P_{T_{N_{01}}} - P_{T_{N_{12}}}$
- Nozzle exit total pressures: $P_{T_{N_i}} = P_{T_{N_{01}}} \cdot \left\{\frac{P_{T_{N_i}}}{P_{T_{N_1}}}\right\}$ — Quotient is from lab calibration of nozzle
- Ejector nozzle pressure drop: $\Delta P_{T_{N_i}} = P_{T_5} - P_{T_{N_i}}$
- Ejector nozzle pressure loss ratios:

$Q_5 = \frac{1}{2}\gamma P_{s_5} M_5^2$

$P_{s_5} = P_{T_5} \div \left(P_{s_5}/P_{T_5}\right)$

$$\left(\frac{P_{s_5}}{P_{T_5}}\right)^{3/\gamma} - \left(\frac{P_{s_5}}{P_{T_5}}\right)^{\frac{\gamma+1}{\gamma}} = \frac{(\gamma-1)R}{2\gamma g^2}\left\{\frac{W\sqrt{T_D}}{A_5 \cdot P_{T_5}}\right\}^2$$

$$M_5 = \left\{\left(\frac{2}{\gamma-1}\right)\left[\left(\frac{P_{T_5}}{P_{s_5}}\right)^{\frac{\gamma-1}{\gamma}} - 1\right]\right\}^{1/2}$$

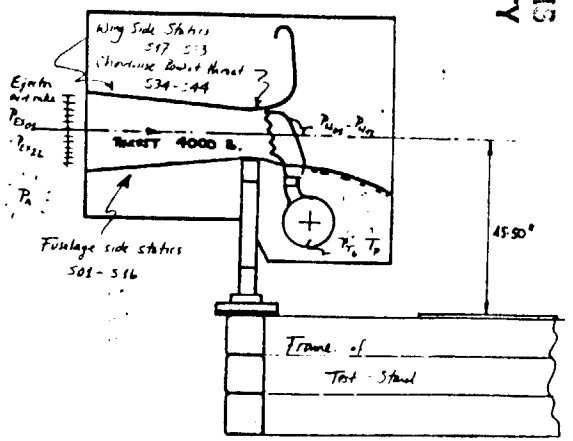

Table 1. Data Summary for Preliminary PLF Tests

Reading	*F-S Temp*	*NPR*	*Thrust*	*PHI*	$\dot{m}$
223	769.70	1.35	945.	1.86	18.70
239	760.60	1.46	1231.	1.87	21.85
225	761.70	1.70	1725.	1.80	27.27
237	763.50	1.82	1977.	1.79	29.66
227	763.50	2.06	2471.	1.78	34.26
235	765.50	2.27	2910.	1.78	37.97
229	763.50	2.38	3066.	1.74	39.96
233	758.40	2.56	3458.	1.76	43.22
231	764.80	2.79	3839.	1.72	46.97

Table 2. Data from PLF Test #223

NASA-LEWIS PRELIMINARY DATA 11/30/87 PDP11TWO REC 07/16/87 19:08:50.656 FAC PLF PGM D003

POWERED LIFT FACILITY SINGLE-SIDED EJECTOR FOR SPEY/E7 MODEL RUN 9
EJECTOR NOZZLE TYPE NOTCHED-CONE NOZZLES FORWARD DUCT VALVE ANGLE 90.0 DEG EXIT-RAKE 1 LOCATION 0.00
EXIT-RAKE 2 LOCATION 0.00

OPTION 1 SUMMARY

RUN	FDVA	NPR	PRIM	PR6	TP	CYCLES
9	90.0	1.354	1.426D	1.370	769.7	10

W	WNOZ	CDN	XM	XM2	XIE	XI6
19.51	18.70	1.0435	945.D	938.	532.	541.

PHINET	PHINET2	ANET6	XMSTD	H	PA	TA
1.7776D	1.7651	1.7469D	967.D	5.97D	14.36	542.8

WF	PR5	XI5	ANET5	XIIN	ANETIN
0.05	1.378D	546.D	1.7308D	573.D	1.6491D

$P_\infty = 2067.84$

$P_0 = 1.354\ P_\infty = 2799.86$

NASA-LEWIS PRELIMINARY DATA 11/30/87 PDP11TWO REC 07/16/87 19:08:50.656 FAC PLF PGM D003

POWERED LIFT FACILITY SINGLE-SIDED EJECTOR FOR SPEY/E7 MODEL RUN 9
EJECTOR NOZZLE TYPE NOTCHED-CONE NOZZLES FORWARD DUCT VALVE ANGLE 90.0 DEG EXIT-RAKE 1 LOCATION 0.00
EXIT-RAKE 2 LOCATION 0.00

OPTION 4 EJECTOR-NOZZLE CALCULATIONS

	01	02	03	04	05	06	07	08	09	10	11	12	A
PM	18.44	18.82	18.88	18.76	18.66	18.99	18.98	18.80	18.92	18.69	18.85	18.70	18.79
PTM	19.18	19.27	19.34	19.40	19.44	19.48	19.49	19.54	19.54	19.57	19.56	19.58	19.45
PRTM	1.336	1.342	1.346	1.351	1.354	1.357	1.357	1.361	1.360	1.363	1.362	1.363	1.354
DELPTM	0.61D	0.52D	0.45D	0.39D	0.35D	0.31D	0.30D	0.25D	0.26D	0.22D	0.23D	0.21D	0.34D
DELPTM/PT5	0.031D	0.027D	0.023D	0.020D	0.018D	0.016D	0.015D	0.012D	0.013D	0.011D	0.012D	0.011D	0.017D
DELPTM/(PT5-PA)	0.113D	0.097D	0.084D	0.071D	0.064D	0.057D	0.055D	0.045D	0.047D	0.040D	0.042D	0.039D	0.063D
DELPTM/Q5	0.821D	0.705D	0.611D	0.521D	0.466D	0.416D	0.400D	0.332D	0.344D	0.295D	0.310D	0.286D	0.459D

Table 3. Data from PLF Test #225

NASA-LEWIS PRELIMINARY DATA 11/30/87 PDP11TWO REC 07/16/87 19:13:08.544 FAC PLF PGM D003

POWERED LIFT FACILITY SINGLE-SIDED EJECTOR FOR SPEY/E7 MODEL RUN 9
EJECTOR NOZZLE TYPE NOTCHED-CONE NOZZLES FORWARD DUCT VALVE ANGLE 90.0 DEG EXIT-RAKE 1 LOCATION 0.00
EXIT-RAKE 2 LOCATION 0.00

OPTION 1 SUMMARY

RUN	FDVA	NPR	PRIN	PR6	TP	CYCLES
9	90.0	1.697	1.801D	1.715	761.7	10

W	WNOZ	CDN	XM	XM2	XIE	XI6
27.45	27.29	1.0056	1725.D	1719.	967.	976.

PHINET	PHINET2	ANET6	XMSTD	H	PA	TA
1.7835D	1.7773	1.7675D	1765.D	6.46D	14.36	540.3

WF	PR5	XI5	ANET5	XIIN	ANETIN
0.06	1.726D	981.D	1.7583D	1016.D	1.6985D

NASA-LEWIS PRELIMINARY DATA 11/30/87 PDP11TWO REC 07/16/87 19:13:08.544 FAC PLF PGM D003

POWERED LIFT FACILITY SINGLE-SIDED EJECTOR FOR SPEY/E7 MODEL RUN 9
EJECTOR NOZZLE TYPE NOTCHED-CONE NOZZLES FORWARD DUCT VALVE ANGLE 90.0 DEG EXIT-RAKE 1 LOCATION 0.00
EXIT-RAKE 2 LOCATION 0.00

OPTION 4 EJECTOR-NOZZLE CALCULATIONS

	01	02	03	04	05	06	07	08	09	10	11	12	A
PN	22.65	23.26	23.34	23.17	23.02	23.54	23.54	23.26	23.43	23.06	23.33	23.08	23.22
PTN	23.92	24.15	24.24	24.30	24.33	24.48	24.51	24.53	24.53	24.49	24.54	24.51	24.38
PRTN	1.665	1.681	1.688	1.692	1.694	1.704	1.706	1.708	1.708	1.705	1.709	1.707	1.697
DELPTN	0.87D	0.64D	0.54D	0.48D	0.45D	0.31D	0.28D	0.26D	0.25D	0.29D	0.24D	0.27D	0.41D
DELPTN/PT5	0.035D	0.026D	0.022D	0.020D	0.018D	0.012D	0.011D	0.010D	0.010D	0.012D	0.010D	0.011D	0.016D
DELPTN/(PT5-PA)	0.083D	0.061D	0.052D	0.047D	0.043D	0.029D	0.027D	0.025D	0.024D	0.028D	0.023D	0.026D	0.039D
DELPTN/Q5	0.738D	0.544D	0.463D	0.413D	0.385D	0.261D	0.236D	0.219D	0.215D	0.248D	0.206D	0.231D	0.347D

Appendix L

Jet Boundary Streamline

Equivalent Secondary Mass Flow

In the exchange of kinetic energy between mixing streams, quantifying the kinetic energy gained or lost by a single stream requires definition of a dividing streamline for the flow. Figure 1 marks the dividing streamline with the jet boundary parameter b^*. This is different than the boundary defined by point f on the figure, which simply marks the volume consumed by turbulent jet expansion.

The dividing streamline easily derives from the mass flow relation

$$\dot{m} = \int_s \rho v dA$$

from which we have

$$2NW(B-b_0)\rho_{1S}v_{e,1} = 2NWb\rho_2\int_{b^*/b}^{B/b} v d\xi$$

Completing the integration

$$\int_{b^*/b}^{B/b} v d\xi = \int_{\xi_1}^{\xi_2} \{v_e(1-\Phi)+v_m\Phi\} d\xi = F_1 v_m + F_3 v_e + F_4 v_e$$

where

$$F_1 = 0.45-(+0.25\xi_1^4-0.8\xi_1^{2.5}+\xi_1)$$
$$F_3 = 0.55-(-0.25\xi_1^4+0.8\xi_1^{2.5})$$
$$F_4 = \xi_2-1$$

Substitution and cancellation of like terms yields

$$c_1\xi_1^4+c_2\xi_1^{2.5}+c_3\xi_1+c_4 = 0$$

where

$$\zeta = \frac{b^*}{b}$$

$$c_1 = 0.25(v_{m,2} - v_{\theta,2})$$

$$c_2 = 0.80(v_{\theta,2} - v_{m,2})$$

$$c_3 = v_{m,2}$$

$$c_4 = \frac{\rho_{1S}}{\rho_2}\frac{B - b_0}{b_j} v_{\theta,1} - c_1 - c_2 - c_3 - \left(\frac{B}{b} - 1\right) v_\theta$$

The root to this equation provides the location of the dividing streamline, b^*, at desired axial location, station 2.

Numerical Solution

The polynomial describing the dividing streamline location does not have an convenient analytic solution, so numerical methods are used. In the present work the modified Newton's method is used. For this method two derivatives are required:

$$f(\zeta) = c_1\zeta^4 + c_2\zeta^{2.5} + c_3\zeta + c_4$$

$$f'(\zeta) = 4c_1\zeta^3 + 2.5c_2\zeta^{1.5} + c_3$$

$$f''(\zeta) = 12c_1 + 3.75c_2\zeta^{0.5}$$

The iterative method of solution calls for the following steps

1) Assume an initial value for the root; here $\zeta \leftarrow \zeta_0 = b_0/b$

2) $u(\zeta) = f(\zeta)/f'(\zeta)$

3) $u'(\zeta) = 1 - f(\zeta)f''(\zeta)/(f'(\zeta))^2$

4) $\delta = -u(\zeta)/u'(\zeta)$

5) If $\delta < \epsilon$ then exit otherwise refine the approximation for the root $\zeta = \zeta + \delta$ and repeat steps 2-4.

Figure L1. Jet Boundary Streamline

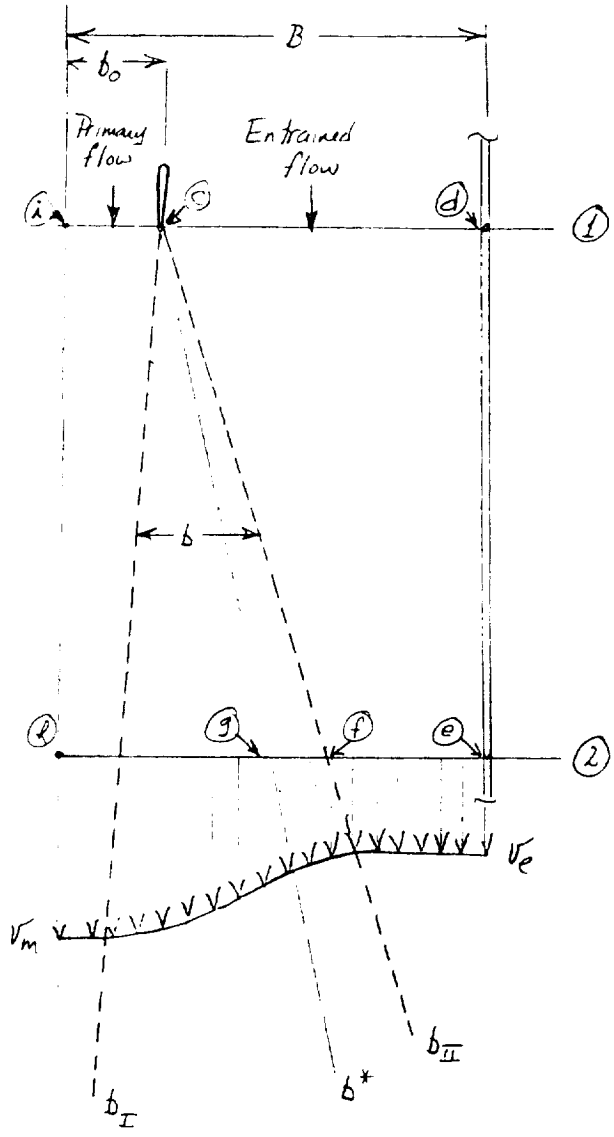

NASA
National Aeronautics and Space Administration

Report Documentation Page

1. Report No.	2. Government Accession No.	3. Recipient's Catalog No.
NASA CR-182203		

4. Title and Subtitle	5. Report Date
A Control-Volume Method for Analysis of Unsteady Thrust Augmenting Ejector Flows	November 1988
	6. Performing Organization Code

7. Author(s)	8. Performing Organization Report No.
Colin K. Drummond	None (E-4461)
	10. Work Unit No.
	505-62-71

9. Performing Organization Name and Address	11. Contract or Grant No.
Sverdrup Technology, Inc. NASA Lewis Research Center Group Cleveland, Ohio 44135	NAS3-25266
	13. Type of Report and Period Covered Contractor Report Final

12. Sponsoring Agency Name and Address	14. Sponsoring Agency Code
National Aeronautics and Space Administration Lewis Research Center Cleveland, Ohio 44135-3191	

15. Supplementary Notes

Project Manager, James R. Mihaloew, Propulsion Systems Division. NASA Lewis Research Center.

16. Abstract

A new method for predicting transient thrust augmenting ejector characteristics is presented. The analysis blends classic self-similar turbulent jet descriptions with a control volume mixing region descretization to solicit transient effects in a new way. Division of the ejector into an inlet, diffuser, and mixing region corresponds with the assumption of viscous-dominated phenomenon in the latter. Inlet and diffuser analyses are simplified by a quasi-steady analysis, justified by the assumption that pressure is the forcing function in those regions. Details of the theoretical foundation, the solution algorithm, and sample calculations are given.

17. Key Words (Suggested by Author(s))	18. Distribution Statement
Unsteady flow Thrust augmenting ejector Control-volume	Unclassified – Unlimited Subject Category 07

19. Security Classif. (of this report)	20. Security Classif. (of this page)	21. No of pages	22. Price*
Unclassified	Unclassified	168	A08

*For sale by the National Technical Information Service, Springfield, Virginia 22161